2010

CHARACTERISTICS AND DESIGN OF DOWNBURST LOADED TRANSMISSION LINES

Mohamed Mohamed Salah El-Din Darwish

CHARACTERISTICS AND DESIGN OF DOWNBURST LOADED TRANSMISSION LINES

(Spine title: Characteristics and Design of Downburst Loaded Transmission Lines)

(Thesis format: Integrated-Article)

By

Mohamed Mohamed Salah El-Din Darwish

Graduate Program in Engineering Science
Department of Civil and Environmental Engineering

A thesis submitted in partial fulfillment
of the requirements for the degree of
Doctor of Philosophy

School of Graduate and Postdoctoral Studies
The University of Western Ontario
London, Ontario, Canada
August, 2010

THE UNIVERSITY OF WESTERN ONTARIO
SCHOOL OF GRADUATE AND POSTDOCTORAL STUDIES

CERTIFICATE OF EXAMINATION

Supervisor	Examiners
Dr. Ashraf El Damatty	Dr. Jon Galsworthy
Supervisory Committee	Dr. Hanping Hong
Dr. Giles Santyr	Dr. Eric Savory
Dr. Charles McKenzie	Dr. Bruce Sparling

The thesis by

Mohamed Darwish

entitled:

Characteristics and Design of Downburst Loaded Transmission Lines

is accepted in partial fulfillment of the
requirements for the degree of
Doctor of Philosophy

Date August 09, 2010 David Gray
Chair of the Thesis Examination Board

ABSTRACT

During the past years, many electrical transmission lines have failed during downbursts. This thesis is part of a research program aimed to understand the behaviour of transmission lines under localized winds. The first part of the thesis assesses the dynamic behaviour of the conductors under downburst loading. A non-linear numerical model is utilized to predict the natural frequencies and mode shapes of the conductors at various loading stages. A turbulence signal is added to the mean component of the downburst wind field previously evaluated from a CFD analysis. Dynamic analysis is performed using various downburst configurations.

The second part of the thesis focuses on evaluating the sensitivity of the forces in the members of guyed towers to changes in the downburst configuration, tower height, guys' configuration, turbulence, and the conductors' pretensioning force. The axial forces in the members are compared to those resulting from normal wind loading and the broken wire load case.

The third part of the thesis focuses on developing simplified loads, equivalent to the critical downburst loads causing the guyed transmission tower to fail. Different options are considered in terms of the location and nature of the design velocity associated to different critical cases. The profile of the horizontal velocity is developed. The equivalent load corresponding to each of the critical cases is developed. Detailed steps of the conductors' reactions calculations are provided. A loading procedure is developed for designing downburst loaded guyed transmission towers.

The fourth part of the thesis involves studying the behaviour of self supported transmission line towers under downburst loading. A parametric study is performed to determine the critical downburst configurations causing maximum axial forces for various members of the tower. The sensitivity of the internal forces developing in the tower's members to changes in the downburst size and location is studied. The structural behaviour associated with the critical downburst configurations is described and compared to the behaviour under normal wind loads.

KEYWORDS: Downburst, High Intensity Wind, Transmission Line, Transmission Tower, Finite Element, Failure, Turbulence

CO-AUTHORSHIP

This thesis has been prepared in accordance with the regulation for an Integrated-Article format thesis stipulated by the School of Graduate and Post-doctoral Studies at the University of Western Ontario and has been co-authored as:

Chapter 2: Dynamic Characteristics of Transmission Line Conductors and its Behaviour under Turbulent Downburst Loading

Numerical modeling work was conducted by M. Darwish under supervision of Dr. A. A. El Damatty. The turbulence estimation process was performed by M. Darwish in coordination with Dr. H. Hangan and Dr. A. A. El Damatty. Drafts of Chapter 2 were written by M. Darwish and modifications were done under close supervision of Dr. A. A. El Damatty. A paper coauthored by M. Darwish, A. A. El Damatty and H. Hangan has been published in the *Journal of Wind and Structures*.

Chapter 3: Sensitivity of Transmission Line Guyed Towers to Downburst Loading

All the analytical work was conducted by M. Darwish under close supervision of Dr. A. A. El Damatty. Drafts of Chapter 3 were written by M. Darwish and modifications were done under supervision of Dr. A. A. El Damatty. A version of this work co-authored by M. Darwish and A. A. El Damatty will be submitted to the *Journal of Engineering Structures*.

Chapter 4: Equivalent Loading of Guyed Transmission Line Towers to Resist Downbursts

All the analytical work was conducted by M. Darwish under close supervision of Dr.

A. A. El Damatty. Drafts of Chapter 4 were written by M. Darwish and modifications were done under supervision of Dr. A. A. El Damatty. A version of this work co-authored by A. A. El Damatty and M. Darwish will be submitted to Proceeding of the **13th International Conference on Wind Engineering**

Chapter 5: Behavior of Self Supported Transmission Line Towers under Downburst Loading

All the analytical work was conducted by M. Darwish under close supervision of Dr. A. A. El Damatty. Drafts of Chapter 3 were written by M. Darwish and modifications were done under supervision of Dr. A. A. El Damatty. A version of this work co-authored by M. Darwish and A. A. El Damatty will be submitted to the *Journal of Wind & Structures.* .

DEDICATION

I would like to dedicate this thesis to my family for their extensive love and support.

In the memory of Mohamed Moftah.

ACKNOWLEDGMENT

The author would like to express his appreciation and sincere gratitude to his research supervisor, Dr. Ashraf El Damatty, for his valuable guidance and advice throughout the course of this research work, it has been a privilege to work under his supervision.

The author is obliged to the Natural Sciences and Engineering Research Council of Canada (NSERC), CEATI and Manitoba Hydro Company, Canada, for the financial and in-kind support provided to this research work. Also, the author deeply appreciates the SHARCNET supercomputer facility and staff at the University of Western Ontario, Canada. Also, the author deeply appreciates the help provided by Dr. Shehata, A.Y. and Dr. Moftah, M.. The author acknowledges the efforts of the research group at the BLWTL, the University of Western Ontario, Canada, for their efforts in providing the downburst wind data and continuous scientific assistance allover the last four years. Above all, the author wishes to express his sincere gratitude to his family and friends for their continuous support and encouragement.

TABLE OF CONTENTS

		Page
	CERTIFICATE OF EXAMINATION	ii
	ABSTRACT	iii
	CO-AUTHORSHIP	v
	DEDICATION	vii
	ACKNOWLEDGMENT	viii
	TABLE OF CONTENTS	ix
	LIST OF TABLES	xiv
	LIST OF FIGURES	xiv
	LIST OF SYMBOLS	xix
	CHAPTER 1	
	INTRODUCTION	
1.1	GENERAL	1
1.2	BACKGROUND ON DOWNBURSTS	2
1.3	NUMERICAL MODELING OF DOWNBURST WIND	6
1.4	RESPONSE OF TRANSMISSION LINES TO DOWNBURST LOADS	7
1.5	OBJECTIVES OF THE STUDY	10
1.6	SCOPE OF THE THESIS	10
	1.6.1 DYNAMIC CHARACTERISTICS OF TRANSMISSION LINE CONDUCTORS AND ITS BEHAVIOUR UNDER TURBULENT DOWNBURST LOADING	11
	1.6.2 SENSITIVITY OF TRANSMISSION LINE GUYED TOWERS TO DOWNBURST LOADING	12
	1.6.3 EQUIVALENT LOADING OF GUYED TRANSMISSION LINE TOWERS TO RESIST DOWNBURSTS	12
	1.6.4 BEHAVIOR OF SELF SUPPORTED TRANSMISSION LINE	13

TOWERS UNDER DOWNBURST LOADING

1.7 MAJOR RESEARCH CONTRIBUTIONS 13

1.8 REFERENCES 13

CHAPTER 2

DYNAMIC CHARACTERISTICS OF TRANSMISSION LINE CONDUCTORS AND THEIR BEHAVIOUR UNDER TURBULENT DOWNBURST LOADING

2.1 INTRODUCTION 16

2.2 NUMERICAL MODELLING OF THE CONDUCTORS 23

2.2.1 FINITE ELEMENT MODEL FOR THE CONDUCTORS 23

2.2.2 PHYSICAL AND GEOMETRIC PROPERTIES OF THE CONDUCTOR 24

2.2.3 VALIDATION 25

2.3 INCREMENTAL FREE VIBRATION ANALYSIS OF THE CONDUCTOR 26

2.3.1 INCREMENTAL FREE VIBRATION ANALYSIS OF THE CONDUCTOR UNDER UNIFORM LOADING 26

2.3.2 VARIATION OF THE PRETENSIONING LEVEL OF THE CABLES 27

2.3.3 EFFECT OF THE BOUNDARY CONDITIONS 29

2.3.4 ANALYSIS OF THE CONDUCTOR UNDER DOWNBURST LOADING 29

2.4 FULL SCALE DATA AND TURBULENCE EXTRACTION 31

2.4.1 FULL SCALE DATA 31

2.4.2 TURBULENCE EXTRACTION 32

2.5 DYNAMIC ANALYSIS 35

2.5.1 VALIDATION 35

2.5.2 DAMPING 37

2.5.3 ANALYSIS AND RESULTS 38

2.6 CONCLUSIONS 45

2.7 REFERENCES 46

CHAPTER 3

SENSITIVITY OF TRANSMISSION LINE GUYED TOWERS TO DOWNBURST LOADING

3.1 INTRODUCTION 50

3.2 DESCRIPTION OF THE NUMERICAL MODEL 54

3.2.1 TOWER AND GUYS MODELING 54

3.2.2 FINITE ELEMENT MODEL FOR THE CONDUCTORS 56

3.3 SENSITIVITY ANALYSIS OF GUYED TOWERS 57

3.3.1 SENSITIVITY OF THE FORCES IN THE TOWER MEMBERS TO CHANGING THE DOWNBURST CONFIGURATIONS 58

3.3.2 THE EFFECT OF TOWER HEIGHT AND GUYS CONFIGURATION 68

3.3.3 THE EFFECT OF TURBULENCE ON THE FORCE IN THE TOWER MEMBERS 80

3.3.4 THE EFFECT OF MAGNITUDE OF CONDUCTORS PRETENSIONING 82

3.4 CONCLUSIONS 85

3.5 REFERENCES 86

CHAPTER 4

EQUIVALENT LOADING OF GUYED TRANSMISSION LINE TOWERS TO RESIST DOWNBURSTS

4.1 INTRODUCTION 89

4.2 DESCRIPTION OF THE MODELED TOWERS 95

4.3 SELECTION OF THE REFERENCE VELOCITY 97

4.3.1 CONSTANT REFERENCE VELOCITY AT 10 m HEIGHT 98

4.3.2 CONSTANT REFERENCE VELOCITY AT 44 m HEIGHT 100
4.3.3 CONSTANT JET VELOCITY 101
4.4 CONVECTIVE VELOCITY EFFECT 102
4.4.1 CRITICAL DOWNBURST CASES 103
4.4.2 EFFECT OF THE CONVECTIVE VELOCITY COMPONENT 105
4.5 EQUIVALENT PATCH LOAD APPROACH 107
4.5.1 APPROACH 1: SIMULATING CRITICAL LOAD CASE 1 108
4.5.2 APPROACH 2: SIMULATING CRITICAL LOAD CASE 2 111
4.5.3 APPROACH 3: SIMULATING CRITICAL LOAD CASE 3 112
4.6 EVALUATION OF LOADS FOR GUYED TRANSMISSION TOWERS 112
4.6.1 THE ASYMMETRIC LOAD CASE 113
4.6.2 LOAD CASE 2 113
4.6.3 LOAD CASE 3 114
4.6.4 SPEED METEOROLOGICAL DATA 115
4.6.5 THE EFFECT OF TURBULENCE 116
4.7 SOLVED EXAMPLE 117
4.7.1 THE ASYMMETRIC LOAD CASE 118
4.7.2 THE SYMMETRIC LOAD CASES 119
4.7.3 COMPARISON OF THE RESULTS 120
4.8 CONCLUSIONS 120
4.9 REFERENCES 122

CHAPTER 5

BEHAVIOR OF SELF SUPPORTED TRANSMISSION LINE TOWERS UNDER DOWNBURST LOADING

5.1 INTRODUCTION 124

5.2 DESCRIPTION OF NUMERICAL MODEL 127

5.3 PARAMETRIC STUDY OF A SELF SUPPORTED TOWER 132

5.3.1 MAXIMUM MEMBER FORCES AND CRITICAL DOWNBURST PARAMETERS 133

5.3.2 SENSITIVITY OF THE TOWER MEMBERS TO CHANGING THE DOWNBURST CONFIGURATION 135

5.4 BEHAVIOUR OF THE SELF SUPPORTED TOWER UNDER DOWNBURST AND NORMAL WIND LOADINGS 145

5.4.1 CASE I ($\theta = 0^{o}$) 145

5.4.2 CASE II ($\theta = 15^{o}$) 147

5.4.3 CASE III ($\theta = 30^{o}$) 151

5.4.4 CASE IV ($\theta = 90^{o}$) 153

5.5 CONCLUSIONS 154

5.6 REFERENCES 156

CHAPTER 6

CONCLUSIONS

6.1 SUMMARY AND CONCLUSIONS 158

6.1.1 DYNAMIC CHARACTERISTICS OF TRANSMISSION LINE CONDUCTORS AND THEIR BEHAVIOUR UNDER TURBULENT DOWNBURST LOADING 159

6.1.2 CHARACTERISTICS OF TRANSMISSION LINE GUYED TOWERS AND ITS BEHAVIOUR UNDER DOWNBURST LOADING 160

6.1.3 EQUIVALENT LOADING OF GUYED TRANSMISSION LINE TOWERS TO RESIST DOWNBURSTS 161

6.1.4 BEHAVIOR OF SELF SUPPORTED TRANSMISSION LINE TOWERS UNDER DOWNBURST LOADING 163

6.2 RECOMMENDATIONS FOR FUTURE RESEARCH 164

CURRICULUM VITAE 165

LIST OF TABLES

Table	Description	Page
2.1	Physical parameters employed for the conductor, (Oakes, 1971).	24
2.2	Results of the Eigen-value Analysis of the 6 Spanned Conductor.	26
2.3	Effects of turbulence on the quasi-static and dynamic responses of the conductors.	45
3.1	Effect of turbulence on the axial forces in the members of Tower A-402-0	68
3.2	Parametric study for the Manitoba Hydro tower type A-401-0	79
4.1	Parametric study measuring the effect of the convective velocity.	107
4.2	Results of the analysis of tower 402 under the equivalent loads in comparison to the downburst load.	118
5.1	Parametric study for the Manitoba Hydro tower type A-501-0	135

LIST OF FIGURES

Figure	Description	Page
1.1	Transmission towers having different structural systems.	2
1.2	Schematic illustration of a thunderstorm, (Bureau of Meteorology, 1999).	3
1.3	Cloud proceeding rain and hail column of a thunderstorm, (CIGRE, 2004).	4
1.4	Typical scales of motion of ground-level winds, (CIGRE, 2004).	4
1.5	Range of peak winds for varying space scales, (CIGRE, 2004).	5
2.1	Schematic diagram of computational domain of downburst CFD model, (Hangan et al, 2003).	17
2.2	Two-Dimensional Consistent Curved Frame Element, (Shehata et al, 2005).	23
2.3	Modeling of the transmission line under study.	25

2.4	Comparisons between mode shapes predicted by model and SAP 2000.	25
2.5	First three mode shapes of the conductor under uniform load.	27
2.6	Mode shapes of the conductor for different levels of pretensioning.	28
2.7	First two mode shapes together with the normalized deflected shape of the conductor under load case 1.	30
2.8	Full scale velocity at a height of 10 m and the turbulence associated with it.	33
2.9	Power spectra of the measured velocities.	34
2.10	Analysis of a simply supported shallow arch under time-dependent loading.	36
2.11	Deflection with varying damping due to downburst with 30s filtering time.	40
2.12	Deflection due to downburst for different filtering periods.	41
3.1	Horizontal projection of transmission tower and downburst, (Shehata et al., 2005).	55
3.2	Geometry of the modeled lattice transmission tower Type A-402-0, (Shehata et al., 2005).	57
3.3	Variation of the axial force in chord member 14 (Zone 1) with r/D_j and θ, for $D_j = 500$ m.	61
3.4	Variation of the axial force in chord member 86 (Zone 2) with r/D_j and D_j, for $\theta = 90^o$.	61
3.5	Variation of the axial force in chord member 141 (Zone 3) with r/D_j and θ, for $D_j = 500$ m.	62
3.6	Variation of the axial force in diagonal member 275 (Zone 4) with r/D_j and D_j, for $\theta = 0^o$.	62
3.7	Variation of the axial force in chord member 318 (Zone 5) with r/D_j and θ, for $D_j = 500$ m.	63
3.8	Variation of the axial force in diagonal member 406 (Zone 6) with r/D_j and D_j, for $\theta = 45^o$.	63
3.9	Variation of the axial force in the lower chord member 422 (connected to the guy) with the downburst configuration.	64

3.10	Variation of the axial force in the lower chord cross-arm member 538 with the downburst configuration.	65
3.11	Variation of the axial force in the diagonal member 514 (Zone 7) with the downburst configuration.	66
3.12	Variation of the axial force in the Tower A-402-0 guys with r/Dj and θ, for D_j = 500 m.	67
3.13	Geometry of the modeled lattice transmission tower Type A-401-0.	69
3.14	Variation of the axial force in the Tower A-401-0 main guys with r/D_j and θ, for D_j = 500 m.	71
3.15	Variation of the axial force in the Tower A-401-0 secondary guys with r/D_j and θ, for D_j = 500 m.	72
3.16	Variation of the axial force in chord member 42 (Zone 1) with r/D_j and D_j, for θ = 90°.	73
3.17	Variation of the axial force in chord member 75 (Zone 2) with r/D_j and θ, for D_j = 500 m.	73
3.18	Variation of the axial force in chord member 330 (Zone 3) with r/D_j and D_j, for θ = 90°.	74
3.19	Variation of the axial force in chord member 350 (Zone 4) with r/D_j and θ, for D_j = 500 m.	74
3.20	Variation of the axial force in diagonal member 381 (Zone 5) with r/D_j and D_j, for θ = 0°.	75
3.21	Variation of the axial force in diagonal member 538 (Zone 6) with r/D_j and θ, for D_j = 500 m.	75
3.22	Variation of the axial force in the upper chord member 502 (connected to the guys) with r/D_j and θ, for D_j = 500 m.	76
3.23	Variation of the axial force in the upper chord cross-arm member 581 with r/D_j and D_j, for θ = 30°.	76
3.24	Variation of the axial force in the lower chord cross-arm member 616 to changing r/D_j and θ, for D_j = 500 m.	77
3.25	Variation of the axial force in chord member 675 to changing r/D_j and θ, for D_j = 500 m.	77

3.26	Variation of the conductor longitudinal reaction with θ and the pretensioning force, for $r/D_j = 1.6$ and $D_j = 1000$ m.	83
3.27	Variation of the forces in the chord members in Zone 6 with θ and the pretensioning force, for $r/D_j = 1.6$ and $D_j = 1000$ m.	84
4.1	Horizontal projection of transmission line and downburst, (Shehata et al., 2005).	90
4.2	Two-dimensional consistent curved frame element, (Shehata et al., 2005).	92
4.3	Geometry of the modeled lattice transmission tower Type A-402-0, (Shehata et al., 2005).	93
4.4	Geometry of the modeled lattice transmission tower Type A-401-0.	97
4.5	Profiles of the radial velocity having a constant 10 m velocity.	99
4.6	Profiles of the radial velocity having a constant 44 m velocity.	101
4.7	Vertical profiles for the radial velocity keeping the jet velocity constant.	102
4.8	The three critical downburst load cases.	105
4.9	The load distribution along the conductor for case 1.	110
4.10	Forces transferred from the conductors to the cross-arms due to case 1.	111
5.1	Horizontal projection of transmission tower and downburst parameters, (Shehata et al., 2005).	129
5.2	Geometry of MH Tower Type A-501	131
5.3	Variation of the axial force in member 45 (Zone 1) with the downburst parameters.	138
5.4	Variation of the axial force in member 402 (Zone 2) with r/D_j and θ, for $D_j = 500$ m.	138
5.5	Variation of the axial force in member 402 (Zone 2) with r/D_j and D_j, for $\theta = 0^o$.	139
5.6	Variation of the axial force in member 605 (Zone 3) with r/D_j and θ, for $D_j = 500$ m.	140
5.7	Variation of the axial force in member 577 (Zone 3) with r/D_j and D_j,	140

for $\theta = 0^{o}$.

5.8 Variation of the axial force in member 750 (Zone 4) with r/D_j and θ, for $D_j = 500$ m. 141

5.9 Variation of the axial force in member 770 (Zone 4) with r/D_j and θ, for $D_j = 1000$ m. 141

5.10 Variation of the axial force in member 925 (Zone 5) with r/D_j and θ, for $D_j = 500$ m. 142

5.11 Variation of the axial force in member 324 (Zone 5) with r/D_j and D_j, for $\theta = 0^{o}$. 142

5.12 Variation of the axial force in member 1104 (Zone 6) with r/D_j and θ, for $D_j = 1000$ m. 143

5.13 Variation of the axial force in member 1241 (Zone 5) with r/D_j and D_j, for $\theta = 0^{o}$. 143

5.14 Variation of the conductor reactions with r/Dj and θ, for $D_j = 500$ m. 144

5.15 Vertical profile of wind loading at a projection angle of 0^{o}. 146

5.16 Structural behavior at a projection angle of 0^{o}. 147

5.17 Vertical profile of wind loading at a projection angle of 15^{o}. 149

5.18 Structural behavior at a projection angle of 15^{o}. 150

5.19 Forces transferred from conductors under different wind loads. 152

5.20 Vertical profile of wind loading at a projection angle of 90^{o}. 153

5.21 Structural behavior at a projection angle of 90^{o}. 154

LIST OF SYMBOLS

Symbol	Unit	Description
A_c	m^2	The conductor cross-sectional area.
A_{cref}	m^2	The reference conductor cross-sectional area.
B	---	Background component of the undamped turbulent response.
C_D	---	Drag coefficient.

D_c	m	Conductor diameter.
D_j	m	Full-scale downburst jet diameter.
E	Pa	Modulus of elasticity
F_c	N	The axial member force causing the member to fail
F_i	Hz	Natural frequency of the conductor for mode (i)
NT	---	Non turbulent response
L	m	Horizontal wind span length of the conductor cable.
m_c	Kg/m	Mass of the conductor per unit length
QT	---	Quasi-static turbulent response
r	m	Full-scale horizontal distance between the centers of the tower and the downburst.
R	---	Resonant component of the undamped turbulent response.
R_{TRANS}	N	Transverse conductor reaction acting at the conductor–tower connection.
R_{LONG}	N	Longitudinal conductor reaction acting at the conductor–tower connection.
S	m	Sag of the conductor cable.
T	N	Tension force in the conductor cable.
T_i	s	Natural period of the conductor for mode (i)
UT	---	Undamped turbulent response
u	m	Translational degree of freedom of the consistent curved frame element in the axial direction.
V_c	m/s	Convective velocity.
V_j	m/s	Full-scale downburst jet velocity.
V_{jc}	m/s	Critical downburst jet velocity.
V	m/s	Horizontal velocity normal to the conductor.
$V_{avg(t)}$	m/s	Average horizontal velocity normal to the conductor at time (t).

w	m	Translational degree of freedom of the consistent curved frame element in the transverse direction.
W	N/m	Distributed wind load perpendicular to the conductors.
W_C	N/m	Weight per unit length of the conductor cable.
X_D	m	Cartesian coordinate of the downburst in global X-direction.
Y_D	m	Cartesian coordinate of the downburst in global Y-direction.
Z_D	m	Cartesian coordinate of the downburst in global Z-direction.
ΔT	s	Analysis time step
α	degrees	Rotational degree of freedom of the consistent curved frame element.
φ	degrees	Thickness rotation degree of freedom of the consistent curved frame element.
θ	degrees	Angle between a vertical plane containing the centers of the tower and the downburst and a vertical plane normal to the transmission line.
ρ	Kg/m^3	Air density
ϕ	degrees	Direction of the wind velocity subjected on the conductor.
ζ_{ai}	---	The aerodynamic damping for uniformly loaded cables for mode *(i)*

CHAPTER 1

INTRODUCTION

1.1 GENERAL

Transmission lines have a major role in electrical energy transmission. Disruptions in electrical power due to transmission line structural failures cause devastating economical and social losses. A transmission line is composed of four main components; the conductors, the ground wires, the insulator strings, and the towers. Transmission towers are designed to carry various loads. However, the largest effect usually occurs due to wind and ice loads. Two different structural systems are used in transmission towers; self-supported towers and guyed towers. For self-supporting towers, the loads are transferred through the towers' members to the ground. Under lateral loads, a self-supporting tower behaves similar to a cantilever (White, 1993). On the other hand, guyed towers rely on attached guys, which are anchored to the ground, to transfer a portion of the lateral loads imposed on the tower. A Guyed tower behaves similar to a simple beam with an overhanging cantilever. This equivalent beam can be treated as hinged at its base to the ground and supported near its top by a spring, simulating the guys' stiffnesses (White, 1993). The uppermost part of guyed towers (the zone above the guys) behaves similar to a cantilever where the detailed configuration of this zone depends mainly on the arrangement of the conductors carried by the tower. Figure 1.1 shows skeletons for self-supported and guyed towers. Self-supported structures are more commonly used and, therefore, are considered the typical form of transmission towers. However, guyed structures are deemed to be more economical (White, 1993).

In a typical transmission line configuration, the conductors are attached to the towers via insulator strings, while the ground wires are attached directly to the top edges of the towers for lightening protection. The transmission towers, together with the conductors, are the focus of the current study.

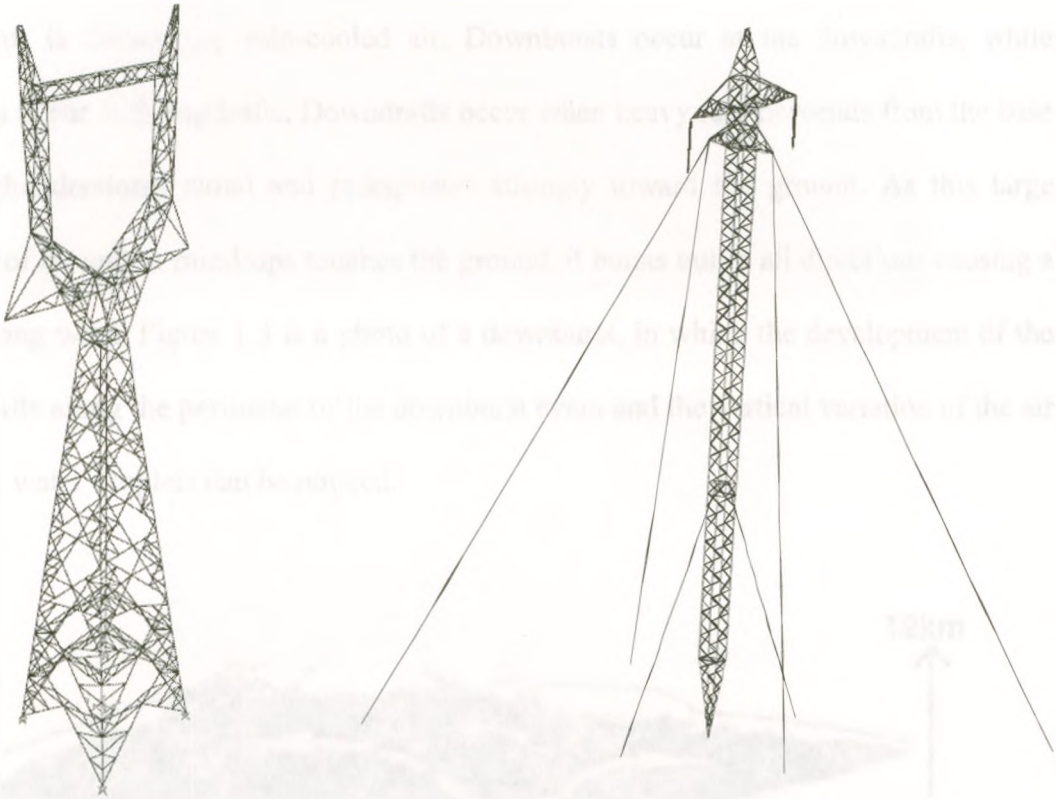

Figure 1.1 Transmission towers having different structural systems.

1.2 BACKGROUND ON DOWNBURSTS

Downbursts and tornados – referred to as high intensity wind (HIW) events – are localized wind events having velocities that are usually higher than 45 m/s (CIGRE, 2004). Although these events constitute approximately 10% of all thunderstorms, they cause 90% of all damages and injuries due to wind loading (CIGRE, 2004). Despite the large number of failures attributed to localized events, the wind loads specified in most codes and standards used for designing transmission line structures are based on large-

scale wind storms in the form of typhoons and hurricanes. Only the ASCE (2010) gives some guidance on tornados loadings.

A thunderstorm can be defined as a combination of rising air (updraft) and descending air (downdraft), as shown in Figure 1.2. The updraft is formed by warm moist air and the downdraft is formed by rain-cooled air. Downbursts occur at the downdrafts, while tornados occur at the updrafts. Downdrafts occur when heavy rain descends from the base of the thunderstorm cloud and precipitates strongly toward the ground. As this large amount of air and/or raindrops touches the ground, it bursts out in all directions causing a very strong wind. Figure 1.3 is a photo of a downburst, in which the development of the downdrafts along the perimeter of the downburst event and the vertical variation of the air carrying water droplets can be noticed.

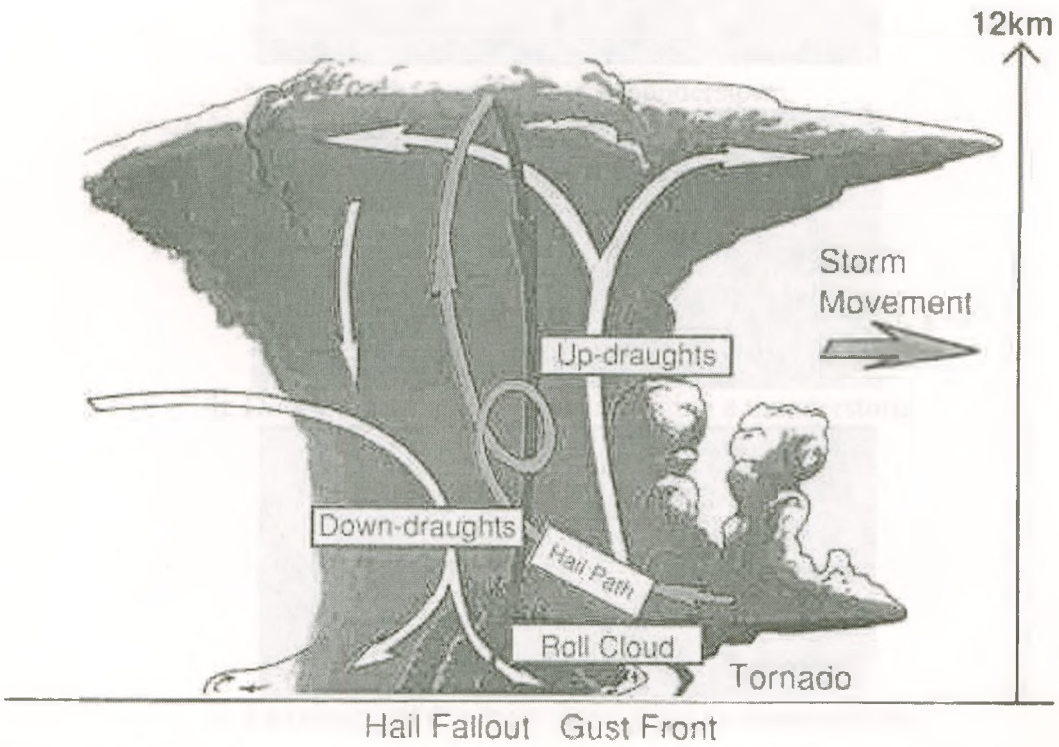

Figure 1.2 Schematic illustration of a thunderstorm, (Bureau of Meteorology, 1999).

Figure 1.3 Cloud proceeding rain and hail column of a thunderstorm, (CIGRE, 2004).

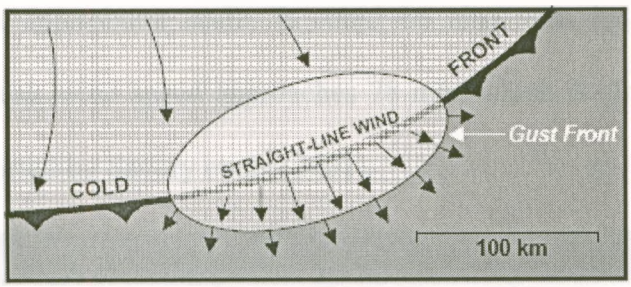

a. The gust front of a thunderstorm.

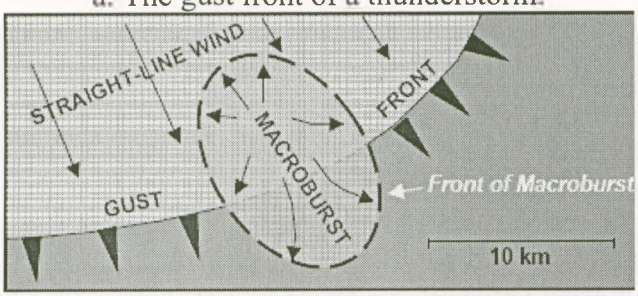

b. Development of a macroburst within a thunderstorm.

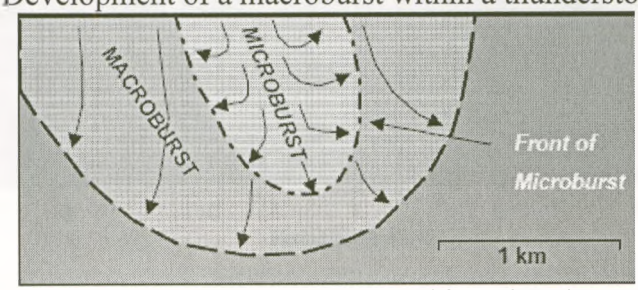

c. Development of a microburst within a thunderstorm.

Figure 1.4 Typical scales of motion of ground-level winds, (CIGRE, 2004).

Figure 1.4 was presented by CIGRE (2004), in lieu of the concepts explained by Fujita (1981), describing the different scales of thunderstorms. Figure 1.4a shows the upper bound of a thunderstorm (in terms of size), where severe straight-line winds can accompany a gust front ahead of a cold frontal system. This scale of motion is typically in the order of 100 km. Figure 1.4b shows the potential further development of a macroburst within the gust front flow at a scale of order 10 km. Finally, a microburst may develop at a scale of order 1 km, as shown in Figure 1.4c.

Figure 1.5 shows the variation in the peak wind speeds within different scales of a thunderstorm. It could be seen that the peak wind speed of the microburst occurs near the lower bound of the microburst scale. It could be also seen in Figure 1.5 that the magnitude of that peak wind speed approaches 78 m/s, which is close to the peak wind speed of 80 m/s reported by Savory et al.. (2001).

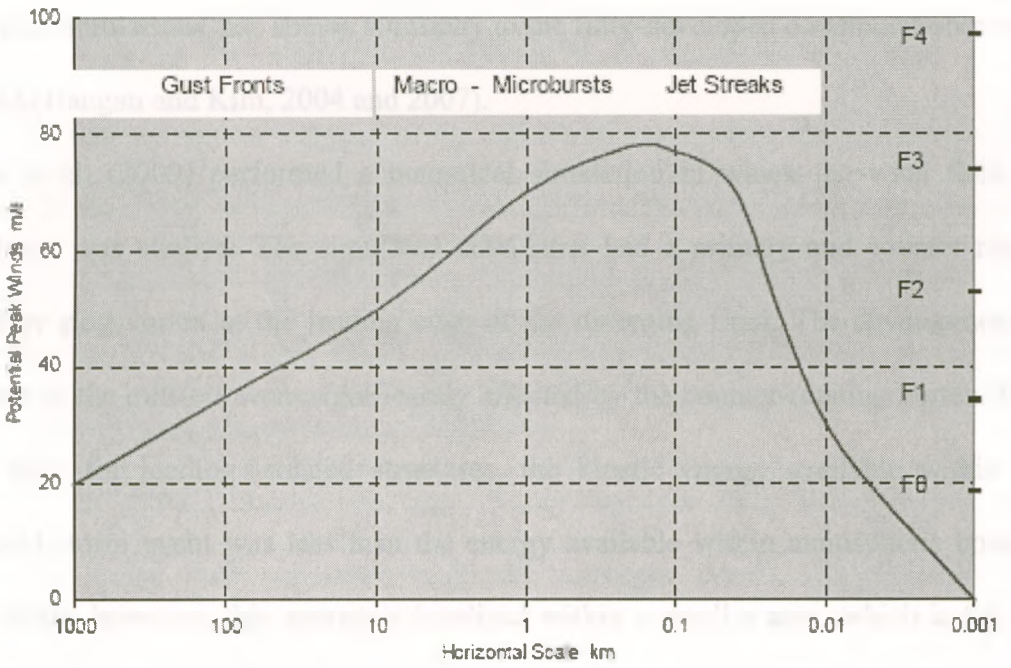

Figure 1.5 Range of peak winds for varying space scales, (CIGRE, 2004).

1.3 NUMERICAL MODELING OF DOWNBURST WIND

The wind field associated with a downburst event differs from that of a large-scale event. The major special characteristic of the downburst phenomenon is its local high intensity wind and its relatively short duration (2.0 ~ 30.0 minutes), such that its scale and intensity cannot readily be measured in the field by traditional recording stations. As such, the simulation of those events relies on numerical and analytical modelling.

Vicory (1992) reported the two essential models developed in the literature to simulate the wind field associated with a downburst; namely the "ring vortex" model and the "impinging wall jet" model. The ring vortex model simulates the downward column of air that forms a vortex ring prior to reaching the ground. The impinging wall jet model simulates the radial-flow of the downburst after touching down at ground level. The radial flow pattern produced by the impinging wall jet, through laboratory experiments and numerical simulations, has shown similarity to the fully-developed downburst observed in the field (Hangan and Kim, 2004 and 2007).

Mason et al. (2009) performed a numerical simulation in which the wind field of a microburst was studied. The simulated downburst had a primary and counter rotating secondary ring vortex at the leading edge of the diverging front. The development and structure of the outflow were significantly affected by the counter-rotating vortex. It was found that, for loading isolated structures, the kinetic energy available within each simulated storm event was less than the energy available within atmospheric boundary layer winds; however, this energy is localized within a smaller area, which is the most unique feature of a microburst, causing it to cause high damage within its locality.

Hangan and Kim (2004, 2007) developed and validated a computational fluid dynamic (CFD) model simulating the spatial and time variations of the wind field associated with

downbursts. This fluid dynamic model simulates the large-scale mean component of the downburst velocity field. The numerical simulation was conducted for stationary downbursts using the commercial software FLUENT 6.0 (2001). An experimental program was carried out using an impinging jet facility, where pressure and velocity measurements were employed to validate the assumptions used in the CFD simulation (Hangan and Kim, 2004 and 2007). The CFD analysis was done assuming a jet diameter of 0.0381 m and a jet velocity of 7.5 m/s. The produced downburst field had two components; a radial (horizontal) component and a vertical (axial) component. The CFD model produced time history series for the velocity field of these two components. The values of the two velocity components at a specific point in space were found to be functions of its location relative to the centre of the jet and its height relative to the ground.

1.4 RESPONSE OF TRANSMISSION LINES TO DOWNBURST LOADS

A major cause of power outages is the failure of the towers during severe natural disasters. These costly failures have been often attributed to high localized wind events, in the form of tornadoes and downbursts (Manitoba Hydro, 1999). However, and as mentioned before, the design codes of transmission towers are based on large-scale synoptic events, such as hurricanes and typhoons.

Savory et al.. (2001) studied the time history response of a lattice self-supported transmission tower under transient tornado and microburst events. The microburst event was modeled using the impinging jet model. The dynamic analyses, performed for the two HIW events, predicted a shear failure due to the tornado similar to that observed in the field. However, the microburst did not cause a failure due to its lower intensity in

comparison to the tornado. It is worth to note that the loads transferred from the conductors and ground wire were taken into consideration; however, the conductors and ground wires were not modeled as structural elements, which is a valid approximation only for the case of symmetric loading.

Xie et al. (2006) investigated tower collapses of a transmission line caused by a downburst. The results of field investigations of ten downburst-loaded towers that failed in the east of China where presented in this study. The collapsed towers were classified according to the level of collapse severity observed in the field; each mode of failure observed was recorded in terms of the shape and extent of the failure. Based on this investigation, Xie et al. (2006) recommended taking the dynamic effects of the transmission towers and the conductors into account when designing the lines.

The wind-induced dynamic response of high-rise transmission towers under downburst wind load was studied by Wang et al. (2009). Wind tunnel tests were used to obtain the wind load coefficients of the transmission towers; however, the variation in the vertical angle of wind projection was not taken into consideration in this study. On the other hand, Mara (2007) studied the effect of varying the horizontal and vertical angles of wind projection. In this study, wind tunnel tests were conducted on two diverse lattice models and the variation in the drag coefficient for unique lattice sections was assessed by exposing these sections to inclined winds with different angles of inclination in both the vertical and horizontal planes. Significant differences in the aerodynamic drag measured for each lattice model were observed at specific angles. However, these angles are much larger than the angles occurring within the most critical downburst cases.

Shehata et al. (2005) developed a structural analysis numerical model for the evaluation of the response of transmission lines under the effect of downbursts. The CFD data

developed by Hangan and Kim (2004, 2007) were incorporated in this model, and were scaled-up based on the relative values between the characteristics of a prototype downburst and those used in the CFD model. The Shehata et al. (2005) structural analysis model was based on the finite element method, and used three-dimensional linear frame elements to simulate the tower members and two-dimensional non-linear curved frame elements to simulate the conductors.

A guyed transmission tower located in Manitoba, Canada, which collapsed in 1996 due to a downburst event, was used by Shehata and El Damatty (2007) to perform this parametric study. Using the previously mentioned structural analysis model, Shehata and El Damatty (2007) conducted a parametric study by varying the jet diameter (D_j) and the location of the centre of the downburst relative to centre of the tower (defined by the polar coordinates r and θ). The study revealed that the critical downburst parameters (D_j, r and θ) vary based on the type and location of the members. Shehata and El Damatty (2008) extended their numerical scheme by including a failure model for the tower members, which was used to study the progressive collapse of the guyed tower that failed in Manitoba, Canada, in 1996. Based on the findings of the extensive parametric study, Shehata et al. (2008) extended the structural analysis model by including an optimization routine. This model is capable of automatically predicting the critical downburst parameters and the corresponding forces.

All the above studies were conducted in a quasi-static manner using the large-scale mean components of the downburst wind field, as predicted numerically by Hangan et al. (2004, 2007).

In view of the above literature, further studies related to the effect of downbursts on guyed transmission lines are needed as follows:

- The effect of turbulence and the dynamic response of the conductors under downburst loads, needs to be assessed.
- Ultimately, a simplified procedure to estimate the loads associated with various critical downburst configurations needs to be developed.
- In addition, the behaviour of self-supported transmission tower lines under various downburst configurations needs to be addressed.

1.5 OBJECTIVES OF THE STUDY

The main objectives of the current research are summarized in the following points:

1. To assess and quantify the effect of the turbulent component of downbursts on the structural response of the conductors and the guyed transmission towers.
2. To assess the variations of the internal axial forces of guyed towers with the downburst characteristics and the towers' configuration.
3. To develop approaches to evaluate equivalent loads simulating the critical downburst configurations to be used in the design of guyed towers.
4. To study the behavior of self-supported transmission towers under downburst loading and determine the critical downburst configurations causing maximum axial forces for various members of the tower.

1.6 SCOPE OF THE THESIS

This thesis has been prepared in an "Integrated-Article" format. In the present chapter, a review of the studies and approaches related to transmission line structures and downburst meteorological phenomenon is provided. The objectives of the study are then illustrated.

Chapters 2, 3, 4 and 5 address the thesis objectives. Chapter 6 presents relevant conclusions of the study together with suggestions for further research work.

1.6.1 DYNAMIC CHARACTERISTICS OF TRANSMISSION LINE CONDUCTORS AND BEHAVIOUR UNDER TURBULENT DOWNBURST LOADING

The objective of chapter 2 is to quantify the effect of turbulence on the conductor reactions through performing a dynamic analysis of the conductor. The dynamic characteristics of the conductors, including their natural frequencies and mode shapes, are determined. In addition to that, a turbulence model for downbursts is identified. The numerical model for the conductors, adopted by Shehata et al. (2005), is extended to include a dynamic analysis, as well as free vibration analysis for identification of the natural frequencies and mode shapes. Due to the high flexibility of the conductors, their natural frequencies can be affected by the pretensioning axial forces, the sagging and the stresses resulting from the downburst loading. As such, the free vibration analysis is conducted at each time increment, using an updated stiffness matrix that incorporates all of these effects. Full scale data obtained from field measurements of the velocity wind field during a downburst event are presented in the second part of the study. The turbulent component of this set of data is extracted and used as the basis of the turbulence model for downburst simulation. Using the numerical model developed in the first part, and the turbulence model proposed in the second part, along with the large-scale fluctuating mean component of the downburst wind field obtained from the CFD model, a set of dynamic analyses are conducted to assess the effects of turbulence and dynamic behaviour on the response of the conductors to downbursts.

1.6.2 SENSITIVITY OF TRANSMISSION LINE GUYED TOWERS TO DOWNBURST LOADING

Chapter 3 assesses the sensitivity of the internal forces of the members of guyed towers to various downburst and structural parameters. The following parameters are considered in this sensitivity analysis: size and location of the downburst, turbulence component of the wind field, conductor pretensioning forces, and the tower height and guys configurations. The maximum axial forces in the members resulting from a downburst are compared to the associated values under normal wind loading calculated using the ASCE standards, including the broken wire load case.

1.6.3 EQUIVALENT LOADING OF GUYED TRANSMISSION LINE TOWERS TO RESIST DOWNBURSTS

The focus of chapter 4 is to develop approaches that can be used by engineers in analyzing and designing guyed transmission line systems to resist downbursts. These approaches are developed in view of the outcome of the studies conducted by previous researchers and the findings of the previous chapters of this thesis. An investigation related to the relation between the jet velocity and the reference wind speed is first conducted. The effect of the convective velocity component, which usually exists during downbursts, is carried out. The study then focuses on three critical downburst configurations identified in previous studies. Simple approaches for evaluating the external forces on the conductors and the towers due to each one of these critical downburst configurations are developed. An example is worked out for illustration.

1.6.4 BEHAVIOUR OF SELF SUPPORTED TRANSMISSION LINE TOWERS UNDER DOWNBURST LOADING

The purpose of this chapter is to study the behaviour of a self-supported transmission tower under downburst loading. A parametric study is conducted to determine the critical downburst configurations causing maximum axial forces for members located in various parts of the tower. The sensitivity of the tower members forces to changes in the downburst size and location is studied. The structural behaviour of the transmission tower under the identified critical downburst configurations is then studied.

1.7 MAJOR RESEARCH CONTRIBUTIONS

The main research contributions of the current research are summarized in the following points:

1. Quantified the effect of turbulence on the transmission line.
2. Studied the sensitivity of guyed transmission towers to various downburst parameters.
3. Developed an equivalent load corresponding to each of the three modes of failure of guyed transmission towers.
4. Studied the sensitivity and behaviour of a self supported tower under downburst and normal wind loadings.

1.8 REFERENCES

American Society of Civil Engineers (ASCE) (2010). "Guidelines for electrical transmission line structural loading." *ASCE Manuals and Reports on Engineering Practice*, No.74, New York.

Bureau of Meteorology (1999) "Tropical cyclone warning directive (eastern region) 1999 - 2000." Queensland Regional Office, Bureau of Meteorology, Australia.

CIGRE SCB2 - 16 Meteorology for Overhead lines (2004), "Report on current practices regarding frequencies and magnitude of high intensity winds", *CIGRE*, B2-04 (WG16).

Fluent Inc. (2001), FLUENT version 6.0, Lebanon, USA.

Fujita T T (1981) "Tornadoes and downbursts in the context of generalised planetary scales" *Journal of Atmospheric Sciences*, 38(8), 1511-1534.

Hangan, H. and Kim, J.D., "Numerical simulation of downbursts", ASCE Structural Congress, Nashville, Te, USA, June, 2004. *(pp.1657-1664)*

Hangan, H. and Kim, J. (2007). "Numerical simulations of impinging jets with application to downbursts" *Journal of Wind Engineering and Industrial Aerodynamics*, 95(4), 279–298.

Manitoba Hydro Transmission and Civil Design Department (1999), "Bipole 1 & 2 HVDC Transmission Line Wind Storm Failure on September 5, 1996 – Review of Emergency Response, Restoration and Design of These Lines", *Manitoba Hydro*, 98-L1/1-37010-06000, 54.

Mason, M. S., Wood, G. S. and Fletcher, D. F. (2009). "Numerical simulation of downburst winds" *Journal of Wind Engineering and Industrial Aerodynamics*, 97(11-12), 523–539.

Mara, T. 2007. The effects of multi-directional winds on lattice sections. MEsc. Thesis, University of Western Ontario, London, Canada.

Savory, E., Parke, G., Zeinoddini, M., Toy, N., and Disney, P. (2001). "Modelling of tornado and microburst-induced wind loading and failure of a lattice transmission tower." *Engineering Structures*, 23, 365-375.

Shehata, A. Y., El Damatty, A. A., and Savory, E. (2005). "Finite element modelling of transmission line under downburst wind loading." *Finite Element in Analysis and Design*, 42(1), 71-89.

Shehata, A.Y. and El Damatty, A.A. (2007). "Behaviour of guyed transmission line structures under downburst wind loading" *Wind and Structures*, 10(3), 249-268

Shehata, A.Y. and El Damatty, A.A. (2008). "Failure analysis of a transmission tower during a microburst" *Wind and Structures*, 11(3), 193-208

Shehata, A. Y., Nassef, A.O. and El Damatty, A. A. (2008). "A coupled finite element-optimization technique to determine critical microburst parameters for transmission towers." *Finite Element in Analysis and Design*, 45(1), 1-12.

Vicory, D. D. (1992). "Assessment of microburst models for downdraft estimation." *Journal of Aircraft*, 29, 1043-1048.

Wang, X., Lou, W., Li, H. and Chen, Y (2009). "Wind-induced dynamic response of high-rise transmission tower under downburst wind load" *Journal of Zhejiang University*, 43(8), 1520-1525.

White, H. B. (1993). "Guyed structures for transmission lines." *Engineering Structures*, 15(4), 289-302.

Xie, Qiang, Zhang, Yong and Li, Jie (2006). "Investigation on tower collapses of 500 kV Renshang 5237 transmission line caused by downburst 2." *Power System Technology*, 30(10), 59-63.

CHAPTER 2

DYNAMIC CHARACTERISTICS OF TRANSMISSION LINE CONDUCTORS AND THEIR BEHAVIOUR UNDER TURBULENT DOWNBURST LOADING

2.1 INTRODUCTION

Electricity is one of the most essential resources for the modern world. Because of this dependence, it is important to prevent the disruptions in the distribution of power, as disruptions can have severe social and economical consequences. Electricity is transmitted through conductors, supported by transmission towers. A major cause of power outages is the failure of the towers during severe natural disasters. These failures, causing losses of millions of dollars, have been often attributed to high localized wind events, in the form of tornadoes and downbursts (Manitoba Hydro, 1999). Despite this fact, the design codes of transmission towers have typically considered only wind loads associated with large-scale synoptic events, such as hurricanes and typhoons. The resulting downburst velocity profiles are quintessentially different from these boundary layer wind profiles and can, therefore, produce completely different loading and collapse modes, as shown by Kim et al. (2007) for the case of tall buildings.

A downburst is defined as a strong downdraft that induces an outburst of damaging winds on, or near the ground (Fujita, 1990). "A short-duration localized wind event results during a downburst, when the downdraft forms ring vortices and spreads radially as it strikes the ground, producing high horizontal wind velocities." (Fujita, 1990). The localized nature of the event (both spatially and in time) and the associated vortex dominated flow complexity are the biggest challenges in performing structural analysis, since the intensity of the wind velocity varies significantly with the characteristics of the

downburst. The jet diameter (D_j), the location of the downburst center relative to the tower (represented by the polar coordinates r and θ) and the jet velocity (V_j) are the primary downburst characteristics, which significantly influence the distribution and magnitude of the forces acting on the tower and the conductors, as described by Shehata and El Damatty (2007) and Shehata et al. (2008).

Hangan and Kim (2004, 2007) developed and validated the computational fluid dynamic (CFD) model shown in Figure 2.1, simulating the spatial and time variations of the wind field associated with downbursts. This fluid dynamic model simulates the large-scale mean component of the downburst velocity field.

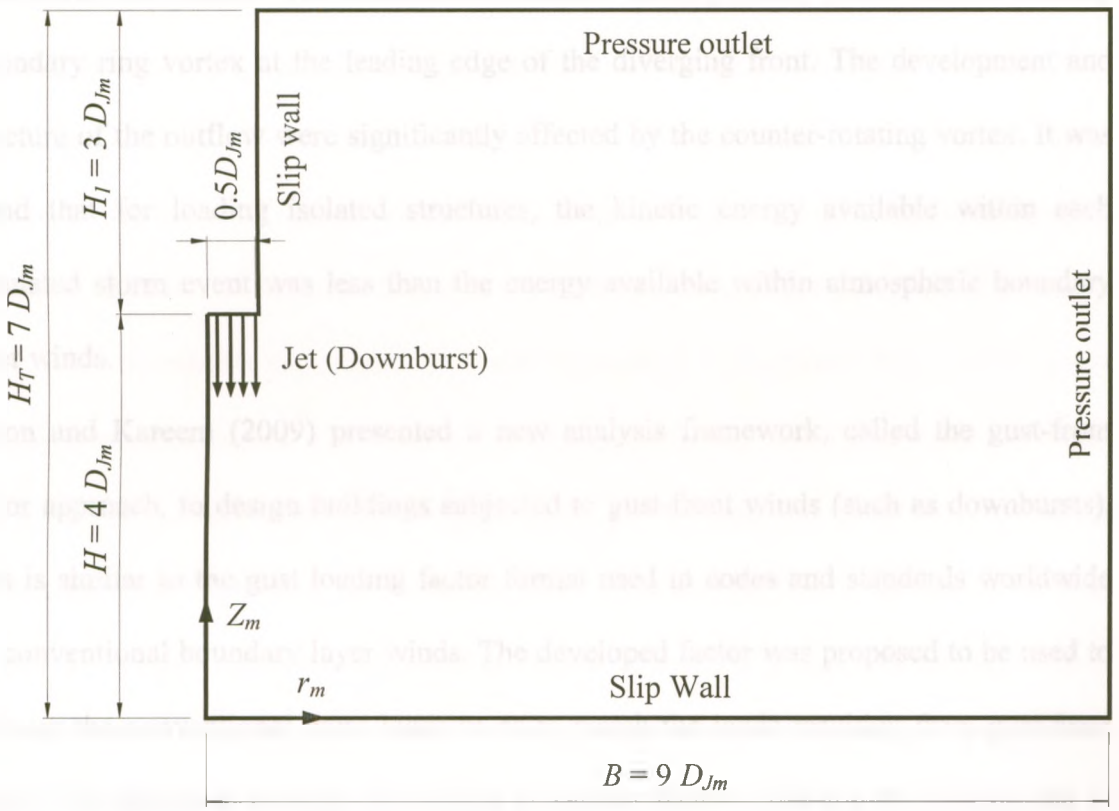

Figure 2.1 Schematic diagram of computational domain of downburst CFD model, (Hangan et al., 2003).

Wang et al. (2009) studied the wind-induced dynamic response of high-rise transmission towers under downburst wind load. Wind tunnel tests were used to obtain the wind load coefficients of the transmission towers. Following on that, a numerical model was developed in which the time history of the moving downburst horizontal fluctuating wind velocity was generated numerically considering the wind azimuth's continuous change. The transmission tower was dynamically analyzed under downburst loading. The analysis showed that the downburst size had the major effect on the displacement response of the transmission tower, while its dynamic effect on the tower was minor.

Mason et al. (2009) performed a numerical simulation in which the wind field of a microburst was studied. The simulated microburst had a primary and a counter-rotating secondary ring vortex at the leading edge of the diverging front. The development and structure of the outflow were significantly affected by the counter-rotating vortex. It was found that for loading isolated structures, the kinetic energy available within each simulated storm event was less than the energy available within atmospheric boundary layer winds.

Kwon and Kareem (2009) presented a new analysis framework, called the gust-front factor approach, to design buildings subjected to gust-front winds (such as downbursts). This is similar to the gust loading factor format used in codes and standards worldwide for conventional boundary layer winds. The developed factor was proposed to be used to scale-up the conventional wind loads so as to match the loads resulting from gust-front winds. This approach includes the effects of various factors affecting the loading due to gust-front winds. This factor is the product of four factors representing the variation in the vertical profile of wind speed (kinematic effects factor), dynamic effects introduced by the sudden rise in wind speed (pulse dynamics factor), nonstationarity of turbulence in

gust-front winds (structural dynamics factor), and transient aerodynamics (potential load modification factor).

Shehata et al. (2005) developed a structural analysis numerical model for the evaluation of the response of transmission lines under the effect of downbursts. This model incorporated the CFD data developed by Hangan et al. (2004). The data was scaled-up based on the relative relationship between the characteristics of a prototype downburst and those used in the CFD model. The structural analysis model developed by Shehata et al. (2005) was based on the finite element method. This model used two-dimensional non-linear curved frame elements to simulate the conductors and three-dimensional linear frame elements to simulate the tower members.

Using this structural analysis model, Shehata and El Damatty (2007) conducted a parametric study by varying the jet diameter (D_j) and the location of the downburst center relative to the tower. A guyed transmission tower located in Manitoba, Canada, which collapsed in 1996 due to a downburst event, was used to perform this parametric study. The critical downburst parameters (D_j, r and θ), leading to maximum forces in the tower members, were identified. The study revealed that the critical downburst parameters vary based on the type and location of the members. For example, the chord members of the tower main body, the diagonal members of the tower main body, and the cross arms members were all found to have different critical downburst parameters. Shehata and El Damatty (2008) extended their numerical scheme by including a failure model for tower members, which was used to study the progressive collapse of the guyed tower that failed in Manitoba, Canada in 1996. As a result of the extensive parametric study, Shehata et al. (2008) extended the structural analysis model by including an optimization routine. This

model is capable of predicting the critical downburst parameters and the corresponding forces in an automated procedure.

All the above studies were performed quasi-statically, making use of the downburst wind field large-scale fluctuating mean components as predicted numerically by Hangan et al. (2004, 2007). The use of a quasi-static analysis was justified based on the fact that the period of the large-scale fluctuating mean component of the downburst load is significantly larger than the fundamental periods of oscillation of both the conductors and the tower. However, the inclusion of the turbulent component in the analysis can magnify the response due to combined effects of the fluctuating (background) component and the resonant component. An assessment of the effects of turbulence necessitates the incorporation of a turbulence model for the downburst wind field and also requires conducting a dynamic analysis. It is expected that the dynamic effect will be of more importance in analyzing the conductors rather than the tower, as the conductors typically have larger fundamental periods compared to the tower that, consequently, are closer to the dominant periods of the turbulent component. The focus of this chapter is the assessment of the effect of turbulence on the response of the conductors to downbursts.

Barbieri et al. (2004) studied the dynamic behavior of transmission line conductors numerically using the finite element method and verified their results experimentally with three different sample lengths using five accelerometers placed along half the sample. The modal parameters were optimized through a gradient search routine, the complex envelope, and the single degree-of-freedom method. A reduced damping matrix was fitted by considering the first five free vibration modes. The study was extended to identify the structural damping of the conductors, which was found to be negligible in comparison to the aerodynamic damping. Barbieri et al. (2008) extended their previous studies to

include the nonlinear characteristics of the transmission line conductors, presenting the results for simply supported inclined conductors. Experimental data obtained in an automated testing system for the conductors were used to validate the results.

Gattulli et al. (2007) assessed the ability of various numerical techniques to accurately reproduce the dynamic response of a suspended cable subjected to an artificially generated 3D turbulent wind field. Due to the high level of aerodynamic damping, weak nonlinear modal coupling was found in the dynamic responses of the studied cable. The high level of aerodynamic damping was also discussed by Loredo-Souza and Davenport (1998) in their study conducted to assess the dynamic behavior of transmission lines under severe normal wind loading. This study was performed experimentally, and the results were verified statistically. The effect of scale turbulence was studied, and the response of the structure was found to depend strongly on the turbulence intensity. In this study, it was concluded that the background response (the quasi-static component) is the largest contributor to the total fluctuating response, in most typical cases. The resonant component can hold importance only when cable characteristics and flow conditions dictate a smaller value for the aerodynamic damping.

Chay et al. (2008) studied the variation of the peak gust intensity in non-stationary winds of different durations. A typical downburst was simulated repeatedly using a numerical model of downburst non-turbulent winds, and an amplitude-controlled Gaussian stochastic process for the turbulent component. The peak gust strength of each event was expressed as a peak factor (ratio) in relation to the largest non-turbulent speed. It was found that the peak factor increased when the downburst event duration increases, and also increased when the turbulence intensity increased.

In order to assess the dynamic response of transmission line conductors under downburst loading, the dynamic characteristics of the conductors, including their natural frequencies and mode shapes, have to be determined. In addition, a turbulence model for downbursts has to be identified. Accordingly, the research presented in this chapter is divided into three parts. In the first part of the study, the numerical model for the conductors adopted by Shehata et al. (2005), is extended to include dynamic analysis, as well as free vibration analysis for identification of the natural frequencies and mode shapes. Due to the high flexibility of the conductors, their natural frequencies can be affected by the pretensioning axial forces, the sagging, and the stresses resulting from the downburst loading. As such, the free vibration analysis is conducted at each time increment, using an updated stiffness matrix that incorporates all of these effects. Full scale data obtained from field measurements of the velocity wind field during a downburst event are presented in the second part of the study. The turbulent component of this set of data is extracted, and is used as the basis of the turbulence model for downburst simulation. Using the numerical model developed in the first part and the turbulence model proposed in the second part, along with the large-scale fluctuating mean component of the downburst wind field obtained from the CFD model, a set of dynamic analyses are conducted to assess the effects of turbulence and dynamic behaviour on the response of the conductors to downbursts.

A brief description of the finite element model, along with the extension of the model to include dynamic and free vibration analysis of non-linear flexible systems, is first provided. The three parts of the study described above are then presented followed by a discussion for the main conclusions obtained from the study.

2.2 NUMERICAL MODELLING OF THE CONDUCTORS

2.2.1 FINITE ELEMENT MODEL FOR THE CONDUCTORS

The numerical model is based on a two dimensional consistent curved frame element that was developed by Koziey and Mirza (1994), and was then extended to include the geometric non-linear effect by Gerges and El Damatty (2002). A sketch of a typical consistent curved frame element is shown in Figure 2.2. The element formulation is based on C_o continuity – which provides inter-element continuity of all degrees of freedom without providing this continuity for the first derivatives of the degrees of freedom. The interpolations of displacements (u and w) and through thickness rotations (α and φ) are conducted independently. Interpolations of displacements are achieved using cubic polynomials considering the degrees of freedom at nodes 1, 2, 4 and 5, while the rotations are interpolated using quadratic polynomials considering the degrees of freedom at nodes 1, 3 and 5. This arrangement of degrees of freedom was done to avoid shear locking.

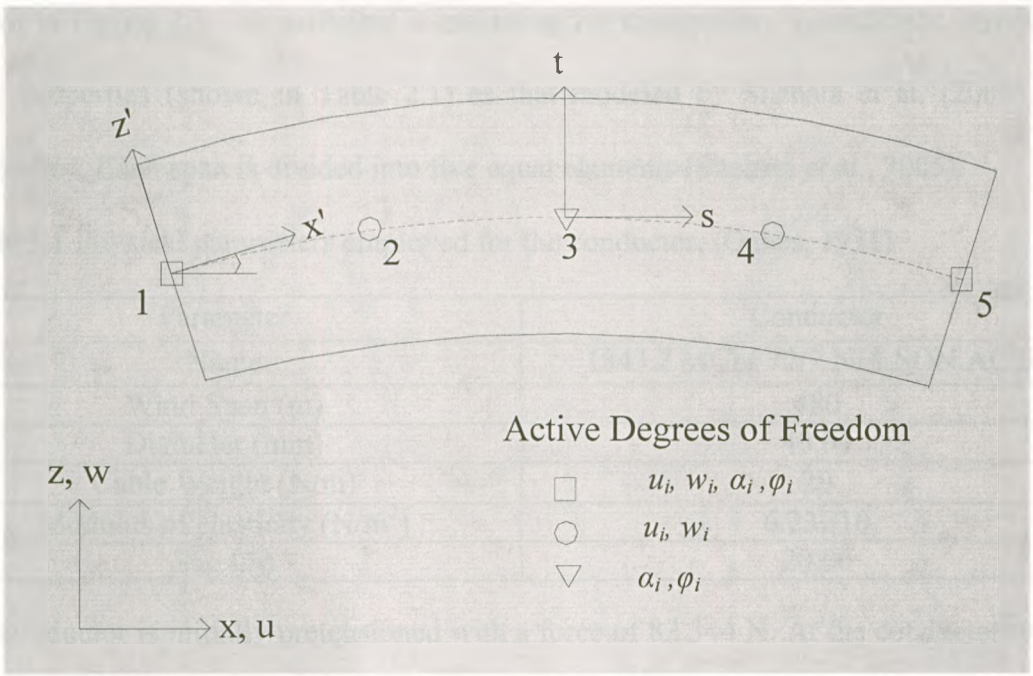

Figure 2.2 Two-dimensional consistent curved frame element, (Shehata et al., 2005).

In the nonlinear model of the consistent frame element, the solution is carried out incrementally while iterations are conducted within each increment until convergence is achieved. In the current study, the nonlinear model is extended by including an eigen-value routine within each increment. As such, the natural frequencies and mode shapes of the modeled structure are evaluated at each increment. Hence, the model can predict the variations of the dynamic characteristics of a conductor due to the large deformations expected from severe wind loading. The nonlinear model is also capable of accounting for the effects of the conductors' pretension force, and initial sagging in estimating the stiffness of the conductors. More details about this finite element model are explained by Shehata et al. (2005).

2.2.2 PHYSICAL AND GEOMETRIC PROPERTIES OF THE CONDUCTOR

Shehata et al. (2005) proved that modeling six spans – having the boundary conditions shown in Figure 2.3 – is sufficient in modeling the conductors. A conductor, having the same properties (shown in Table 2.1) as that modeled by Shehata et al. (2005), was considered. Each span is divided into five equal elements (Shehata et al., 2005).

Table 2.1 Physical parameters employed for the conductor, (Oakes, 1971)

Parameter	Conductor
Name	1843.2 MCM 72/7 NELSON ACSR
Wind Span (m)	480
Diameter (mm)	40.64
Cable Weight (N/m)	29
Modulus of elasticity (N/m^2)	6.23E10
Sag (m)	20.00

The conductor is initially pretensioned with a force of 82,344 N. At the conductor-towers connections, a set of nonlinear springs, simulating the combined stiffness of the tower and

the insulators, is implemented in the model as shown in Figure 2.3. According to ASCE 74 (2010), the drag coefficient (C_d) is equal to 1. More details about the modeling of the conductors, including the evaluation of the springs' characteristics, are explained by Shehata et al. (2005).

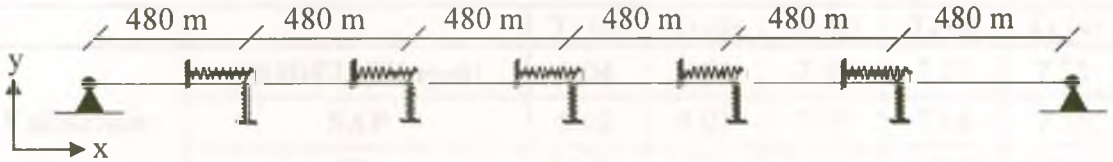

Figure 2.3 Modeling of the transmission line under study.

2.2.3 VALIDATION

The commercial program SAP2000 (Computers and Structures, 2006) is used to validate the free vibration scheme incorporated into the numerical model. It is not possible to account for the effect of nonlinear springs in a free vibration analysis conducted using SAP2000. Accordingly, for validation purposes, the analysis is conducted using SAP2000, while assuming hinge boundary conditions instead of the springs. An initial pretensioning force of 82,344 N is applied in the analysis with initial sag of 20 m.

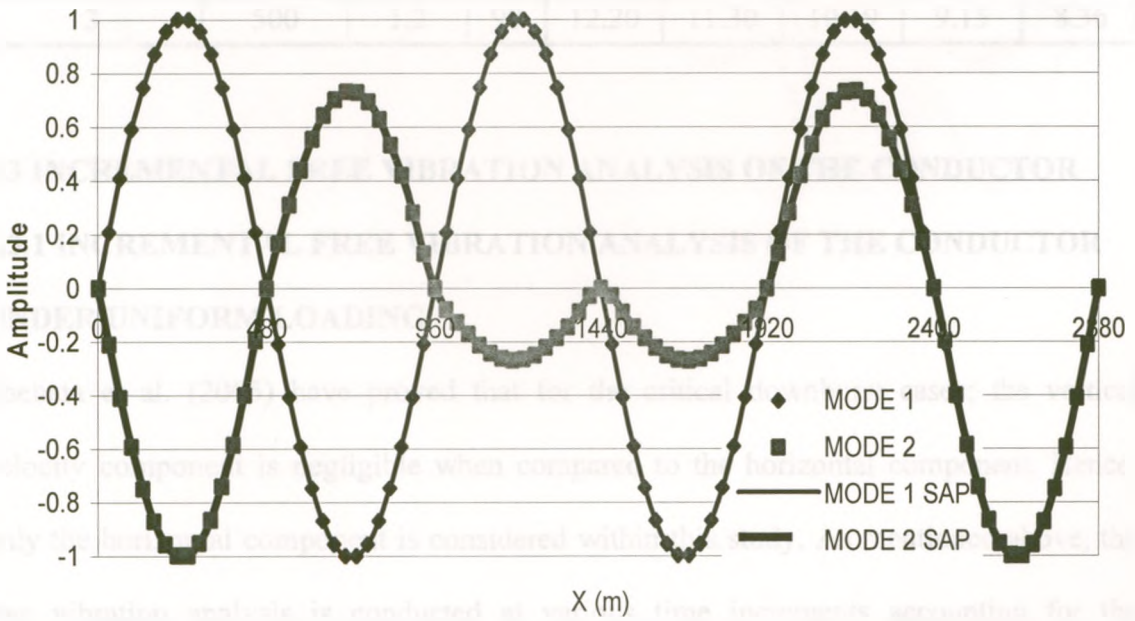

Figure 2.4 Comparisons between mode shapes predicted by model and SAP 2000.

The results of the conducted analysis are summarized in Table 2.2 and Figure 2.4, showing an excellent agreement, for both the mode shapes and the natural periods, between the model and the SAP2000 results.

Table 2.2 Results of the Eigen-value analysis of the 6 spanned conductor.

				T_1 (s)	T_2 (s)	T_3 (s)	T_4 (s)	T_5 (s)
Validation	**MODEL (Hinged)**			8.04	8.01	7.94	7.83	7.75
	SAP			8.02	8.03	7.95	7.84	7.76
	% Difference			0.34%	0.32%	0.18%	0.03%	0.02%
Uniform Load				12.20	11.30	10.19	9.15	8.33
Pretensioning Force Variation	**400%**			10.00	8.14	6.52	5.33	4.21
	200%			10.93	9.61	8.19	7.00	5.98
	100%			12.20	11.30	10.19	9.15	8.33
	50%			14.27	13.68	12.91	12.15	11.45
Boundary Condition Variation	**Springs**			12.20	11.30	10.19	9.15	8.33
	Hinged			8.04	8.01	7.94	7.83	7.75
Downburst Loading Case	**D_J (m)**	**r/D_J**	**θ °**					
1	1000	1.6	30	12.00	11.11	10.03	8.99	7.87
2	1000	1.2	0	12.15	11.28	10.17	9.13	8.01
3	500	1.2	90	12.20	11.30	10.19	9.15	8.36

2.3 INCREMENTAL FREE VIBRATION ANALYSIS OF THE CONDUCTOR

2.3.1 INCREMENTAL FREE VIBRATION ANALYSIS OF THE CONDUCTOR UNDER UNIFORM LOADING

Shehata et al. (2005) have proved that for the critical downburst cases; the vertical velocity component is negligible when compared to the horizontal component. Hence, only the horizontal component is considered within this study. As mentioned above, the free vibration analysis is conducted at various time increments accounting for the

deformations under the applied wind load. The first set of free vibration analyses considers uniformly distributed forces associated with normal wind loads. The velocity of the assumed wind load is increased incrementally from zero to a value of 35 m/s, using ten increments. The results of the free vibration analysis conducted at the ten load increments showed no differences in terms of natural frequencies and mode shapes of the structure. The values of the first five natural periods are shown in Table 2.2, and the mode shapes of the first three modes are plotted in Figure 2.5. This result indicates that the magnitude of loading has no direct effect on the dynamic characteristics of the conductors.

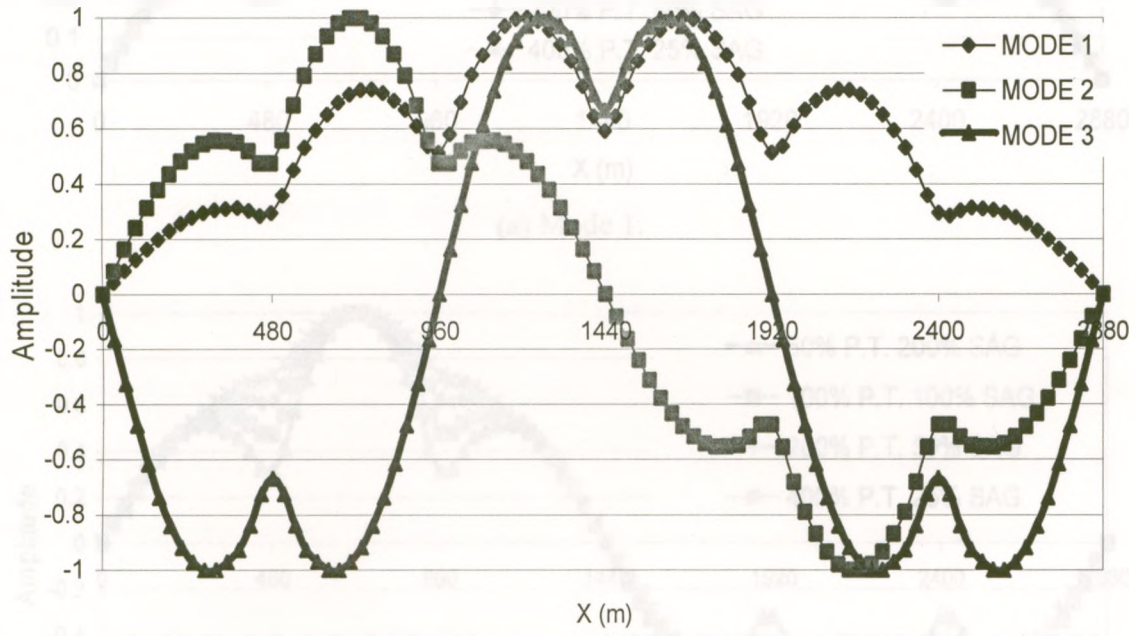

Figure 2.5 First three mode shapes of the conductor under uniform load.

2.3.2 VARIATION OF THE PRETENSIONING LEVEL OF THE CABLES

The analysis under uniform loading is repeated by varying the magnitude of the pretension force. Various values representing 50%, 200% and 400% of the initial pretension force are considered, respectively. The sag is inversely proportional to the

pretension force. Accordingly, the sag values are divided by the same factor used to magnify the pretension force, e.g. when the pretensioning is doubled, the sag is halved. The natural periods and the mode shapes resulting from this set of analyses are given in Table 2.2 and Figures 2.6a and b.

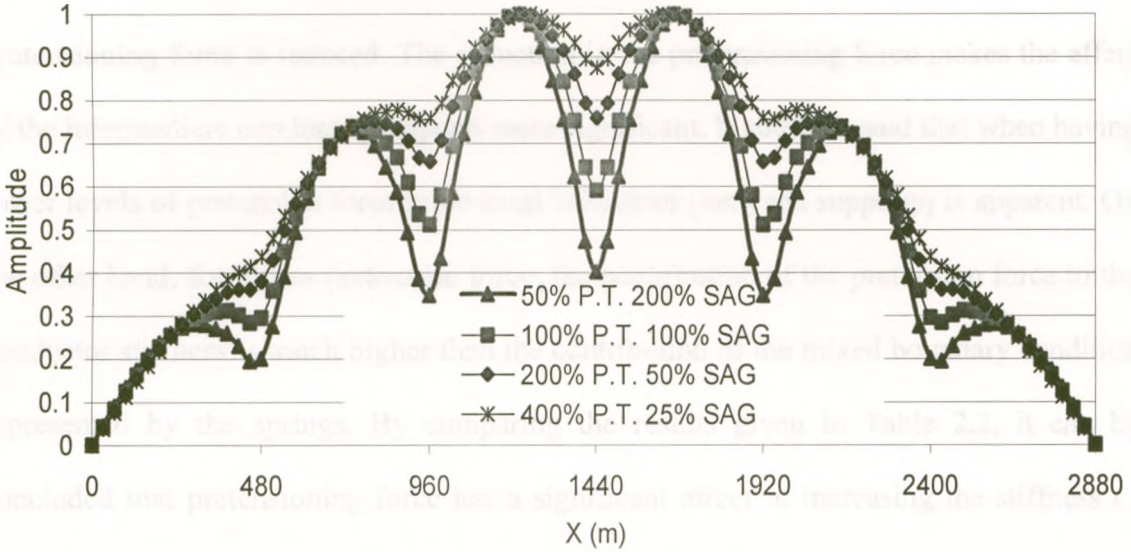

(a) Mode 1.

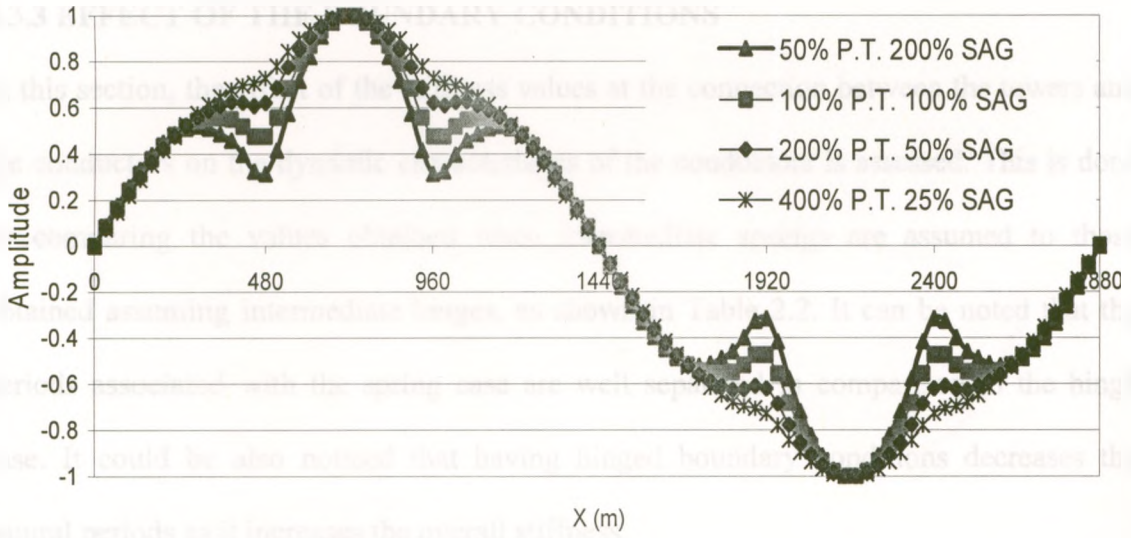

(b) Mode 2.

Figure 2.6 Mode shapes of the conductor for different levels of pretensioning.

The results show that the variation in the level of pretensioning causes some variation in the values of the natural periods. Typically, the periods decrease with the increase of the pretensioning force. The differences between the periods of the first four modes are reduced with the reduction in the pretensioning force. It is also worth noticing the reduction of the mode shape amplitude at the spring locations when the magnitude of the pretensioning force is reduced. The reduction in the pretensioning force makes the effect of the intermediate conductor supports more significant. It could be said that when having lower levels of pretension force more local behaviour (between supports) is apparent. On the other hand, for higher pretension force, the contribution of the pretension force to the conductor stiffness is much higher than the contribution of the mixed boundary condition represented by the springs. By comparing the results given in Table 2.2, it can be concluded that pretensioning force has a significant effect in increasing the stiffness of the conductor and consequently, decreasing its period of vibration.

2.3.3 EFFECT OF THE BOUNDARY CONDITIONS

In this section, the effect of the stiffness values at the connection between the towers and the conductors on the dynamic characteristics of the conductors is assessed. This is done by comparing the values obtained when intermediate springs are assumed to those obtained assuming intermediate hinges, as shown in Table 2.2. It can be noted that the periods associated with the spring case are well separated in comparison to the hinge case. It could be also noticed that having hinged boundary conditions decreases the natural periods as it increases the overall stiffness.

2.3.4 ANALYSIS OF THE CONDUCTOR UNDER DOWNBURST LOADING

The dynamic characteristics of the conductor are then evaluated at different loading stages within a downburst event. The evaluation of the downburst forces followed the approach described by Shehata and El Damatty (2005). The downburst forces acting on the conductor depends on the jet velocity (V_j), the jet diameter (D_j), the ratio between the distance between the centers of the downburst and the jet diameter (r/D_j) and the projection angle (θ) relative to the transverse direction of the transmission line. Three different downburst cases with parameters given in Table 2.2 are considered. They represent the maxima of the most critical three different downburst configurations with respect to the considered transmission line, as predicted by Shehata and El Damatty (2005). The original pretensioning force, defined in section 2.3.1, is considered in all analyses. Free vibration analyses are conducted at the 240 time history load increments defining the entire time history of the loading (Shehata et al., 2005). The results of the analyses of the three load cases are given in Table 2.2. The results indicate almost no variation in the dynamic characteristics of the conductors within various time increments.

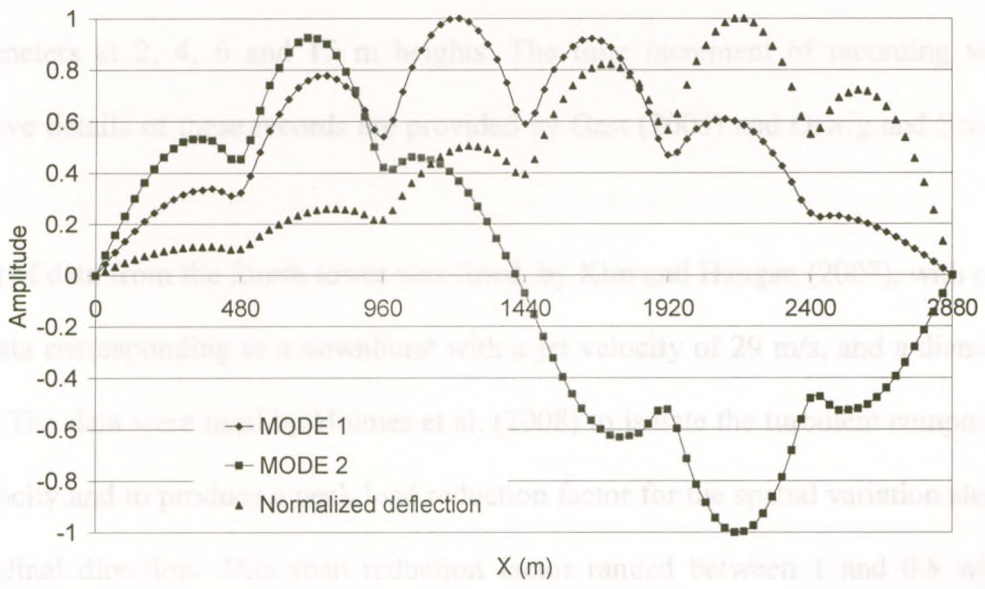

Figure 2.7 First two mode shapes together with the normalized deflected shape of the conductor under load case 1.

The mode shapes shown in Figure 2.7 are similar to those under uniform loading, with the exception of a minor loss of symmetry of the mode shapes. This is due to the asymmetric distribution of the downburst loading associated with this case.

In Figure 2.7, the maximum deflection obtained through the time history analysis is normalized, such that the largest amplitude has a value of unity. It could be noticed from the figure that the asymmetry of the deflected shape is more pronounced than the asymmetry of the mode shape.

2.4 FULL SCALE DATA AND TURBULENCE EXTRACTION

2.4.1 FULL SCALE DATA

The Wind Science and Engineering Research Centre at Texas Tech University recorded the gust front from a downdraft that occurred on the 4th of June 2002 at the former Reese Air force base, located 20 km west of Lubbock, Texas, USA. The anemometers were placed at a 10 m height on four towers with a uniform spacing of 263 m. The line of anemometer towers was in the North – South direction. The fourth tower had additional anemometers at 2, 4, 6 and 15 m heights. The time increment of recording was 1s. Extensive details of these records are provided by Gast (2003) and Orwig and Schroeder (2007).

The set of data from the fourth tower was fitted, by Kim and Hangan (2007), with a set of CFD data corresponding to a downburst with a jet velocity of 29 m/s, and a diameter of 600 m. The data were used by Holmes et al. (2008) to isolate the turbulent component of the velocity and to produce a peak load reduction factor for the spatial variation along the longitudinal direction. This span reduction factor ranged between 1 and 0.8 within a distance of 720 m, which means that the maximum difference between the peak loads at

any two points along the longitudinal direction is 20 %. Hence, the turbulence signal could be considered to be nearly uniform along the longitudinal direction. In the same study, the vertical velocity profiles of the maximum running mean and the gust speeds are found to have negligible variation along the height of tower 4 (from 0 to 15 m). Therefore, the turbulence signal could be considered to be nearly uniform along the height of the transmission tower (44 m).

2.4.2 TURBULENCE EXTRACTION

The turbulence is extracted by calculating the moving average of the velocity over a certain period of time, and subtracting it from the total (instantaneous) velocity within this period of time. The averaging period (called the filtering or running mean period) could be as low as 10s or as high as 120s, based on that used by Gast (2003) and Orwig and Schroeder (2007). In Figure 2.8, the turbulence (light line) has been calculated by subtracting the running average velocity (the black solid line) from the full scale data (shown as dark dots). Holmes et al. (2008) calculated the running turbulence intensity (which is the ratio between the time-varying root mean squared turbulence and the running mean wind speed) for various filtering periods. The study showed that for averaging periods between 20 s and 80 s, the running turbulence intensity is stable between 0.09 and 0.12. Hence, averaging periods within this range are considered to be suitable. According to Holmes et al. (2008), the use of averaging times higher than 80 s can incorrectly include part of the mean component of the velocity and non-stationary wind excitations that should not be considered as random turbulence. On the other hand, averaging times lower than 20 s exclude a large portion of the random component from the residual turbulence, as stated by Holmes et al. (2008).

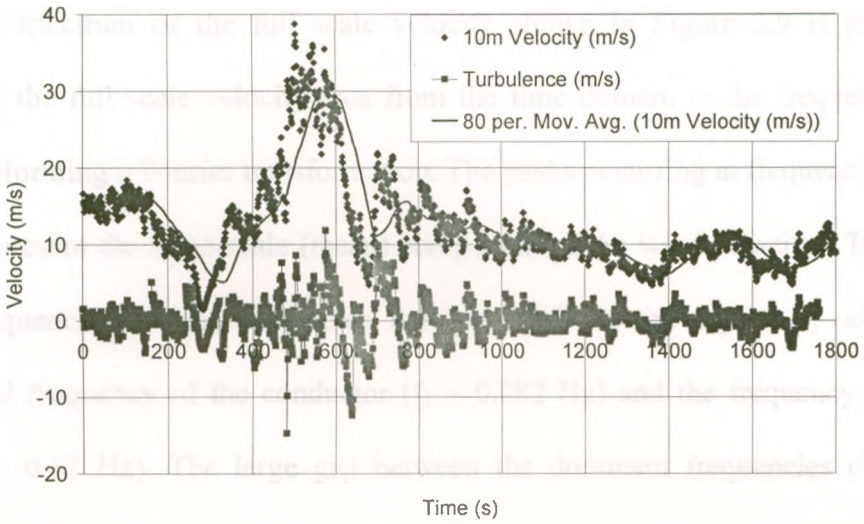

(a) Full scale velocity and the turbulence associated with it (filtering period = 80s).

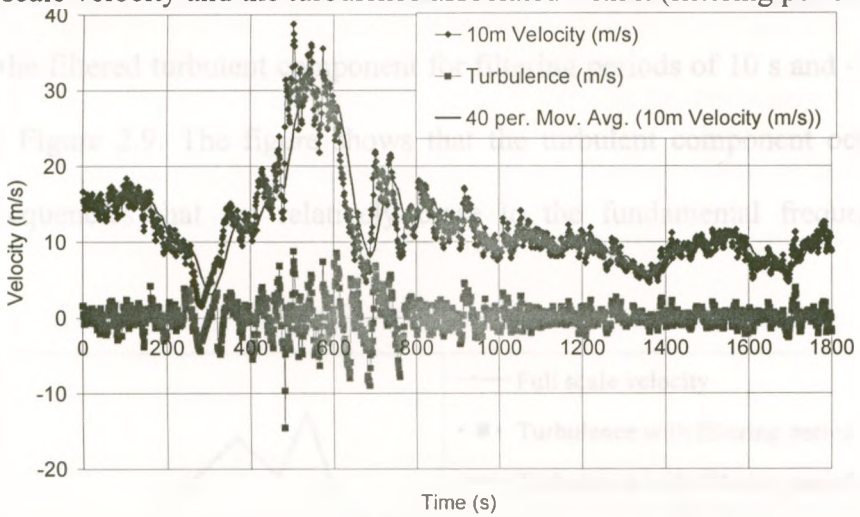

(b) Full scale velocity and the turbulence associated with it (filtering period = 40s).

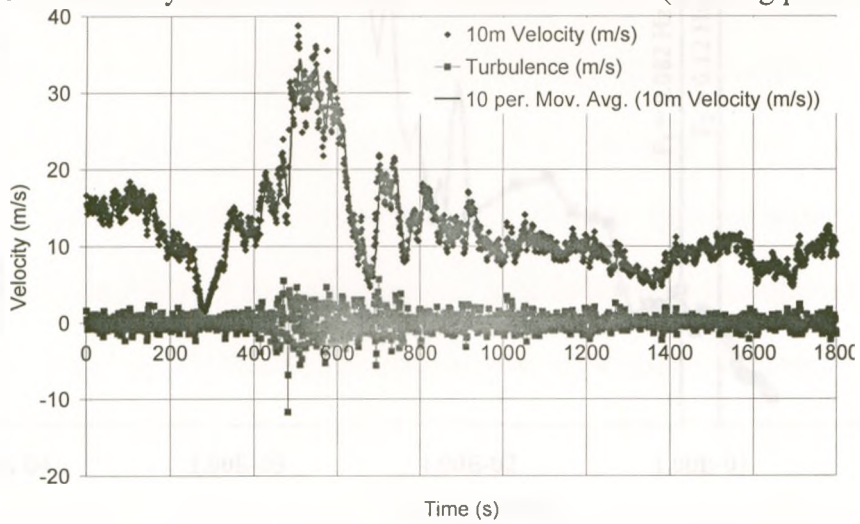

(c) Full scale velocity and the turbulence associated with it (filtering period = 10s).

Figure 2.8 Full scale velocity at a height of 10 m and the turbulence associated with it.

The power spectrum of the full scale velocity shown in Figure 2.9 is produced by transferring the full scale velocity data from the time domain to the frequency domain through performing a Fourier transformation. The peaks occurring at frequencies less than 0.01 Hz represent the large-scale (mean) component of the wind velocity. The range of natural frequencies of the conductor are identified in the figure by showing the fundamental frequency of the conductor (f_1 = 0.082 Hz) and the frequency of the fifth mode (f_5 = 0.12 Hz). The large gap between the dominant frequencies of the mean component and the frequencies of the conductor can be seen in the figure. The power spectra for the filtered turbulent component for filtering periods of 10 s and 40 s are also provided in Figure 2.9. The figure shows that the turbulent component occurs over a range of frequencies that are relatively close to the fundamental frequency of the conductor.

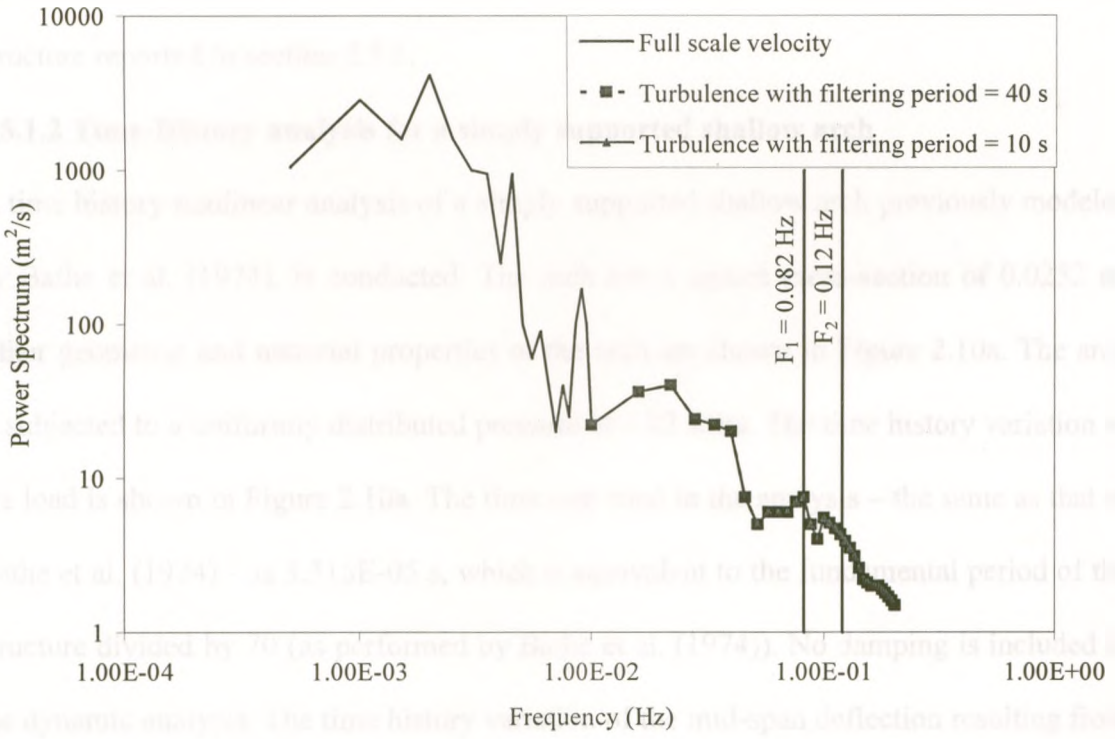

Figure 2.9 Power spectra of the measured velocities

2.5. DYNAMIC ANALYSIS

The numerical model described previously in section 2.2 is used, together with the Newmark direct integration method, to perform nonlinear dynamic analyses. More details about the Newmark method are explained by Bathe (1996).

2.5.1 VALIDATION

2.5.1.1 Sweep test

The first validation is done by conducting a sweep test, where the transmission line analyzed previously in section 2.3.1 is subjected to a uniform load that has a sinusoidal variation with time. The sweep test is conducted by varying the frequency of the applied load and recording the maximum mid-span deflection corresponding to each frequency value. The results of the sweep test show that the absolute maximum deflection occurs at an oscillating period of 12.2 s, which is very close to the fundamental period of the structure reported in section 2.3.1.

2.5.1.2 Time-History analysis for a simply supported shallow arch

A time history nonlinear analysis of a simply supported shallow arch previously modeled by Bathe et al. (1974), is conducted. The arch has a square cross-section of 0.0252 m. Other geometric and material properties of the arch are shown in Figure 2.10a. The arch is subjected to a uniformly distributed pressure of 3.83 MPa. The time history variation of the load is shown in Figure 2.10a. The time step used in the analysis – the same as that of Bathe et al. (1974) – is 3.315E-05 s, which is equivalent to the fundamental period of the structure divided by 70 (as performed by Bathe et al. (1974)). No damping is included in the dynamic analysis. The time history variation of the mid-span deflection resulting from

the analysis is shown in Figure 2.10b, along with the results obtained by Bathe (1974), showing an excellent agreement.

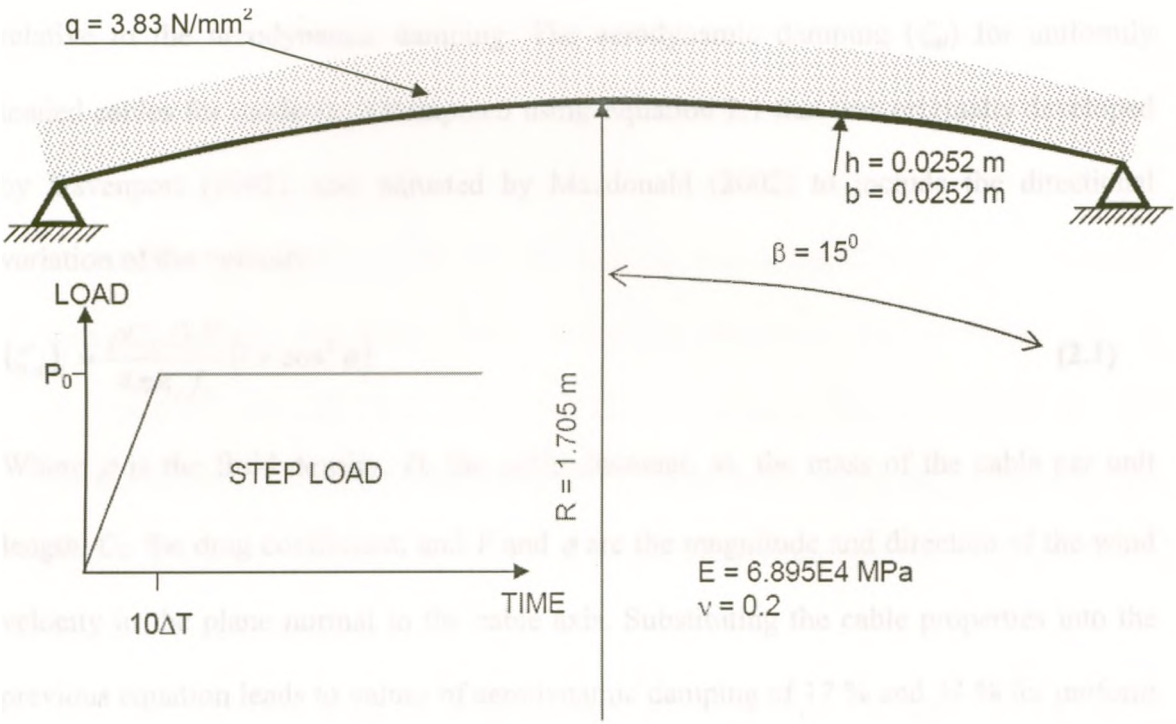

(a) Problem Description.

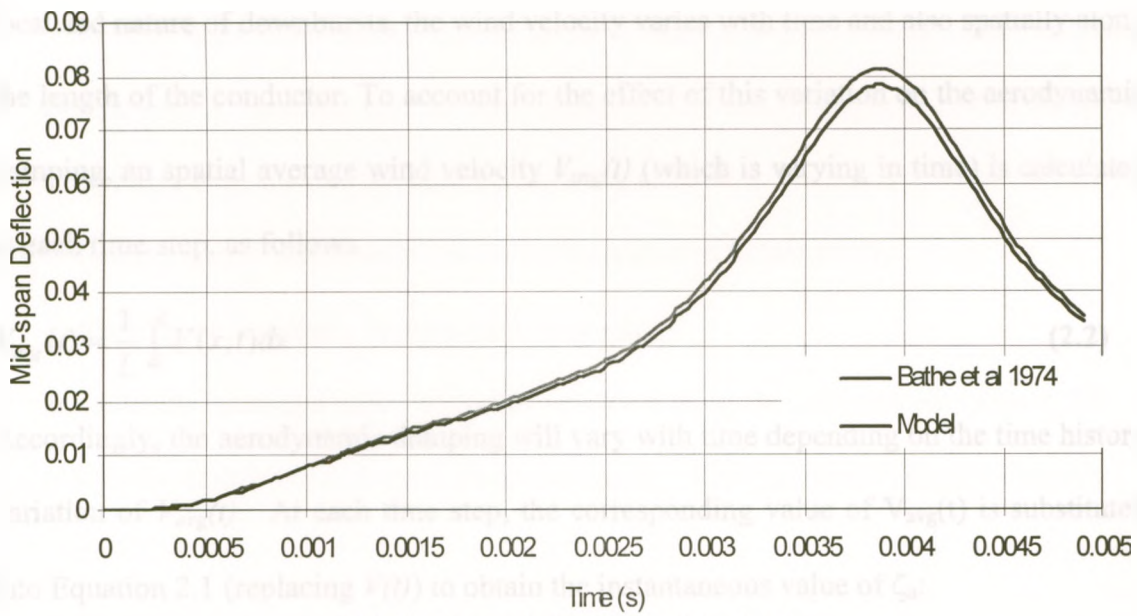

(b) Mid-Span Deflection of the Arch.

Figure 2.10 Analysis of a simply supported shallow arch under time-dependent loading.

2.5.2 DAMPING

The structural damping of the cables is neglected in this study, since it is quite small relative to the aerodynamic damping. The aerodynamic damping (ζ_{ai}) for uniformly loaded cables for mode (i) is computed using Equation 2.1 that was originally developed by Davenport (1962), and adjusted by Macdonald (2002) to include the directional variation of the velocity.

$$(\zeta_a)_i = \frac{\rho C_D D_c V}{4\pi m_c f_i}\left(1+\cos^2\phi\right) \qquad \textbf{(2.1)}$$

Where ρ is the fluid density, D_c the cable diameter, m_c the mass of the cable per unit length, C_D the drag coefficient, and V and ϕ are the magnitude and direction of the wind velocity in the plane normal to the cable axis. Substituting the cable properties into the previous equation leads to values of aerodynamic damping of 17 % and 34 % for uniform wind velocities (normal to the cable) of 10 m/s and 20 m/s, respectively. Due to the localized nature of downbursts, the wind velocity varies with time and also spatially along the length of the conductor. To account for the effect of this variation on the aerodynamic damping, an spatial average wind velocity $V_{avg}(t)$ (which is varying in time) is calculated at each time step, as follows

$$V_{avg}(t) = \frac{1}{L}\int_0^L V(x,t)dx \qquad \textbf{(2.2)}$$

Accordingly, the aerodynamic damping will vary with time depending on the time history variation of $V_{avg}(t)$. At each time step, the corresponding value of $V_{avg}(t)$ is substituted into Equation 2.1 (replacing $V(t)$) to obtain the instantaneous value of ζ_a:

$$(\zeta_a(t))_i = \frac{\rho C_D D_c V(t)}{4\pi m_c f_i}\left(1+\cos^2 0\right) = \frac{2\rho C_D D_c V_{avg}(t)}{4\pi m_c f_i} = \frac{\rho C_D D_c V_{avg}(t)}{2\pi m_c f_i} \qquad \textbf{(2.3)}$$

2.5.3 ANALYSIS AND RESULTS

Two types of time history loads are considered in the conducted analyses:

a) The large-scale, running mean component of the downburst loading associated with the downburst configuration at which the failure has been initiated as described by Shehata and El Damatty (2007), which was: D_j = 1000 m, r/D_j = 1.6 and $\theta = 30^o$. The jet velocity has a value of 29 m/s, the same as that of the CFD-matched full-scale data, by Hangan and Kim (2007). The entire large-scale wind velocity field is obtained from the CFD data. The forces corresponding to this component vary with time and space. As such, the time history of the forces acting on the conductors vary from one point to another, depending on the location of the specific point relative to the center of the downburst.

b) The turbulent component is obtained from the field measurements. As explained before, based on the field measurements at various vertical locations, and based on the relatively high longitudinal correlations (Holmes et al., 2008), the turbulent component is assumed not to vary spatially. The time variation of this turbulent component depends on the employed filtering scheme.

The following set of time history analyses are conducted in this study:

- Analysis 1; Non-turbulent quasi-static analysis:

  Includes the running mean component without adding the turbulent component. The analysis is conducted in a quasi-static manner, i.e. without considering the dynamic effect.

- Analysis 2; Turbulent quasi-static analysis:

  Includes the running mean and the turbulent components. This analysis is repeated

several times, using different values for the filtering period. The filtering periods used are 10 s, 20 s, 30 s, 40 s and 80 s, respectively. The analysis is conducted in a quasi-static manner, i.e. without considering the dynamic effect.

- Analysis 3; Non-turbulent undamped dynamic analysis:

  Includes the running mean component without adding the turbulent component. The dynamic effect is included and zero damping is assumed (undamped).

- Analysis 4; Turbulent undamped dynamic analysis:

  Includes the running mean and the turbulent components. This analysis is repeated several times, using different values for the filtering period. The used filtering periods are 10 s, 20 s, 30 s, 40 s and 80 s, respectively. The dynamic effect is included and zero damping is assumed (undamped).

- Analysis 5; Turbulent 17% damped dynamic analysis:

  Includes the running mean and the turbulent components. This analysis is repeated several times, using different values for the filtering period. The filtering periods used are 10 s, 20 s, 30 s, 40 s and 80 s, respectively. The dynamic effect is included. A constant aerodynamic damping of 17 % (corresponding to a uniform wind velocity of 10 m/s) is assumed.

- Analysis 6; Turbulent 34% damped dynamic analysis:

  Includes the running mean and the turbulent components. This analysis is repeated several times, using different values for the filtering period. The filtering periods used are 10 s, 20 s, 30 s, 40 s and 80 s, respectively. The dynamic effect is included. A constant aerodynamic damping of 34 % (corresponding to a uniform wind velocity of 20 m/s) is assumed.

- Analysis 7; Turbulent dynamic analysis with variable damping:

  Includes the running mean and the turbulent components. This analysis is repeated several times, using different values for the filtering period. The filtering periods used are 10 s, 20 s, 30 s, 40 s and 80 s, respectively. The dynamic effect is included. The time varying aerodynamic damping explained in section 2.5.2, is included in this analysis.

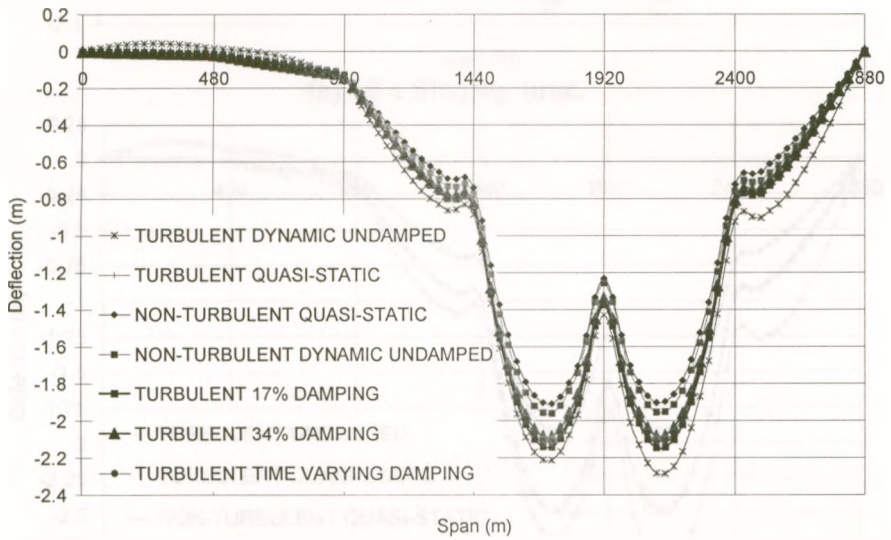

Figure 2.11 Peak transverse deflection with varying damping due to downburst with 30s filtering time.

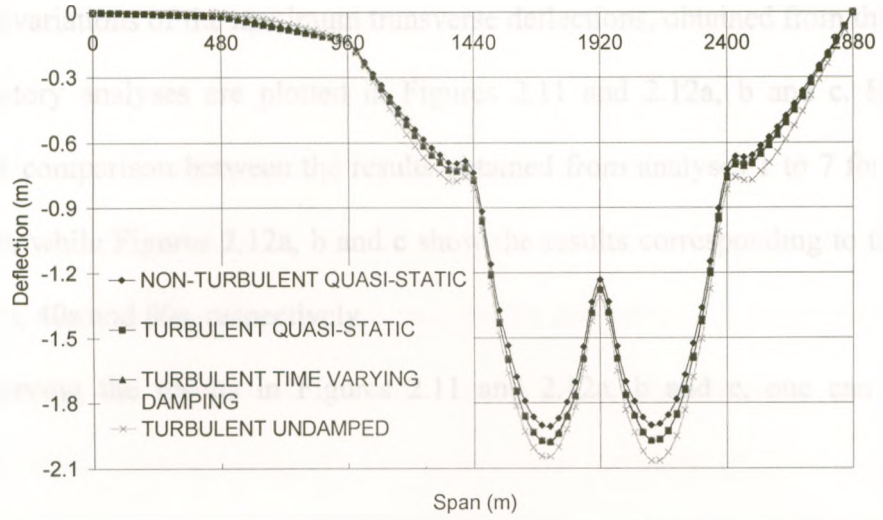

(a) 10 s filtering time.

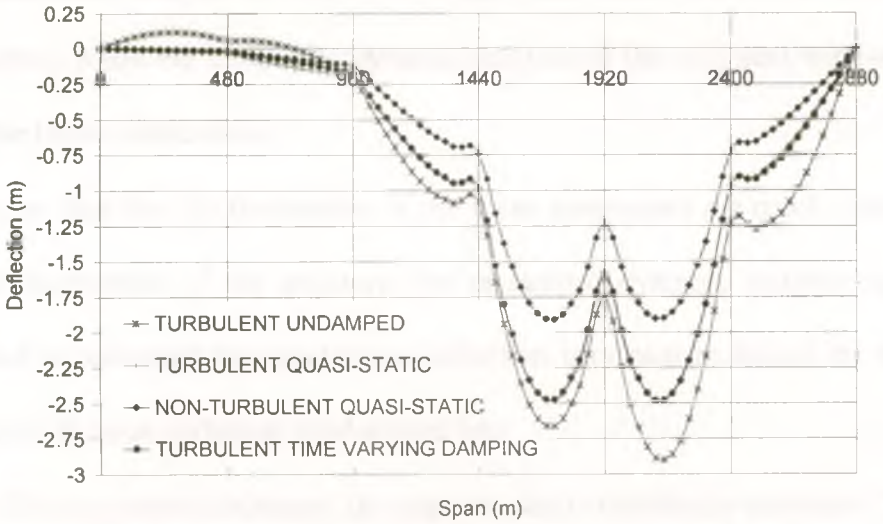

(b) 40 s filtering time.

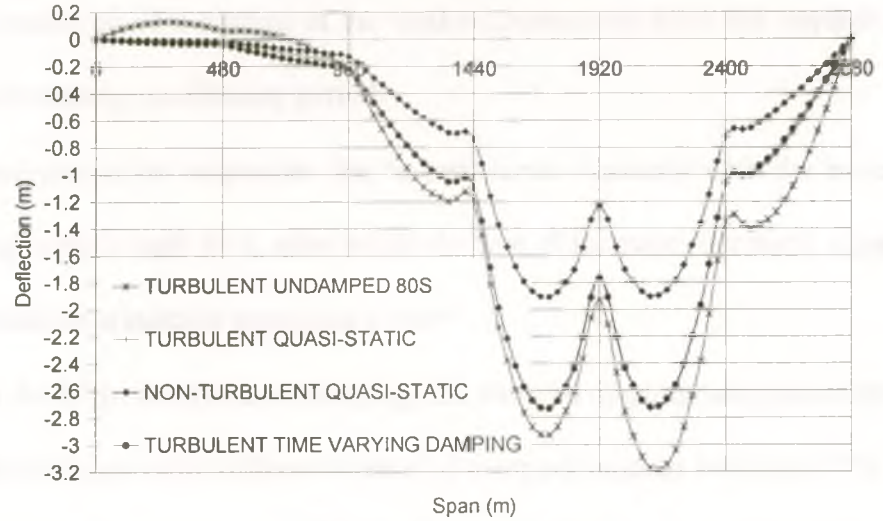

(c) 80 s filtering time.

Figure 2.12 Peak transverse deflection due to downburst for different filtering periods.

The spatial variations of the maximum transverse deflections, obtained from the above set of time history analyses are plotted in Figures 2.11 and 2.12a, b and c. Figure 2.11 illustrates a comparison between the results obtained from analyses 1 to 7 for a filtering time of 30s, while Figures 2.12a, b and c show the results corresponding to the filtering times of 10s, 40s and 80s, respectively.

When observing the results in Figures 2.11 and 2.12a, b and c, one can notice the following:

- The quasi-static analysis of the non-turbulent wind-loaded line results in the smallest deflections, while the undamped dynamic analysis of the turbulent wind-loaded line gives the largest deflections.
- Due to the fact that the frequencies of the mean component are much lower than the natural frequencies of the structure, the undamped dynamic analysis of the non-turbulent wind-loaded line produces a deflection very near to that of the quasi-static analysis of the non-turbulent wind-loaded line.
- As the filtering period decreases, the response due to turbulence decreases. This is due to the exclusion of a portion of the random component from the residual turbulence when decreasing the filtering period.
- The increase in the responses due to turbulence increases with the increase in the filtering periods until 40 s, after which the rate of increase decreases, suggesting that 40 s would be a suitable averaging period.
- Due to the high aerodynamic damping, the damped dynamic analysis of the turbulent wind-loaded line (with different values of damping ranging between 17 % and 34 %) produces a deflection very near to that of the quasi-static analysis of the turbulent

wind-loaded line as the high aerodynamic damping significantly reduces the resonant response.

Some selected results obtained from the analyses are also provided in Table 2.3. The maximum transverse deflections, as well as the maximum transverse and longitudinal reactions at the intermediate spring, are provided in this table. These reactions represent the maximum forces transferred from the conductors to the intermediate tower. The maximum values corresponding to the quasi-static turbulent (QT), undamped non-turbulent dynamic (NT), and undamped turbulent dynamic (UT), are provided. The response of the conductor to turbulence consists of two components: the background component (B) and the undamped resonant component (R). These components are isolated using the following relations:

$B = QT - NT$; $R = UT - QT$.

The percentages of each of these two components relative to the undamped turbulent dynamic (UT) cases are provided in Table 2.3, for filtering times of 10 s, 20 s, 30 s, 40 s and 80 s, respectively. The following observations can be drawn from these results:

- The values of deflections shown in Table 2.3 show that for an undamped line with lower turbulence filtering periods, the resonant response is higher than the background response (for 10 s filtering period). For longer filtering periods (40 s and 80 s), the resonant response is lower than the background response.
- The reactions presented in Table 2.3 show that as the filtering period decreases, the values of the reactions of the undamped dynamic analysis of the turbulent wind-loaded line approach those resulting from the quasi-static analysis of the turbulent wind-loaded line. It could be also noticed that the ratio between the resonant and background components increases when the filtering period decreases.

- As the filtering period decreases, the background component of the turbulence decreases. This is due to the exclusion of a portion of the random component from the residual turbulence when decreasing the filtering period. This excluded portion has a range of frequencies that is significantly less than the natural frequencies of the conductor (as shown in Figures 2.11 and 2.12a, b and c and Table 2.3), causing a decrease in the background component in comparison to the resonant component.
- The resonant component of the turbulence is damped out when the damping is included in the analysis, leaving the background component to play the major role in the quantification of the effect of turbulence. Consequently, the turbulent damped dynamic system produces results very near to those produced from the turbulent quasi-static system.
- Whereas the resonant component is damped out due to the high aerodynamic damping, the background component (B) represents the real increase in the reaction due to turbulence.
- The response due to turbulence significantly increases with the increase in the filtering periods, between filtering periods of 10 s and 40 s. Between filtering periods of 40 s and 80s, the response remains almost unchanged. Hence, a filtering period of 40 s is considered to be sufficient enough for quantifying turbulence, as also concluded by Holmes et al. (2008). Therefore, it could be concluded that the increase in the reactions due to turbulence is 22.5 %, which corresponds to the percentage of background component for a filtering period of 40 s. On the other hand, the increase in the transverse deflection due to turbulence is 19.7 %, which corresponds to the percentage of background component for a filtering period of 40 s.

Table 2.3 Effects of Turbulence on the Quasi-Static and Dynamic Responses of the Conductors.

Transverse Deflection (m)					
FILTER TIME (s)	**10**	**20**	**30**	**40**	**80**
NT: Non turbulent	1.91	1.91	1.91	1.91	1.91
QT: Quasi-Static turbulent	1.97	2.05	2.14	2.48	2.73
UT: Undamped turbulent	2.07	2.19	2.33	2.90	3.19
B: Background Deflection = QT-NT	0.06	0.15	0.23	0.57	0.63
R: Resonant Deflection = UT-QT	0.10	0.13	0.19	0.42	0.46
% Background Component = 100*B/UT	3.1 %	6.6 %	10.0 %	19.7 %	19.9 %
% Resonant Component = 100*R/UT	4.6 %	6.2 %	8.1 %	14.5 %	14.9 %
R/B	1.51	0.93	0.81	0.73	0.73
Transverse Reaction (N)					
FILTER TIME (s)	**10**	**20**	**30**	**40**	**80**
NT: Non turbulent	-5720	-5720	-5720	-5720	-5720
QT: Quasi-Static turbulent	-6030	-6250	-6530	-7600	-8360
UT: Undamped turbulent	-6330	-6630	-6970	-8370	-9250
B: Background reaction = QT-NT	-310	-530	-810	-1890	-2650
R: Resonant reaction = UT-QT	-300	-380	-450	-760	-880
% Background Component = 100*B/UT	4.9 %	8.0 %	11.6 %	22.6 %	28.6 %
% Resonant Component = 100*R/UT	4.8 %	5.8 %	6.4 %	9.1 %	9.5 %
R/B	0.97	0.72	0.55	0.40	0.33
Longitudinal Reaction (N)					
FILTER TIME (s)	**10**	**20**	**30**	**40**	**80**
NT: Non turbulent	13780	13780	13780	13780	13780
QT: Quasi-Static turbulent	14530	15060	15730	18330	20160
UT: Undamped turbulent	15270	16000	16930	20230	22320
B: Background reaction = QT-NT	750	1280	1950	4550	6380
R: Resonant reaction = UT-QT	740	940	1190	1900	2160
% Background Component = 100*B/UT	4.9 %	8.0 %	11.5 %	22.5 %	28.6 %
% Resonant Component = 100*R/UT	4.8 %	5.9 %	7.1 %	9.4 %	9.7 %
R/B	0.99	0.73	0.61	0.42	0.34

2.6 CONCLUSIONS

This chapter assesses the dynamic behaviour of the line conductors under downburst loading. A non-linear numerical model is developed and used to predict the natural frequencies and mode shapes of conductors at various loading stages. A turbulence signal is extracted from a set of full-scale data. It is added to the mean component of the

downburst wind field previously evaluated numerically. Dynamic analysis is performed using various downburst configurations. The following conclusions can be drawn from this chapter:

1. The magnitude of the pretension force has a major effect on the natural frequencies, reactions and mode shapes of the conductor. As the pretension force increases, the natural periods of the structure decreases, and the deflection at the connection between the towers and the cables increases.

2. The inclusion of the flexibility of the towers and insulators at the towers/conductor connections, rather than assuming fully hinged boundary conditions, has a significant effect on the natural frequencies and mode shapes.

3. The level of loading and the downburst load configuration have minor effects on the natural periods and the mode shapes of the conductor.

4. The response due to turbulence increases significantly with the increase in the filtering periods, until a filtering period of 40 s. Beyond this value, the response remains almost unchanged. This suggests that 40 s is a suitable averaging period, agreeing with the findings of Holmes et al. (2008).

5. Due to the large aerodynamic damping, the resonant component of the turbulence is damped out when the damping is included in the analysis, leaving the background component to play the major role in the quantification of the effect of turbulence. Hence, the quasi-static analysis is sufficient enough in assessing the effect of turbulence.

6. Considering the 40 s averaging period, the inclusion of turbulence increases the deflection and the internal forces by about 20 % for the considered downburst intensity.

2.7 REFERENCES

Bathe, K. J.(1996), *Finite Element Procedures in Engineering Analysis*, Prentice-Hall, Englewood Cliffs, New Jersey.

Bathe, K. J., Wilson, E.L. and Ramm, E (1975). "Finite element formulations for large deformation dynamic analysis" *International Journal for Numerical Methods in Engineering*, 9(2), 353-386

Barbieri, N., De Souza, J., Honorato, O. and Barbieri, R. (2004). "Dynamical analysis of transmission line cables. Part 1 - Linear theory " *Mechanical Systems and Signal Processing*, 18(3), 659-669

Barbieri, N., De Souza, J., Honorato, O. and Barbieri, R. (2004). "Dynamical analysis of transmission line cables. Part 2 - Damping estimation" *Mechanical Systems and Signal Processing*, 18(3), 671-681

Barbieri, R., De Souza, J., Honorato, O. and Barbieri, R. (2008). "Dynamical analysis of transmission line cables. Part 3-Nonlinear theory" *Mechanical Systems and Signal Processing*, 22(4), 992-1007

Chay, M., Wilson, R. and Albermani, F. (2008). "Gust occurrence in simulated non-stationary winds" *Journal of Wind Engineering and Industrial Aerodynamics*, 96(10-11), 2161–2172.

Computers and structures (2006), SAP 2000 v11.01

Davenport, A.G., (1962). "Buffeting of a suspension bridge by storm winds." *Journal of the ASCE Structural Division,* 88 (3), 233–264.

Fujita, T. (1990). "Downbursts: meteorological features and wind field characteristics." *Journal of Wind Engineering and Industrial Aerodynamics*, 36(1), 75-86.

Gast, K., 2003. A comparison of extreme wind events as sampled in the 2002 Thunderstorm Outflow Experiment. Master's Thesis, Texas Tech University, Lubbock.

Gattulli, V., Martinelli, L., Perotti, F. and Vestroni, F., (2007). "Dynamics of suspended cables under turbulence loading: Reduced models of wind field and mechanical system." *Journal of Wind Engineering and Industrial Aerodynamics*, 95(3), 183-207.

Gerges, R.R. and El Damatty, A.A. (2002). "Large displacement analysis of curved beams." *Proceeding of CSCE Conference*, Montreal, QC, Canada, ST 100.

Holmes, J., Hangan, H., Schroeder, J., Letchford, C., and Orwig, K. (2008): "A forensic study of the Lubbock-Reese downdraft of 2002" *Wind and Structures,* 11(2), 137-152.

Hangan, H. and Kim, J., "Numerical simulation of downbursts", ASCE Structural Congress, Nashville, Te, USA, June, 2004. *(pp.1657-1664)*

Hangan, H. and Kim, J. (2007). "Numerical simulations of impinging jets with application to downbursts" *Journal of Wind Engineering and Industrial Aerodynamics*, 95(4), 279–298.

Kim, J.D., Hangan, H. and Ho, T.C.E. (2007). "Downburst versus boundary layer induced loads for tall buildings." *Wind and Structures*, 10(5), 481-494.

Koziey, B. and Mirza, F. (1994). "Consistent curved beam element." *Computers and Structures*, 51(6), 643-654.

Kwon, D. and Kareem, A. (2009). "Gust-front factor: New framework for wind load effects on structures." *Journal of Structural Engineering*, 135(6), 717-732.

Loredo-Souza, A. M. and Davenport, A. G. (1998). "The effects of high winds on transmission lines." *Journal of Wind Engineering and Industrial Aerodynamics*, 74-76, 987-994.

Macdonald, J (2002). "Separation of the contributions of aerodynamic and structural damping in vibrations of inclined cables" *Journal of Wind Engineering and Industrial Aerodynamics*, 90(1), 19–39.

Mason, M., Wood, G. and Fletcher, D. (2009). "Numerical simulation of downburst winds" *Journal of Wind Engineering and Industrial Aerodynamics*, 97(11-12), 523--539.

Manitoba Hydro Transmission and Civil Design Department (1999), "Bipole 1 & 2 HVDC Transmission Line Wind Storm Failure on September 5, 1996 – Review of Emergency Response, Restoration and Design of These Lines", *Manitoba Hydro*, 98-L1/1-37010-06000, 54.

Oakes, D. "Nelson river HVDC transmission line towers." Manitoba Power Conference EHV-DC, Winnipeg, Manitoba, Canada, June 7-10, 1971, 17

Orwig, K. and Shcroeder, J. (2007). "Near-surface wind characteristics of extreme thunderstorm outflows" *Journal of Wind Engineering and Industrial Aerodynamics*, 95(1), 565-584.

Shehata, A., El Damatty, A. and Savory, E. (2005). "Finite element modelling of transmission line under downburst wind loading." *Finite Element in Analysis and Design*, 42(1), 71-89.

Shehata, A.Y. and El Damatty, A.A. (2007). "Behaviour of guyed transmission line structures under downburst wind loading" *Wind and Structures*, 10(3), 249-268

Shehata, A.Y. and El Damatty, A.A. (2008). "Failure analysis of a transmission tower during a microburst" *Wind and Structures*, 11(3), 193-208

Shehata, A. Y., Nassef, A.O. and El Damatty, A. A. (2008). "A coupled finite element-optimization technique to determine critical microburst parameters for transmission towers." *Finite Element in Analysis and Design*, 45(1), 1-12.

Wang, X., Lou, W., Li, H. and Chen, Y. (2009). "Wind-induced dynamic response of high-rise transmission tower under downburst wind load" *Journal of Zhejiang University*, 43(8), 1520-1525.

CHAPTER 3

SENSITIVITY OF TRANSMISSION LINE GUYED TOWERS TO DOWNBURST LOADING

3.1 INTRODUCTION

Due to the essentiality of electricity in modern life, preventing disruptions in power distribution is vital, as disruptions can have negative social and economical consequences. Conductors supported on transmission towers are a major mode of electricity transmission. Hence, transmission towers are among the most essential components in the electrical system. A major cause of power disruptions is the failure of the towers during natural disasters. These costly failures have been often attributed to high localized wind events, in the form of tornadoes and downbursts (Manitoba Hydro, 1999).

The most critical load in designing transmission towers is the wind load. The design codes of transmission towers have typically considered only normal wind loads associated with large-scale synoptic events such as hurricanes and typhoons. Within the last decades, high intensity winds associated with localized wind events have been subjected to research studies investigating their effects on transmission lines. Typically, the velocity profiles resulting from high intensity winds are different from the regular boundary layer wind profiles along both the vertical and horizontal planes. They usually produce different loading and collapse modes due to the fact that their effects are intensified within a certain locality, which is not the case for boundary layer winds (Kim et al., 2007).

There are two main types of electrical transmission towers; self-supporting and guyed towers. Self-supporting towers carry and transfer loads only through the towers

members. Under lateral loads, a self-supporting tower behaves similar to a cantilever. On the other hand, guyed towers rely on attached guys, which are anchored to the ground, to transfer some of the lateral loads imposed on the towers. Lateral loads are carried by a guyed tower in a similar manner to a simple beam with a cantilever at the part above the guys' level.

High intensity winds (HIW), in the form of downbursts, originate from thunderstorms. A downburst was defined by Fujita (1990) as "a strong downdraft that induces an outburst of damaging winds on or near the ground". The economic losses in North America due to the failure of electric towers in these events are dramatic.

Xie et al. (2006) investigated tower collapses of a transmission line caused by a downburst. The results of field investigations of ten downburst-loaded towers that failed in the east of China where presented in this study. The collapsed towers were classified according to the level of collapse severity. The destruction characteristics of a downburst and its damage to transmission lines were analyzed. Based on this investigation, Xie et al. (2006) recommended taking the dynamic effects of both the transmission towers and the conductors into account when designing the lines. However, Xie et al. (2006) did not perform a dynamic analysis so as to quantify the increase in the different structural responses due to the vibration of these structures.

Hangan and Kim (2004) developed and validated a computational fluid dynamic (CFD) model simulating the spatial and time variations of the downburst wind field. This fluid dynamic model simulates the large-scale fluctuating mean component of the downburst velocity field. Shehata et al. (2005) developed a structural analysis numerical model capable of evaluating the response of transmission lines under the effect of downbursts. The CFD data developed by Hangan and Kim (2004) was incorporated in this model and

scaled-up based on the relative values between the characteristics of a prototype downburst and those used in the CFD model. The Shehata et al. (2005) structural analysis model was based on the finite element method, using three-dimensional linear frame elements to simulate the tower members and two-dimensional non-linear curved frame elements to simulate the conductors.

Using this structure analysis model, Shehata and El Damatty (2007) conducted a parametric study by varying the jet diameter (D_j) and the location of the downburst center relative to the tower. A guyed transmission tower located in Manitoba, Canada, which collapsed in 1996 due to a downburst event, was used to perform this parametric study. The critical downburst parameters leading to maximum forces in the tower members were identified. The study revealed that the critical downburst parameters vary based on the type and location of the members. Shehata and El Damatty (2008) extended their numerical scheme by including a failure model for the tower members, which was used to study the progressive collapse of the guyed tower that failed in Manitoba, Canada in 1996. An optimization code was coupled to the model by Shehata et al. (2008) to predict the critical downburst parameters and the corresponding forces in an automated procedure.

Mathur et al. (1987) studied the dynamic characteristics of a 21.7 m high guyed transmission tower for which the natural period of the highest mode of interest was found to be 0.64 s. Meanwhile, Oliviera et al. (2007) studied the structural behavior of a 50 m high guyed transmission tower; its first five natural periods ranged between 0.18 s and 0.38 s. Concerning the same issue, Shehata et al. (2005) reported a value of 0.58 s for the natural period of a 44 m high guyed transmission tower. Taking into account that the loading period of the mean velocity in a downburst event is greater than 20 s, Shehata et

al. (2005) performed a quasi-static analysis, negating the need to perform a dynamic analysis.

The downburst velocity wind field produced by Hangan and Kim (2004) CFD model had two components and, hence, the resultant velocity has an inclination with the horizontal direction. The variation in the values of the vertical and horizontal velocity components within a downburst event was discussed by Shehata et al. (2005). It was found that the vertical velocity component was maximized in regions near to the downburst center, (Shehata et al., 2005). Mara (2007) studied the effect of varying the horizontal and vertical angles of wind projection. In this study, wind tunnel tests were conducted on two diverse lattice models and the variation in the aerodynamic behaviour of unique lattice sections was assessed. Significant differences in the aerodynamic drag measured for each lattice model were observed at specific angles (especially for large vertical angles). On the other hand, for the critical load cases reported by Shehata and El Damatty (2007), the vertical velocity component was very small in comparison to the horizontal velocity component. Hence, for these critical cases, the effect of the variation in the vertical angle on the aerodynamic drag could be neglected.

The current study focuses on evaluating the sensitivity of the guyed transmission tower members' forces to changing the downburst configurations. The effect of turbulence is included in this study. The axial forces in the members are compared to those resulting from normal wind loading evaluated using the ASCE # 74 (2010). Both, the symmetric and broken wire load cases are included in the normal wind load calculations. The study includes investigating the effect of increasing the level of pretensioning in the conductors on the longitudinal reaction and the forces in the cross-arm members. The study is conducted numerically based on the numerical model developed by Shehata et al. (2005).

3.2 DESCRIPTION OF THE NUMERICAL MODEL

As mentioned above, the current study is conducted using the numerical model developed by Shehata et al. (2005). The wind field for downbursts utilized in this model is based on the CFD model developed by Hangan and Kim (2007). The variations of the downburst wind field, with time and space, for a small-scale downburst jet having a specific diameter and a certain downward velocity, were provided by this CFD simulation. The downburst velocity field has two components; a radial horizontal component and an axial vertical component. A procedure to scale this wind field up and to estimate the wind forces acting on the tower and the conductors due to a full-scale downburst was provided by Shehata et al. (2005). The magnitude and direction of these forces depend on a number of parameters, which are referred to as "the downburst configurations". These parameters are: a) the jet velocity (V_j), b) the jet diameter (D_j), c) the location of the centre of the downburst relative to centre of the tower, which is defined by the polar coordinates r and θ. Two types of elements are used in Shehata's numerical model. The tower members are modeled using two-node linear three-dimensional frame elements. Meanwhile, the conductors are modeled using an assembly of two-dimensional nonlinear curved consistent frame elements (Gerges and El Damatty, 2002).

3.2.1 TOWER AND GUYS MODELING

A guyed tower transmission line system, belonging to the utility company "Manitoba Hydro" and labelled A-402-0, is considered. A sketch showing the layout of the tower and the downburst relative to the transmission line is shown in Figure 3.1. Four conductors hang between every two consecutive towers; two from each cross-arm side with a sag of 20 m. The conductors are attached to the towers via insulator strings that are

allowed to swing in two perpendicular planes. One ground wire is attached between each two consecutive towers at their top edges for lightning protection. The insulator strings connecting the conductors to the towers have a length of 4.27 m. Each two towers are spaced at a distance of 480 m. Figure 3.2 shows the elevations of the modeled tower from the two faces normal and parallel to the transmission line. As shown in Figure 3.2, the modeled tower consists of seven zones; five zones below the tower-guy connections and two zones above this level. More details concerning the modeling and analysis of this tower and the conductors are provided by Shehata et al. (2005)

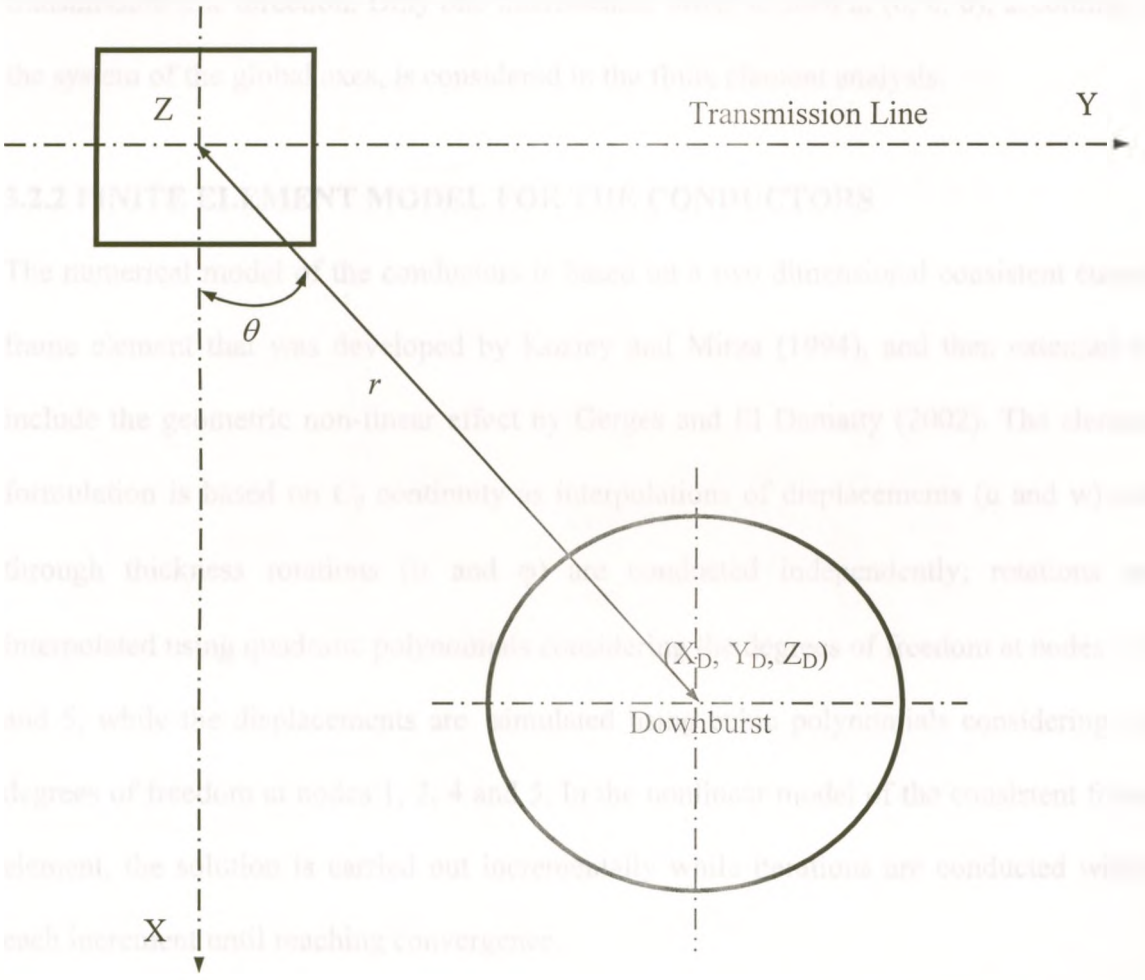

Figure 3.1 Horizontal projection of the transmission tower and downburst, (Shehata et al., 2005).

As mentioned above, two-node linear three-dimensional frame element having three translational and three rotational degrees of freedom for each node is used to model the tower members and the guys. Each tower member is modelled using one element while each guy is divided to five elements. The guys are assumed to be highly pretensioned with a force much higher than the maximum possible compression force. The system of global axes used in the finite element analysis of the entire transmission line/tower system is shown in Figure 3.1, where the Y-axis coincides with the direction of the transmission line, the Z-axis is the vertical direction, and the X-axis is perpendicular to the transmission line direction. Only one intermediate tower located at (0, 0, 0), according to the system of the global axes, is considered in the finite element analysis.

3.2.2 FINITE ELEMENT MODEL FOR THE CONDUCTORS

The numerical model of the conductors is based on a two dimensional consistent curved frame element that was developed by Koziey and Mirza (1994), and then extended to include the geometric non-linear effect by Gerges and El Damatty (2002). The element formulation is based on C_o continuity as interpolations of displacements (u and w) and through thickness rotations (α and φ) are conducted independently; rotations are interpolated using quadratic polynomials considering the degrees of freedom at nodes 1, 3 and 5, while the displacements are simulated using cubic polynomials considering the degrees of freedom at nodes 1, 2, 4 and 5. In the nonlinear model of the consistent frame element, the solution is carried out incrementally while iterations are conducted within each increment until reaching convergence.

A six-span conductor, having the same properties as the conductor modeled by Shehata et al. (2005), was considered. The conductor is initially pretensioned with a force of 82,344

N. Each conductor covers a span of 480 m, has a sag of 20 m, and is divided into five equal elements. At the conductor-towers connections, a set of nonlinear springs, simulating the combined stiffness of the tower and the insulators, is implemented in the model. More details about the modeling of the conductors are explained by Shehata et al. (2005).

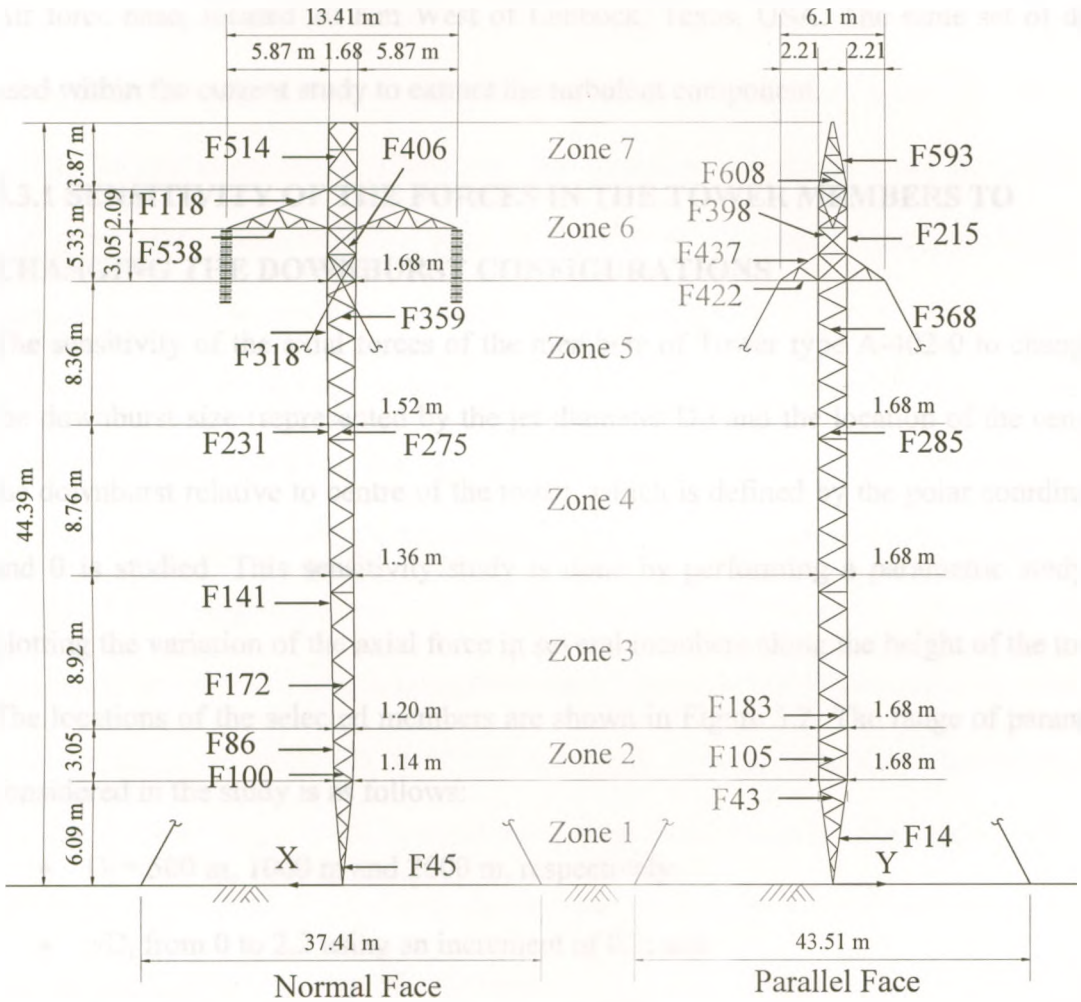

Figure 3.2 Geometry of the modeled lattice transmission tower Type A-402-0, (Shehata et al., 2005).

3.3 SENSITIVITY ANALYSIS OF GUYED TOWERS

All the analyses performed within this chapter is done for a downburst having a constant jet velocity of 29 m/s, in addition to the self weight of the conductors and the ground

wires. Hangan and Kim (2007) validated their CFD model simulating the spatial and time variations of the downburst wind field by matching its results to a real downdraft. The jet velocity that produced the same mean velocity record as that in the field was found to be equal to 29 m/s. This downdraft was recorded by the Wind Science and Engineering Research Centre at Texas Tech University on the 4th of June, 2002, at the former Reese Air force base, located 20 Km West of Lubbock, Texas, USA. The same set of data is used within the current study to extract the turbulent component.

3.3.1 SENSITIVITY OF THE FORCES IN THE TOWER MEMBERS TO CHANGING THE DOWNBURST CONFIGURATIONS

The sensitivity of the axial forces of the members of Tower type A-402-0 to changes in the downburst size (represented by the jet diameter D_j) and the location of the centre of the downburst relative to centre of the tower, which is defined by the polar coordinates r and θ is studied. This sensitivity study is done by performing a parametric study and plotting the variation of the axial force in several members along the height of the towers. The locations of the selected members are shown in Figure 3.2. The range of parameters considered in the study is as follows:

- D_j = 500 m, 1000 m and 2000 m, respectively;
- r/D_j from 0 to 2.2 using an increment of 0.2; and
- θ from 0^o and 90^o using an increment of 15°.

The results of this parametric study are shown in Figures 3.3 – 3.12, as well as in Table 3.1. In the same table, the maximum axial forces resulting from applying the ASCE # 74 guidelines (2010) are provided for the considered members. When applying these guidelines, the reference velocity at 10 m height is matched to the corresponding value (at

the tower) associated with a downburst having a jet velocity of 29 m/s. For each load case, the velocity at a height of 10 m is equated to that resulting from the downburst wind field. The comparison of this normal wind load case and the downburst load case is presented in Section 3.3.3 in which a turbulence signal is added to the downburst wind field. Hence, to compare this newly developed peak downburst wind field to a normal wind load, this load should be calculated based on a gust wind speed. Hence, this reference velocity is increased by 10 % to convert it into a 3 s gust speed (as specified by ASCE 74) so as to be comparable to the turbulent downburst wind field. Both the symmetric and broken wire load case are included in the normal wind load calculations. The results of this analysis are discussed in Section 3.3.3.

The results indicate that the variation in r/D_j has a large effect on the values of the axial forces in all members along the height of the tower. For zones 1 to 5 (the zones beneath the tower-guy connection), the maximum forces in most of the members occur when the values of r/D_j range between 1.2 and 1.4; this is due to the maximum radial velocity occurring for values of r/D_j ranging between 1.2 and 1.4. For these zones, the maximum forces occur at an angle (θ) of 90^o for the chord members and the diagonal members parallel to the transmission line, while the maximum forces occur at an angle of 0^o for the diagonal members perpendicular to the line. For most of the members all over the tower, the minimum forces occur at r/D_j of 0 and 2.2; this is due to the negligible radial velocity at these locations.

In the zones above the guy connection with the tower, the maximum forces happen at intermediate angles (between 15^o and 45^o). This is due to the large value of the longitudinal reaction of the conductors associated with these angles, which leads to an uneven distribution of forces on the conductors adjacent to the tower. It is worth noting

that the maximum forces in these zones occur for r/D_j larger than 1.4. Knowing that the maximum radial velocity occurs for values of r/D_j ranging between 1.2 and 1.4, it is worth pointing out that for the critical cases with intermediate angles, the perpendicular distance from the downburst center to the transmission line is ranging between $1.2D_j$ and $1.4D_j$. This could explain the large loads on the conductors for these load cases. Due to the nonlinear behaviour of the conductors, this loading leads to a net force acting on the cross arms along the longitudinal direction of the conductors.

For most of the members along the height of the tower, the axial forces increase with a decrease in D_j. Therefore, for most of the members, the highest forces occur at a jet diameter of 500 m (which is the lower bound diameter of the study). It could be noticed from Figures 3.3–3.12 that the effect of varying D_j is less significant than the effects of varying r/D_j and θ. This is noticed most for jet diameters of 500 m and 1000 m, as the axial forces produced by these two diameters are very near to each other for most of the members studied. This explains why the jet diameter for the load cases that are critical for the cross-arm chords is 1000 m as the forces caused by a jet diameter of 1000 m are almost equal to those caused by a jet diameter of 500 m. It is worth noting that the jet diameter of 500 m and 1000 m are the most critical due to the highest velocity profiles occurring for these two diameters as shown by Shehata et al. (2005).

Knowing that the guys are highly pretensioned, it is worth noting that the negative force for some cases shown in Figure 3.12 is representing the reduction in the guy pretensioning (not a net compressive force).

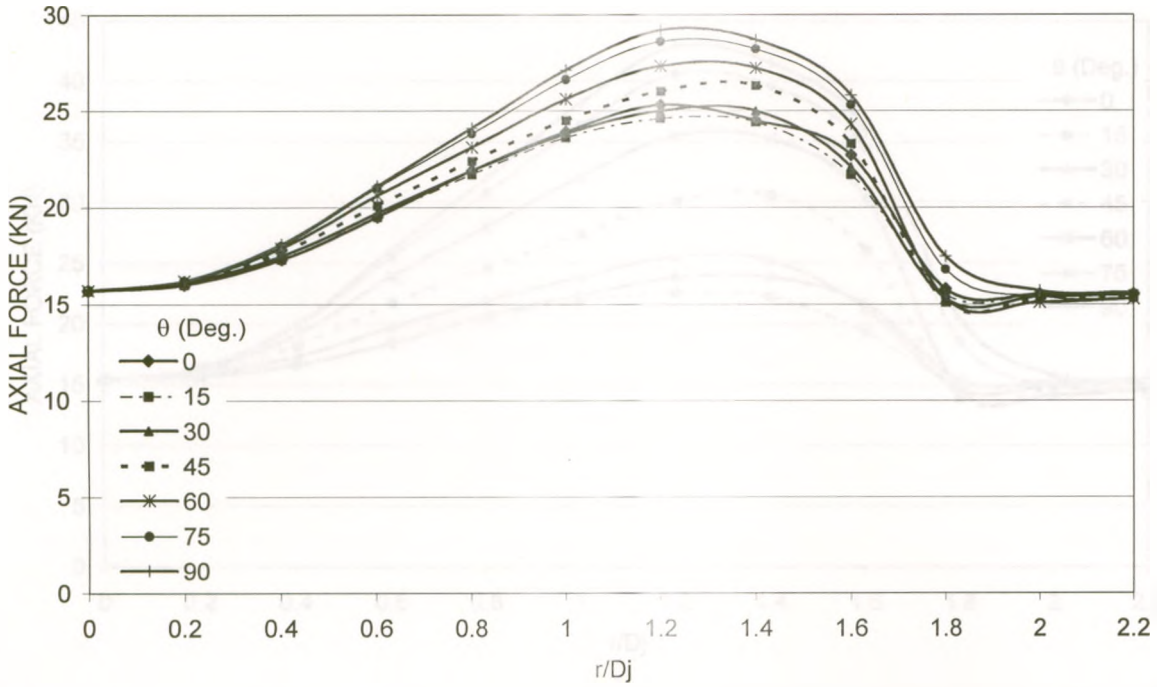

Figure 3.3 Variation of the axial force in chord member 14 (Zone 1) with r/D_j and θ, for D_j = 500 m.

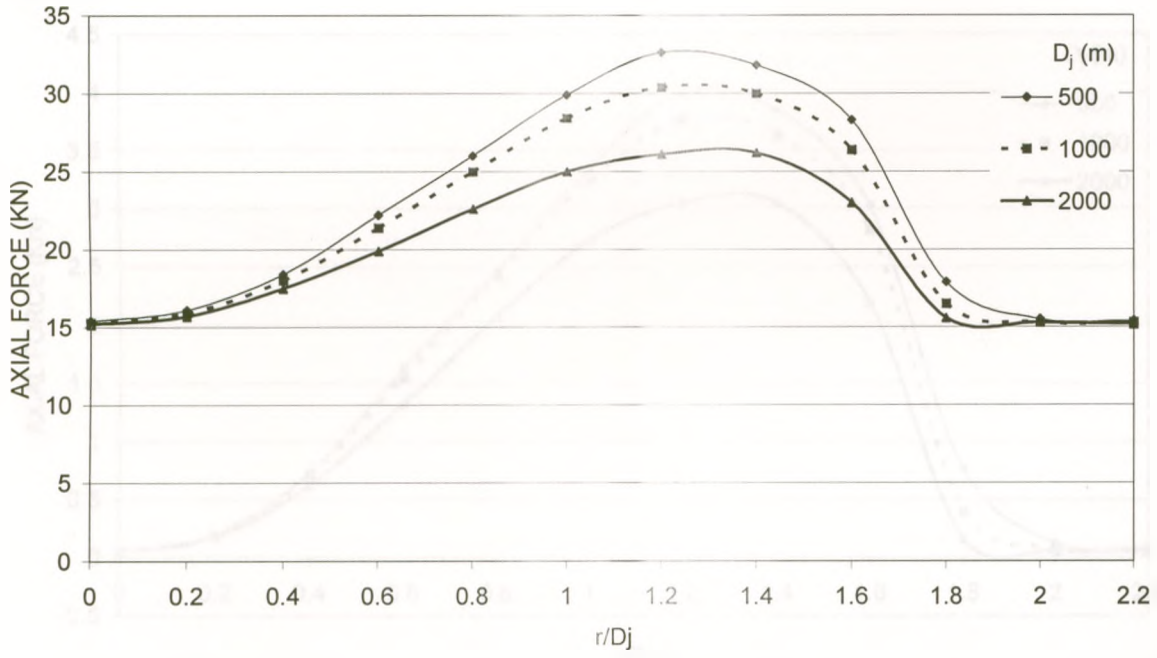

Figure 3.4 Variation of the axial force in chord member 86 (Zone 2) with r/D_j and D_j, for θ = 90°.

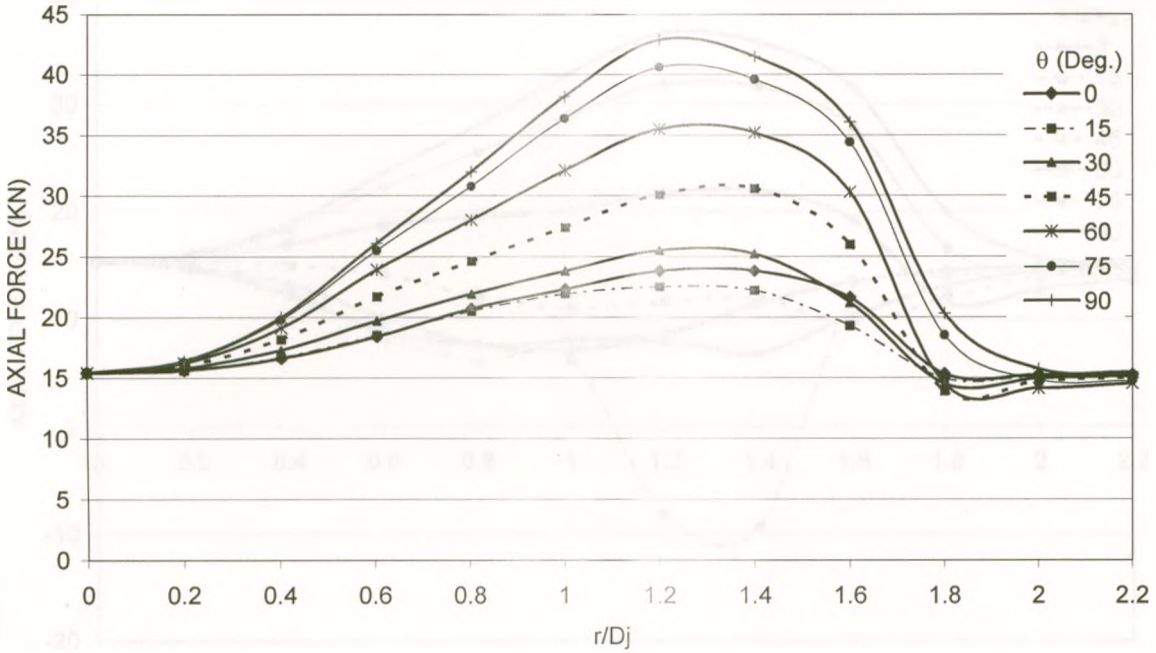

Figure 3.5 Variation of the axial force in chord member 141 (Zone 3) with r/D_j and θ, for D_j = 500 m.

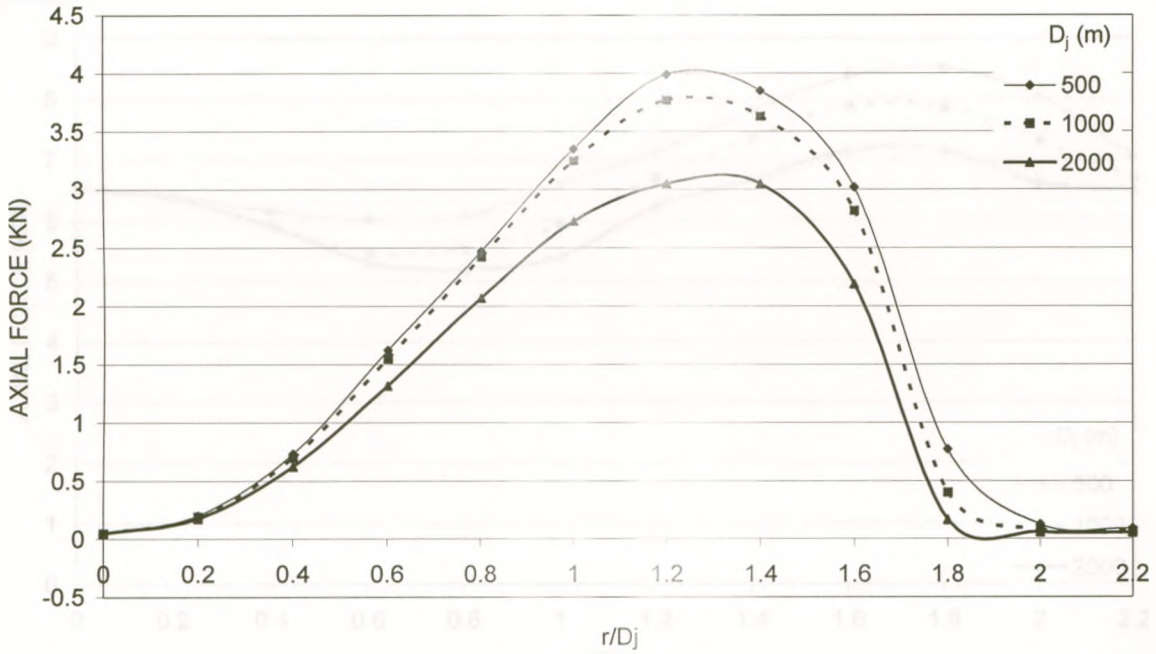

Figure 3.6 Variation of the axial force in diagonal member 275 (Zone 4) with r/D_j and D_j, for $\theta = 0^o$.

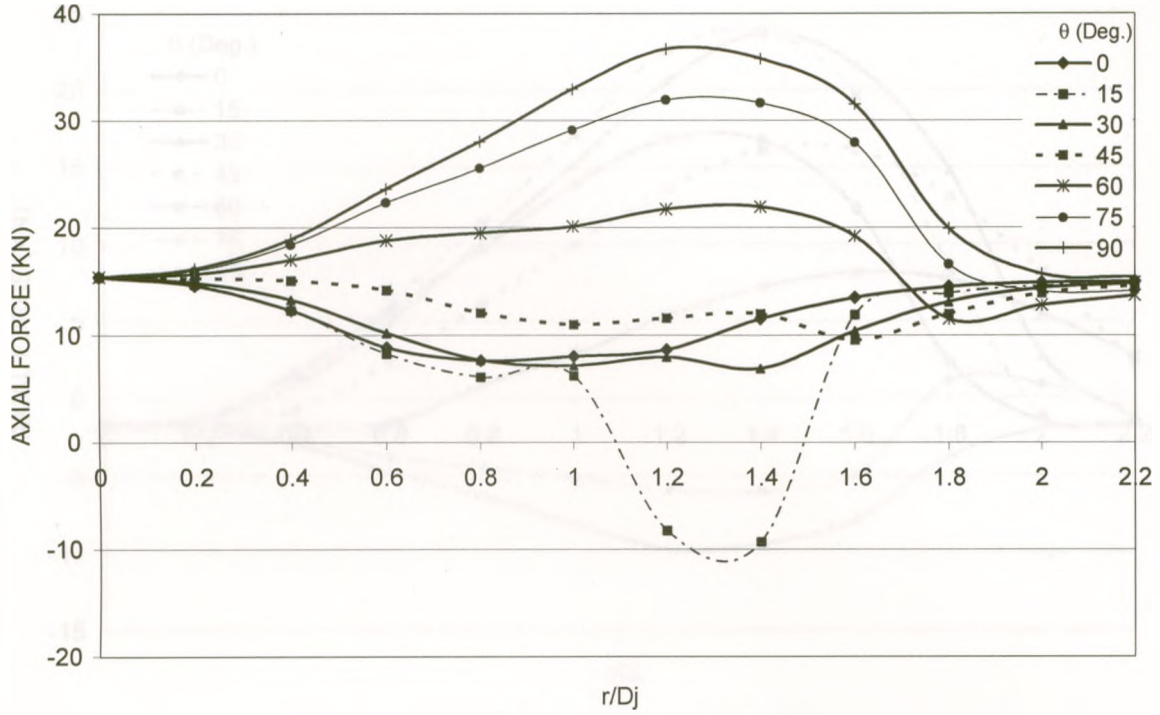

Figure 3.7 Variation of the axial force in chord member 318 (Zone 5) with r/D_j and θ, for D_j = 500 m.

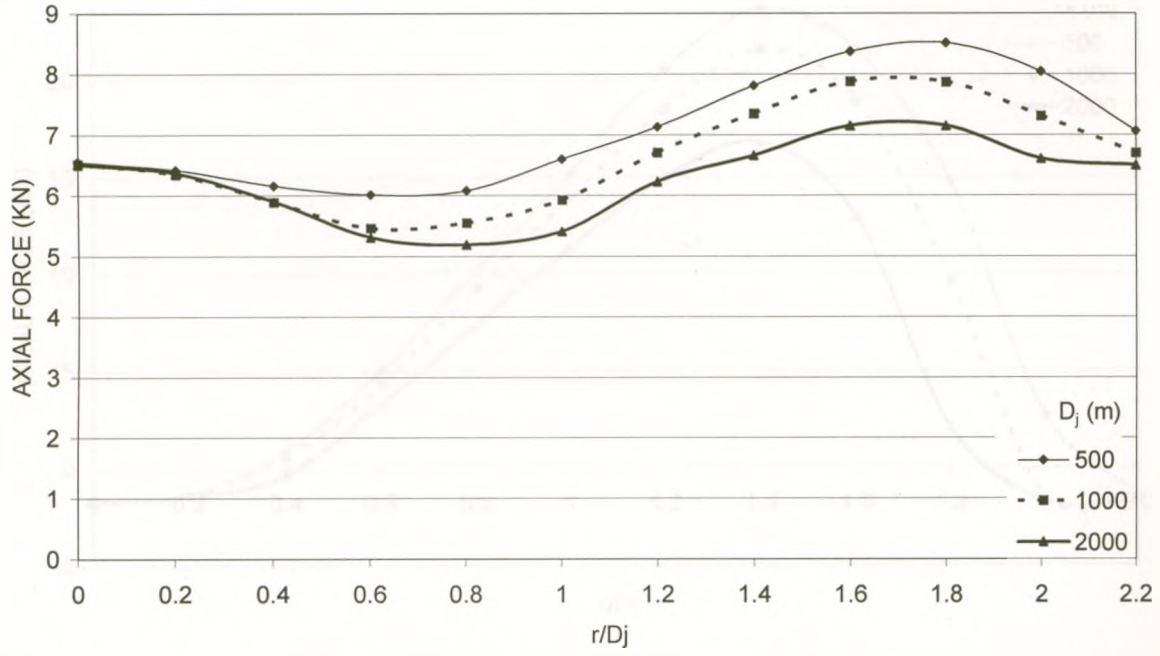

Figure 3.8 Variation of the axial force in diagonal member 406 (Zone 6) with r/D_j and D_j, for $\theta = 45^{\circ}$.

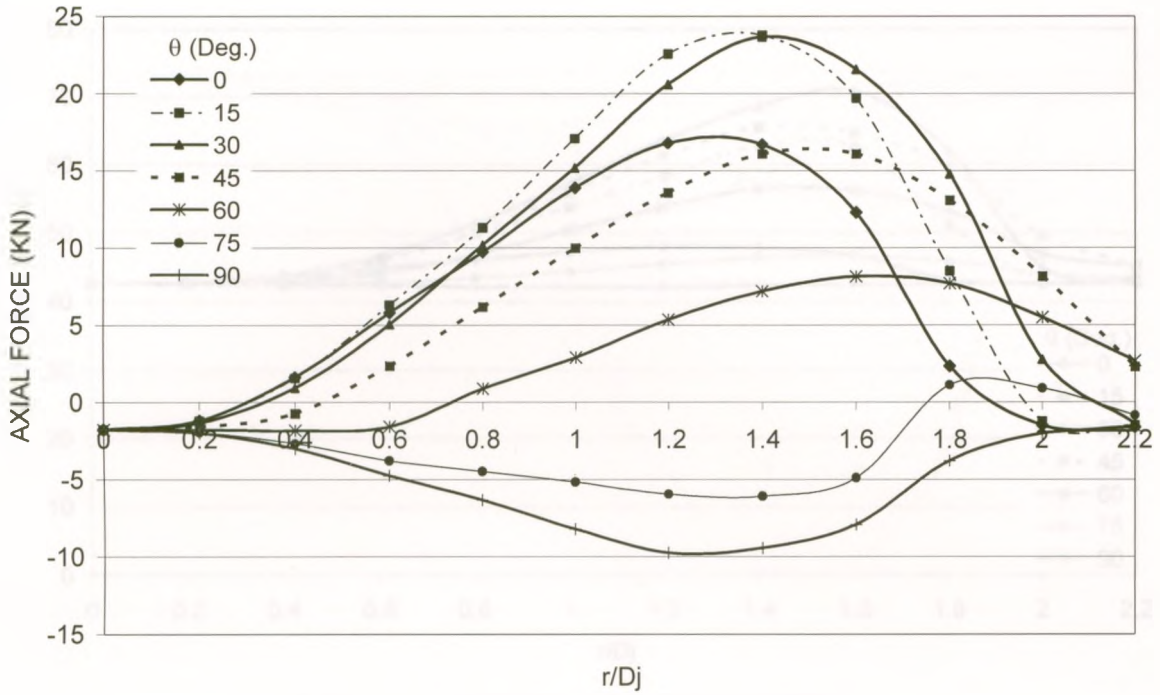

(a) Variation with r/D_j and θ, for D_j = 500 m.

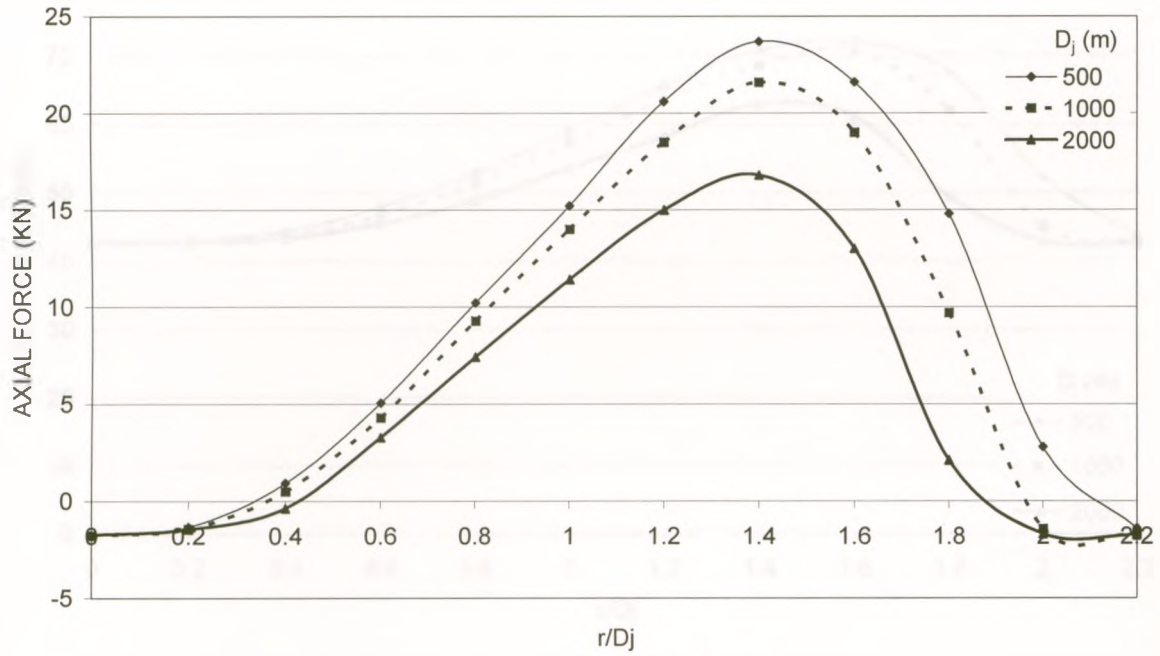

(b) Variation with r/D_j and D_j, for $\theta = 30^o$.

Figure 3.9 Variation of the axial force in the lower chord member 422 (connected to the guy) with the downburst configuration.

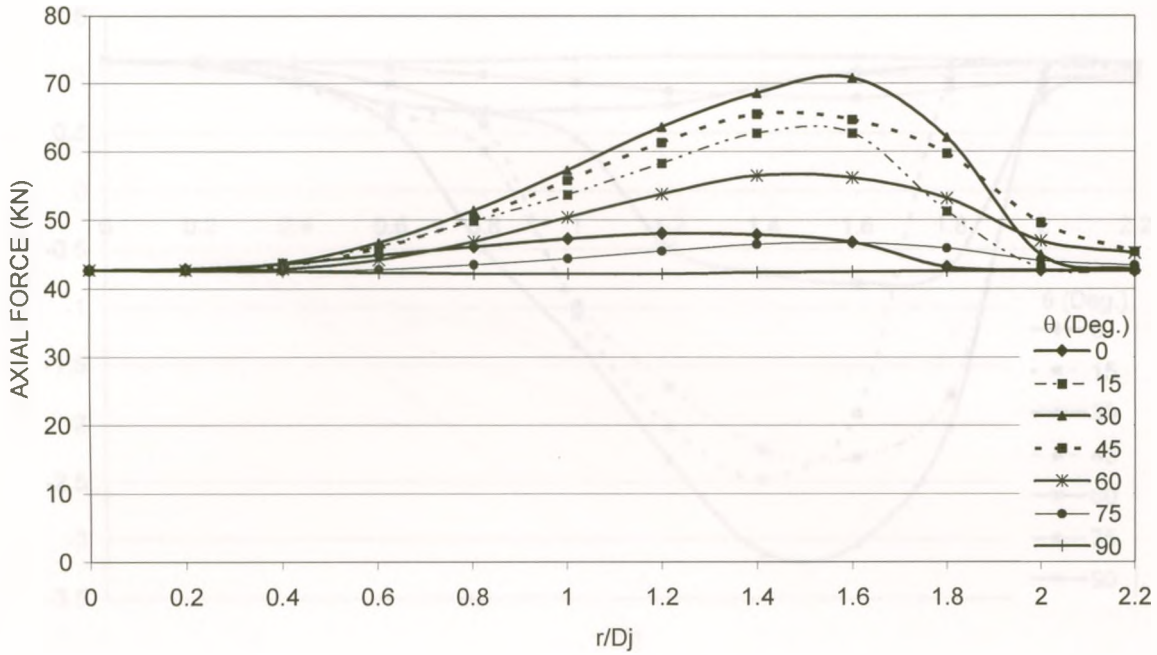

(a) Variation with r/D_j and θ, for D_j = 1000 m.

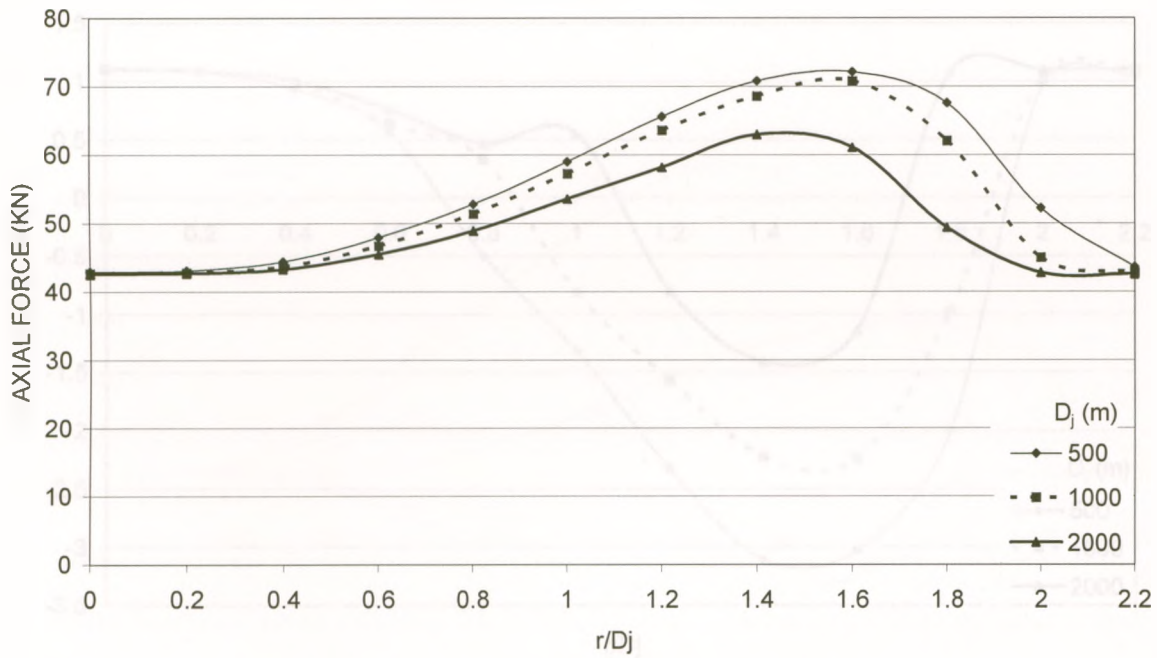

(b) Variation with r/D_j and D_j, for $\theta = 30^{o}$.

Figure 3.10 Variation of the axial force in the lower chord cross-arm member 538 with the downburst configuration.

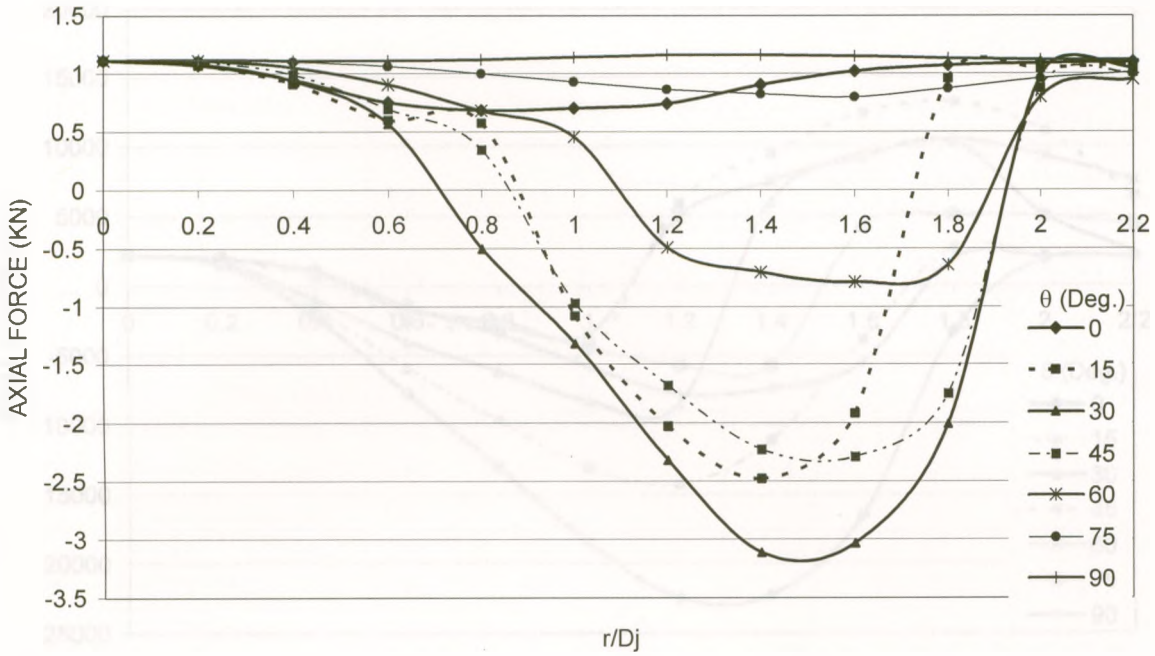

(a) Variation with r/D_j and θ, for D_j = 500 m.

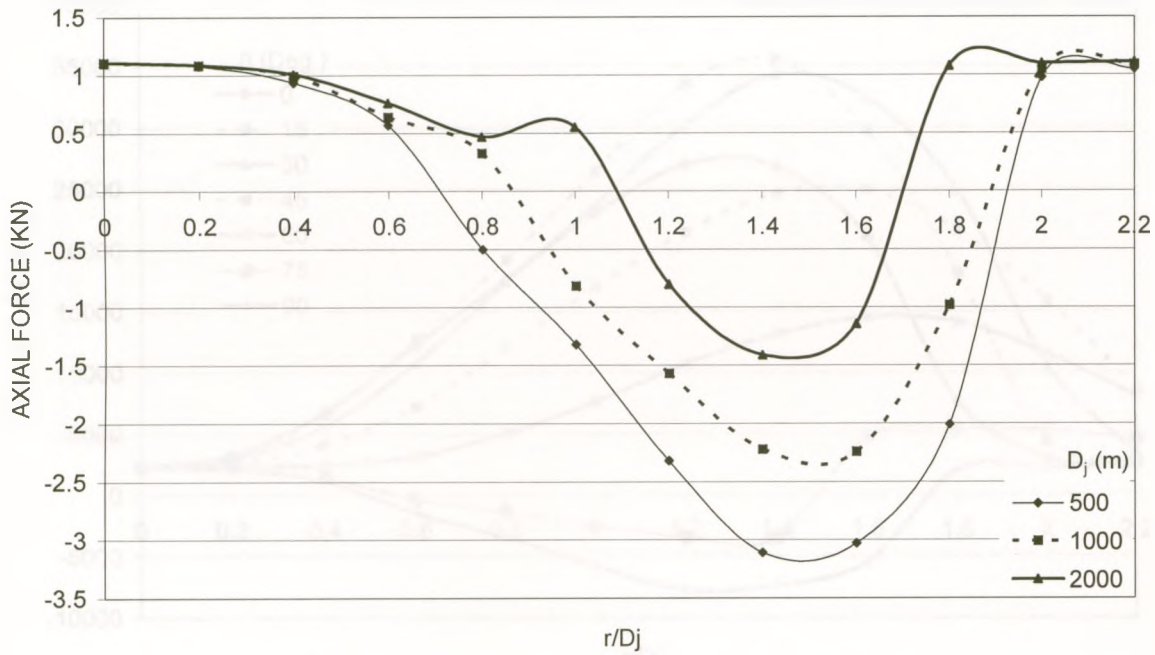

(b) Variation with r/D_j and D_j, for $\theta = 30^o$.

Figure 3.11 Variation of the axial force in the diagonal member 514 (Zone 7) with the downburst configuration.

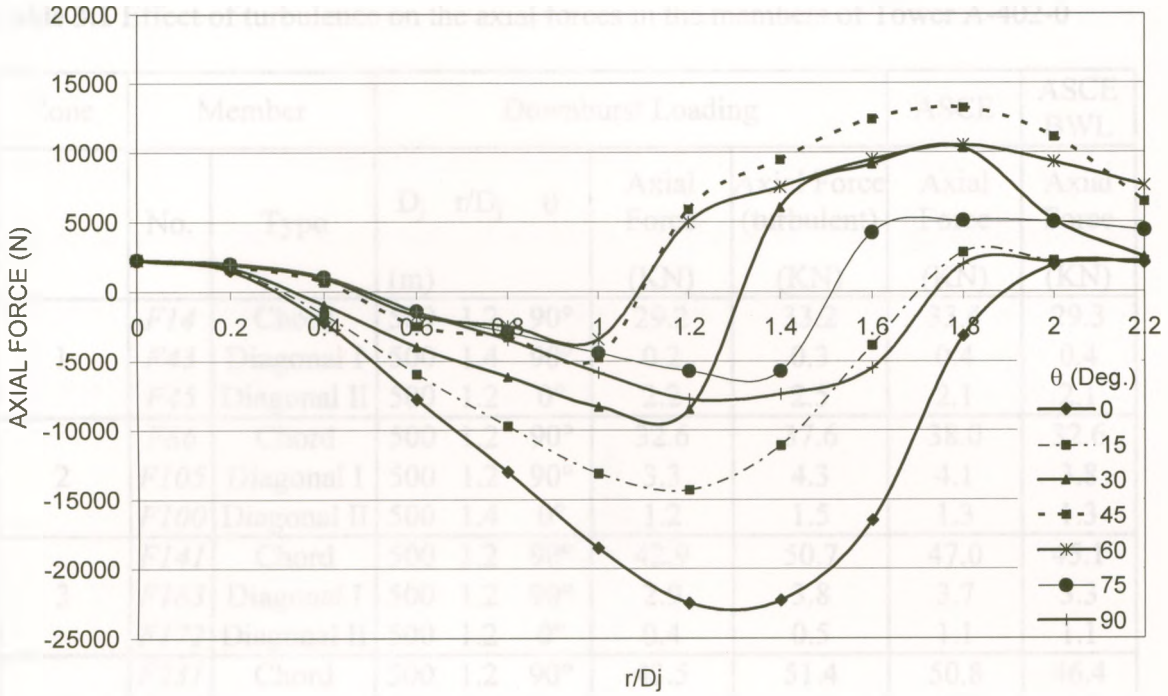

(a) Guy 1.

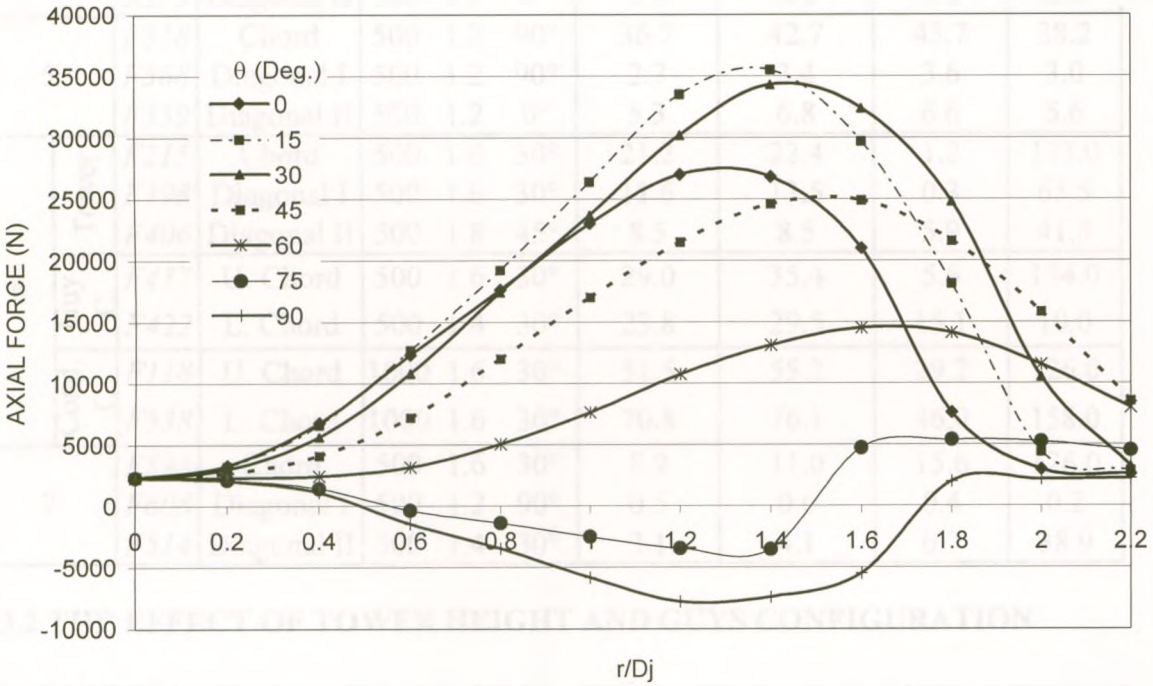

(b) Guy 2.

Figure 3.12 Variation of the axial force in the Tower A-402-0 guys with r/D_j and θ, for $D_j = 500$ m.

Table 3.1 Effect of turbulence on the axial forces in the members of Tower A-402-0

Zone		Member		Downburst Loading					ASCE	ASCE BWL
		No.	Type	D_j (m)	r/D_j	θ	Axial Force (KN)	Axial Force (turbulent) (KN)	Axial Force (KN)	Axial Force (KN)
1		*F14*	Chord	500	1.2	90°	29.2	33.2	33.4	29.3
		F43	Diagonal I	500	1.4	90°	0.2	0.3	0.4	0.4
		F45	Diagonal II	500	1.2	0°	2.2	2.5	2.1	2.1
2		*F86*	Chord	500	1.2	90°	32.6	37.6	38.0	32.6
		F105	Diagonal I	500	1.2	90°	3.3	4.3	4.1	3.8
		F100	Diagonal II	500	1.4	0°	1.2	1.5	1.3	1.3
3		*F141*	Chord	500	1.2	90°	42.9	50.7	47.0	45.1
		F183	Diagonal I	500	1.2	90°	2.9	3.8	3.7	3.3
		F172	Diagonal II	500	1.2	0°	0.4	0.5	1.1	1.1
4		*F231*	Chord	500	1.2	90°	43.5	51.4	50.8	46.4
		F285	Diagonal I	500	1.2	90°	1.1	1.5	1.7	1.6
		F275	Diagonal II	500	1.2	0°	4.0	5.1	5.5	4.5
5		*F318*	Chord	500	1.2	90°	36.7	42.7	43.7	38.2
		F368	Diagonal I	500	1.2	90°	2.7	3.4	3.6	3.0
		F359	Diagonal II	500	1.2	0°	5.3	6.8	6.6	5.6
6	Tower	*F215*	Chord	500	1.6	30°	21.2	22.4	1.2	173.0
		F398	Diagonal I	500	1.6	30°	11.6	13.5	0.3	65.5
		F406	Diagonal II	500	1.8	45°	8.5	8.5	5.9	41.5
	Guy C.	*F437*	U. Chord	500	1.6	30°	29.0	35.4	5.6	174.0
		F422	L. Chord	500	1.4	30°	23.8	29.5	15.1	10.0
	Cond. C	*F118*	U. Chord	1000	1.6	30°	51.5	55.2	29.2	126.0
		F538	L. Chord	1000	1.6	30°	70.8	76.1	46.0	158.0
7		*F593*	Chord	500	1.6	30°	8.9	11.0	15.6	126.0
		F608	Diagonal I	500	1.2	90°	0.5	0.6	0.4	0.2
		F514	Diagonal II	500	1.4	30°	3.1	4.1	0.3	38.9

3.3.2 THE EFFECT OF TOWER HEIGHT AND GUYS CONFIGURATION

The effects of changing the height and guys' configuration are studied through modeling another Manitoba Hydro tower (type A-401-0) in addition to the previously modeled tower. The towers of the A-401-0 line are geometrically similar to those of theA-402-0 line with the exception of having different height and guys' configuration. Tower type A-

401-0 (shown in figure 3.13) is 11 m higher than A-402-0 and has two additional guys. As shown in Figure 3.13, the two additional guys are located in the vertical plane perpendicular to the transmission line at a height of 19.81 m, while the other four guys are connected to the tower at a height of 45.85 m. On the other hand, the conductors are supported at a height of 48.90 m and the ground wire is supported at the top of the tower at a height of 55.07 m.

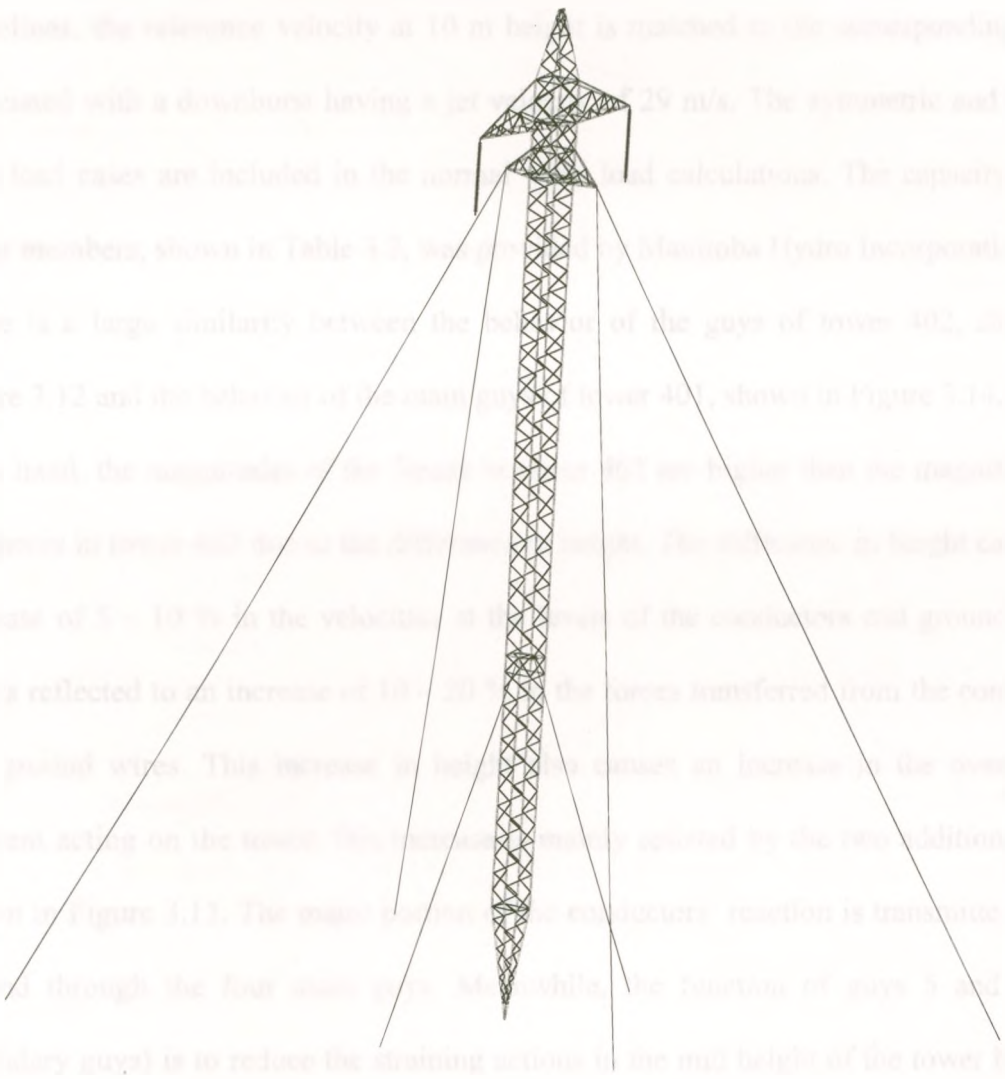

Figure 3.13 Geometry of the modeled lattice transmission tower Type A-401-0

The sensitivity of the axial forces in the tower members to changes in D_j, r/D_j, and θ is studied through performing a parametric study and plotting the variation of the axial force

in several members along the height of the tower. The same ranges and increments used for the variables (D_j, r/D_j and θ) in the analysis of Tower A-402-0 are used in this parametric study.

The results of this parametric study are shown in Figures 3.14 – 3.25 as well as in Table 3.2. In the same table, the maximum axial forces resulting from applying the ASCE # 74 guidelines (2010) are provided for the considered members. When applying these guidelines, the reference velocity at 10 m height is matched to the corresponding value associated with a downburst having a jet velocity of 29 m/s. The symmetric and broken wire load cases are included in the normal wind load calculations. The capacity of the tower members, shown in Table 3.2, was provided by Manitoba Hydro Incorporation.

There is a large similarity between the behavior of the guys of tower 402, shown in Figure 3.12 and the behavior of the main guys of tower 401, shown in Figure 3.14. On the other hand, the magnitudes of the forces in tower 401 are higher than the magnitudes of the forces in tower 402 due to the difference in height. The difference in height causes an increase of 5 – 10 % in the velocities at the levels of the conductors and ground wires; this is reflected to an increase of 10 – 20 % in the forces transferred from the conductors and ground wires. This increase in height also causes an increase in the overturning moment acting on the tower, this increase is mainly resisted by the two additional guys shown in Figure 3.13. The major portion of the conductors' reaction is transmitted to the ground through the four main guys. Meanwhile, the function of guys 5 and 6 (the secondary guys) is to reduce the straining actions in the mid height of the tower body by acting as springs in the middle of the tower body. This explains why the forces in guys 5 and 6, shown in Figure 3.15, are less in magnitude than the forces in the four main guys.

It is worth noting that the negative force for some cases is representing the reduction in the guy pretensioning (not a net compressive force).

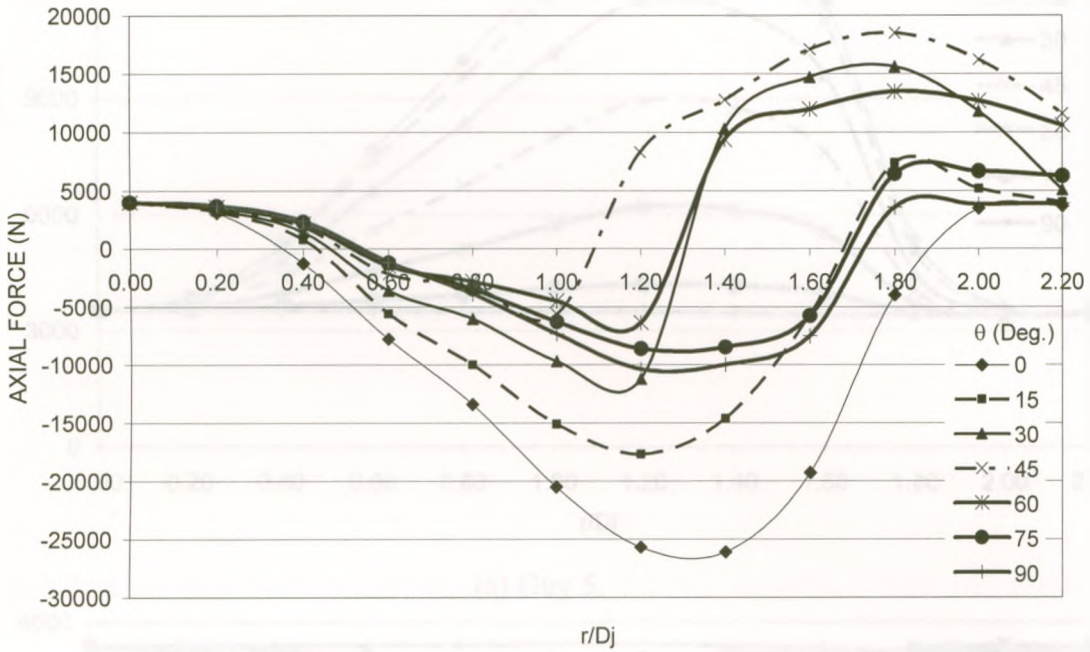

(a) Guy 1.

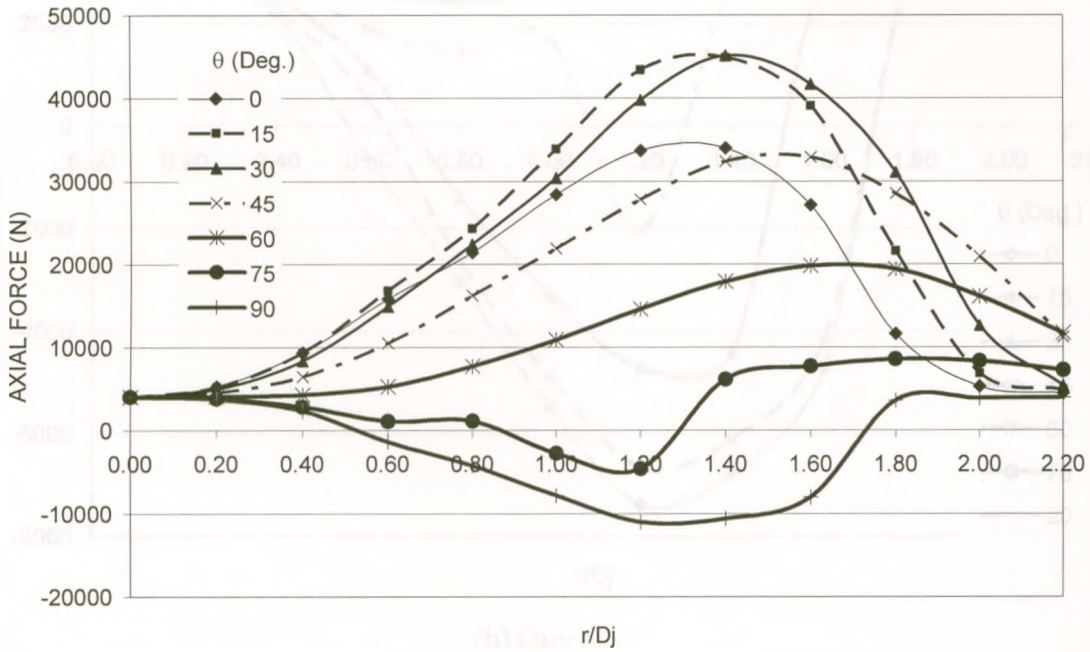

(b) Guy 2.

Figure 3.14 Variation of the axial force in the Tower A-401 main guys with r/D_j and θ, for D_j = 500 m.

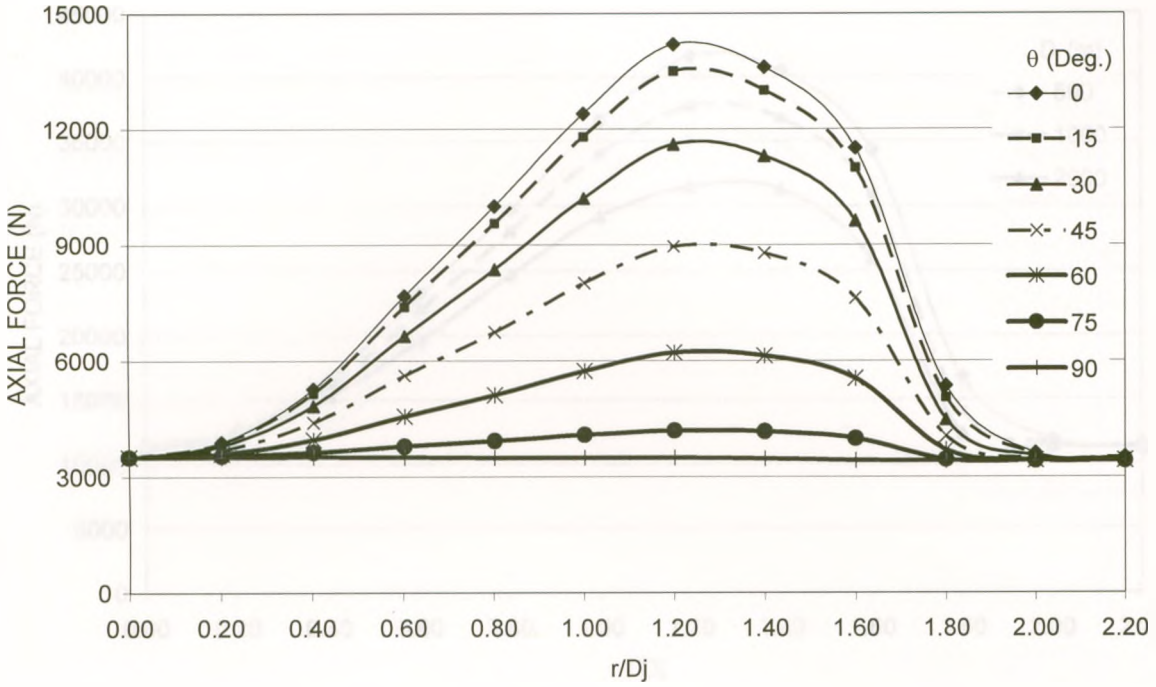

(a) Guy 5.

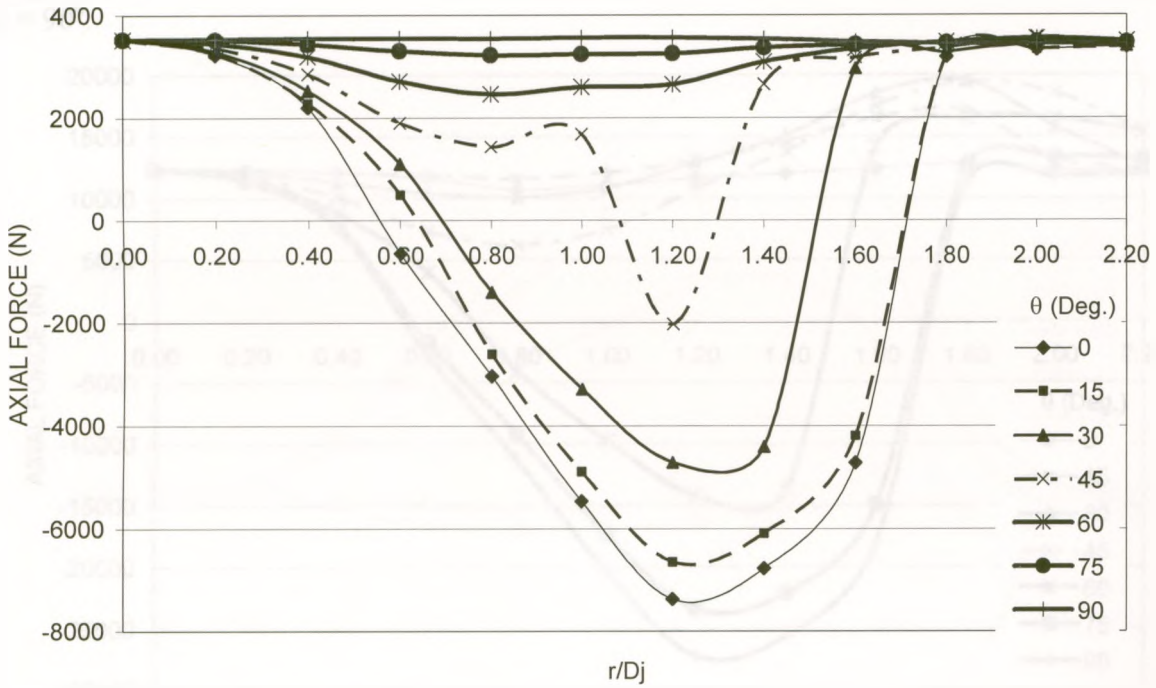

(b) Guy 6.

Figure 3.15 Variation of the axial force in the Tower A-401-0 secondary guys with r/D_j and θ, for D_j = 500 m.

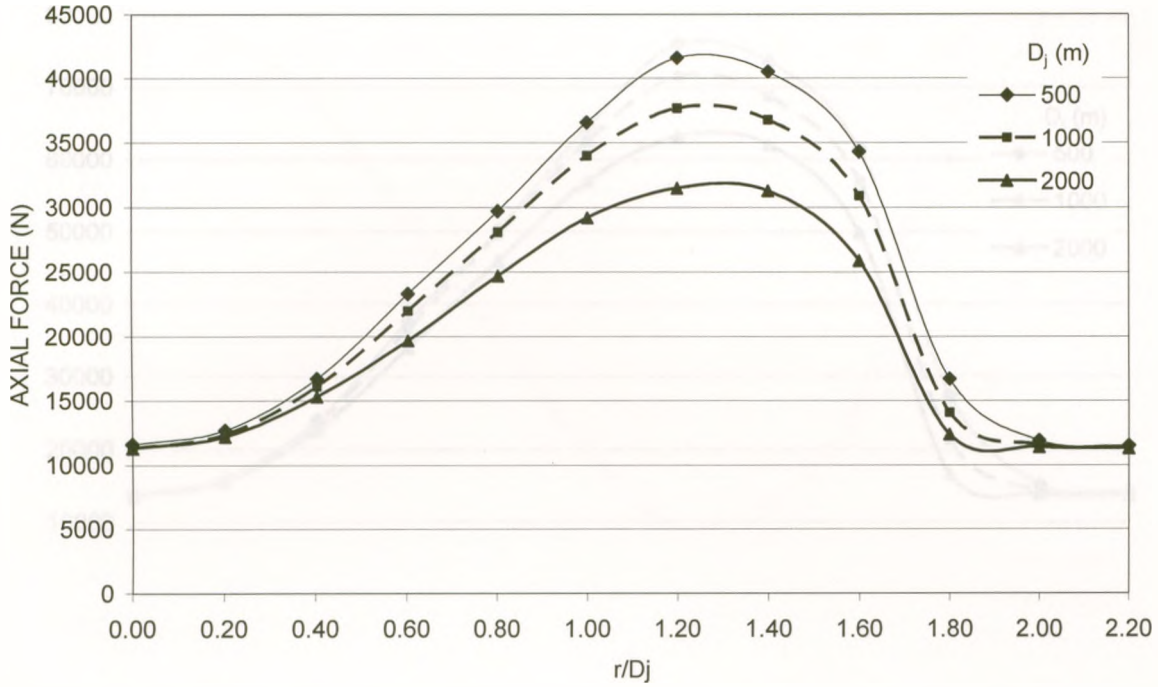

Figure 3.16 Variation of the axial force in chord member 42 (Zone 1) with r/D_j and D_j, for $\theta = 90^o$.

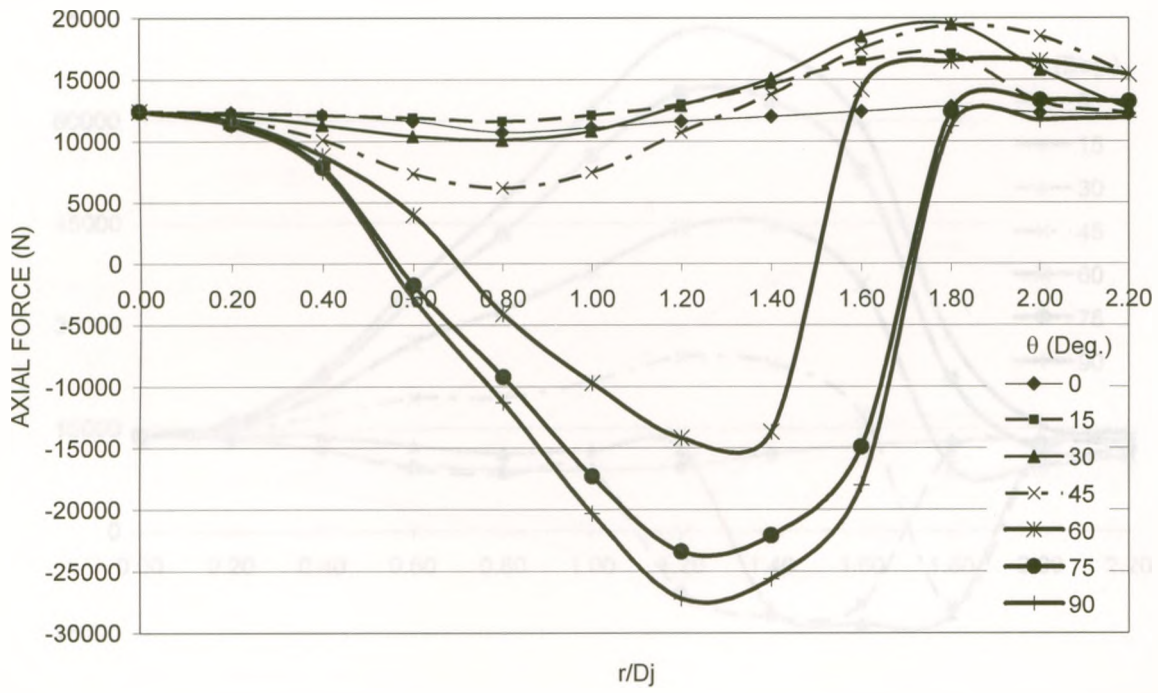

Figure 3.17 Variation of the axial force in chord member 75 (Zone 2) with r/D_j and θ, for D_j = 500 m.

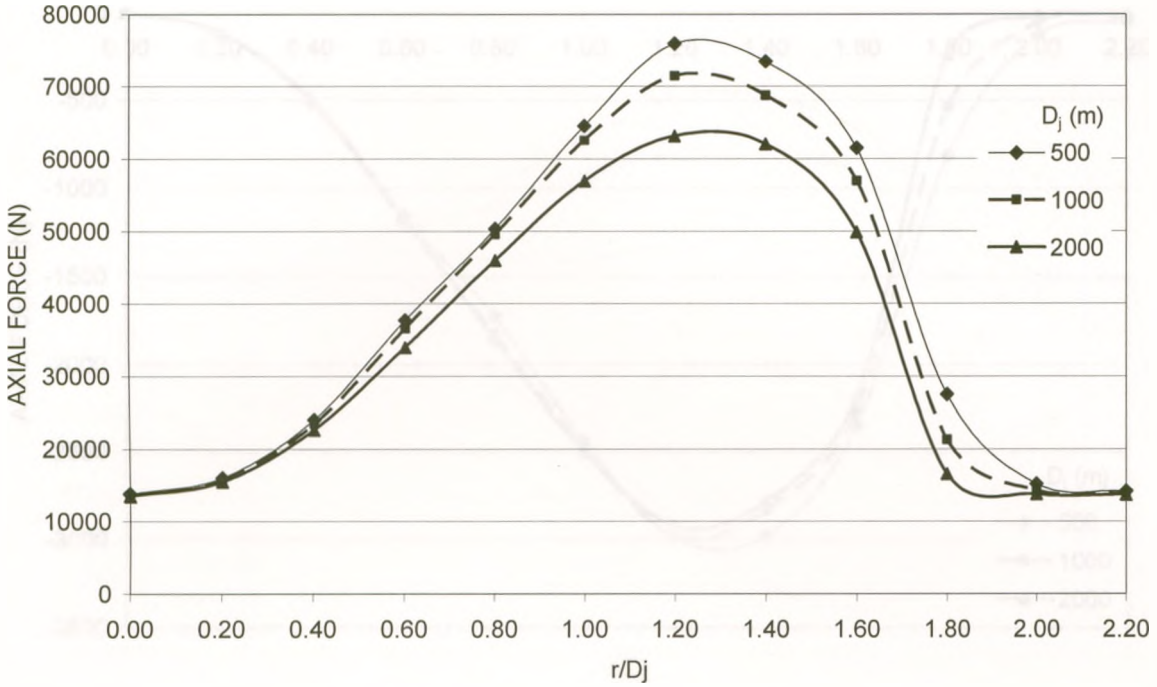

Figure 3.18 Variation of the axial force in chord member 330 (Zone 3) with r/D_j and D_j, for $\theta = 90^{\circ}$.

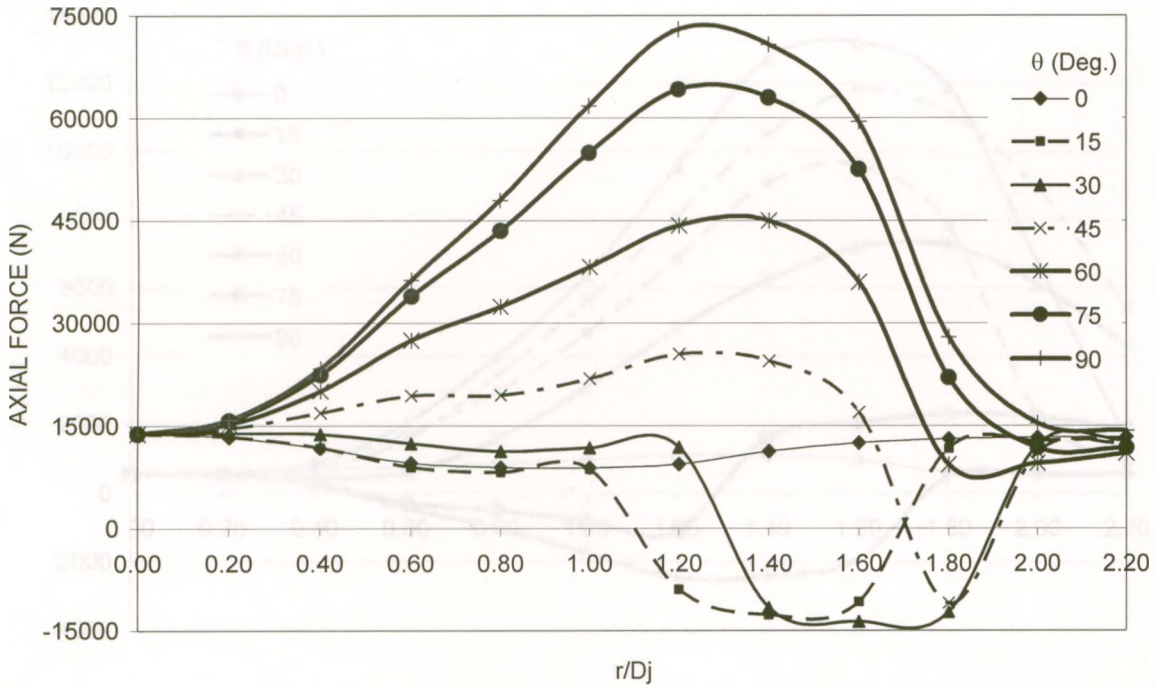

Figure 3.19 Variation of the axial force in chord member 350 (Zone 4) with r/D_j and θ, for $D_j = 500$ m.

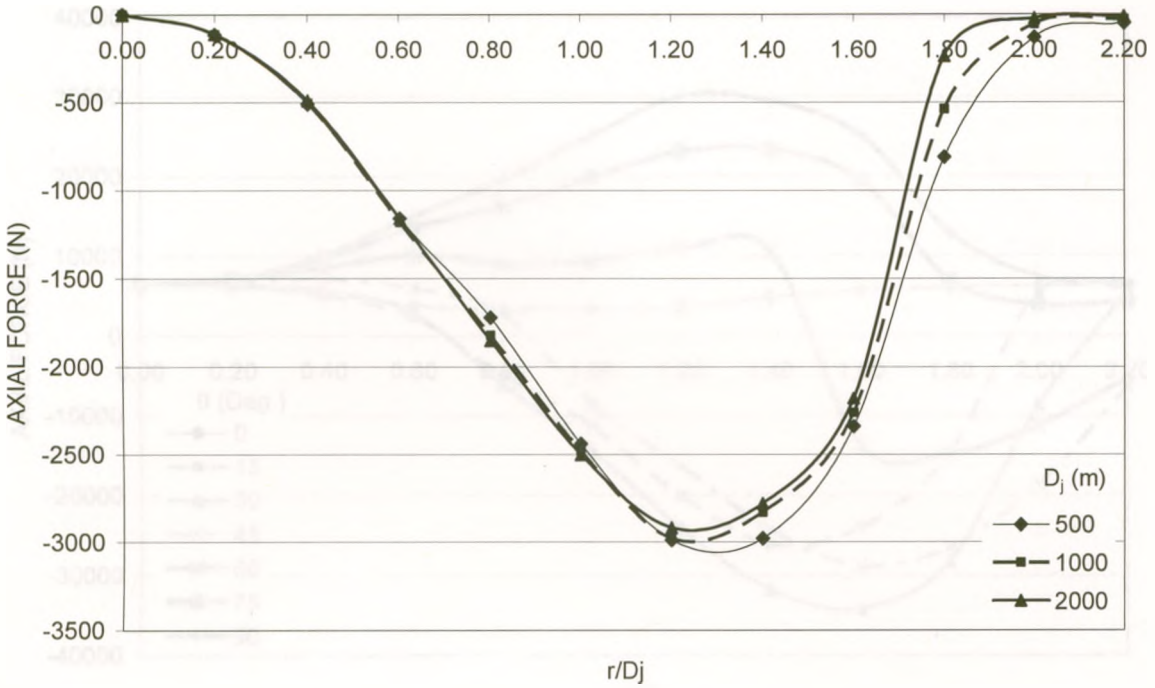

Figure 3.20 Variation of the axial force in diagonal member 381 (Zone 5) with r/D_j and D_j, for $\theta = 0^o$.

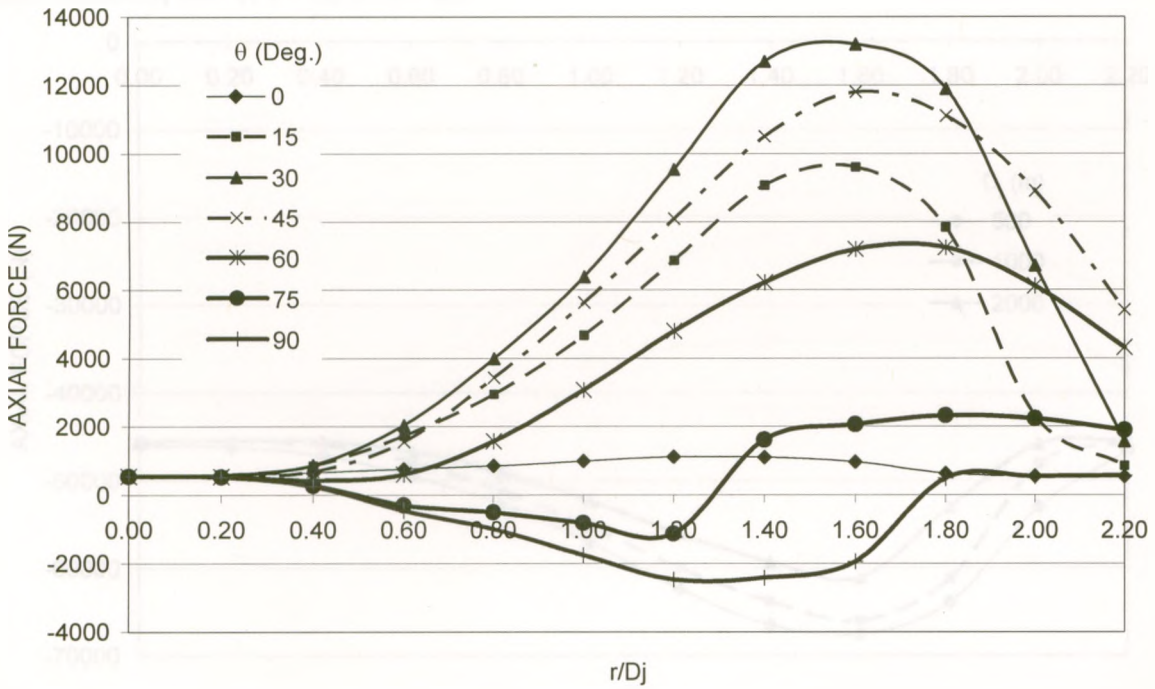

Figure 3.21 Variation of the axial force in diagonal member 538 (Zone 6) with r/D_j and θ, for $D_j = 500$ m.

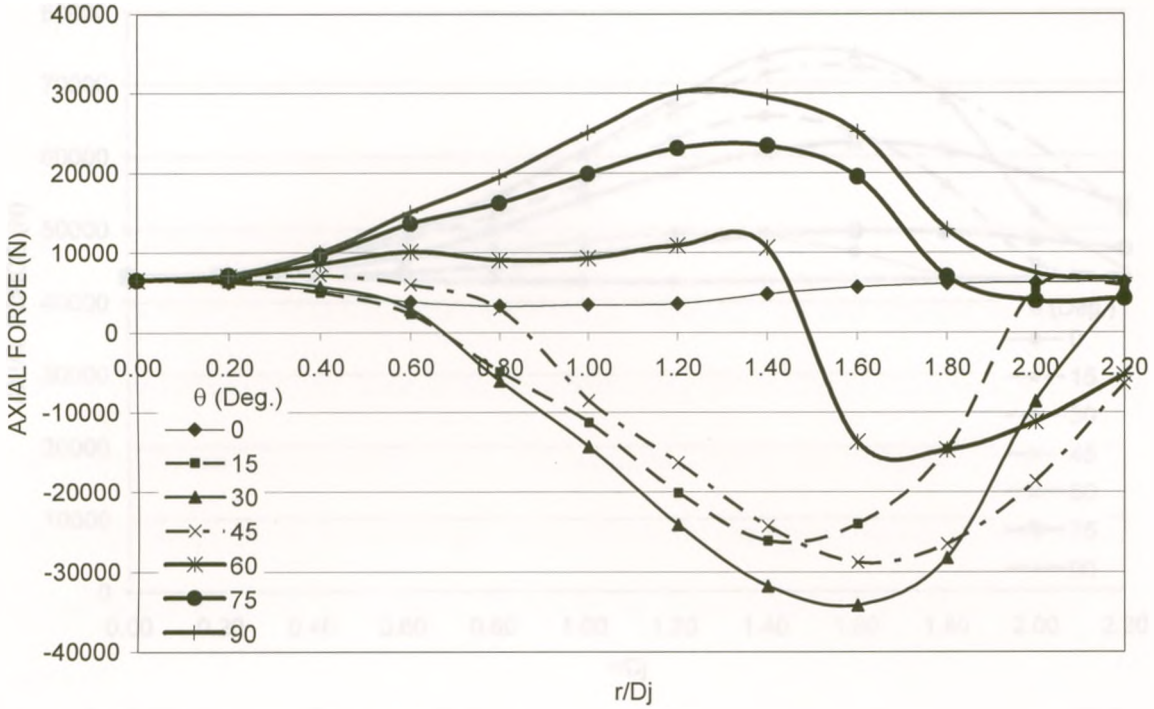

Figure 3.22 Variation of the axial force in the upper chord member 502 (connected to the guys) with r/D_j and θ, for D_j = 500 m.

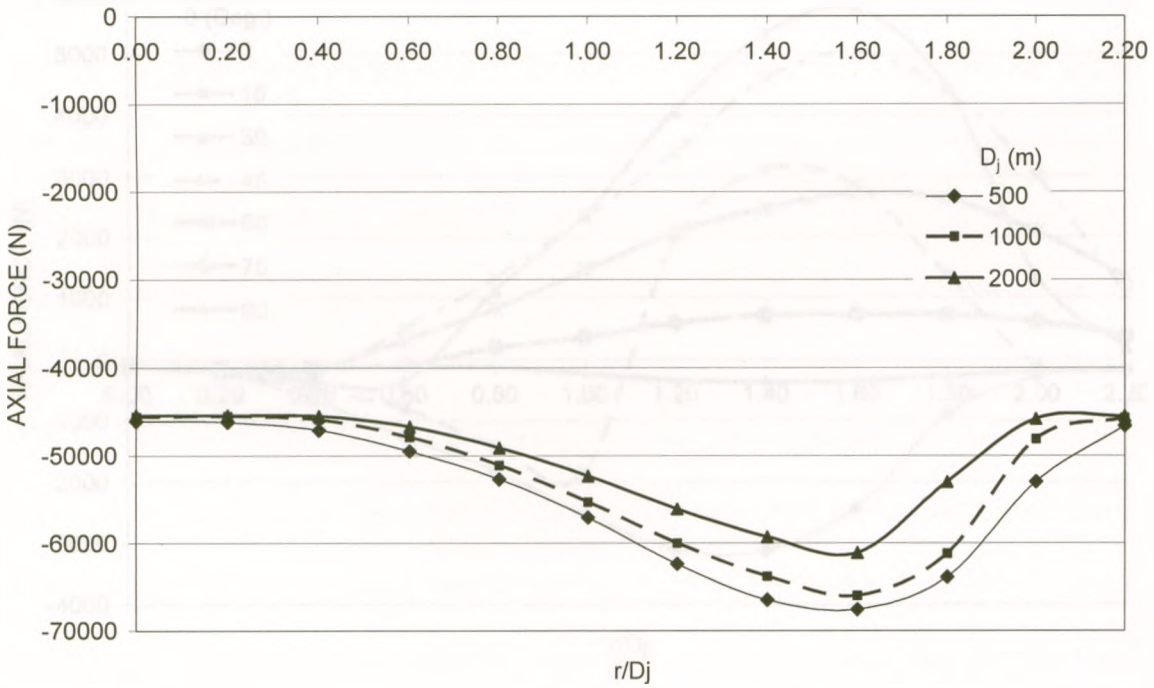

Figure 3.23 Variation of the axial force in the upper chord cross-arm member 581 with r/D_j and D_j, for $\theta = 30^o$.

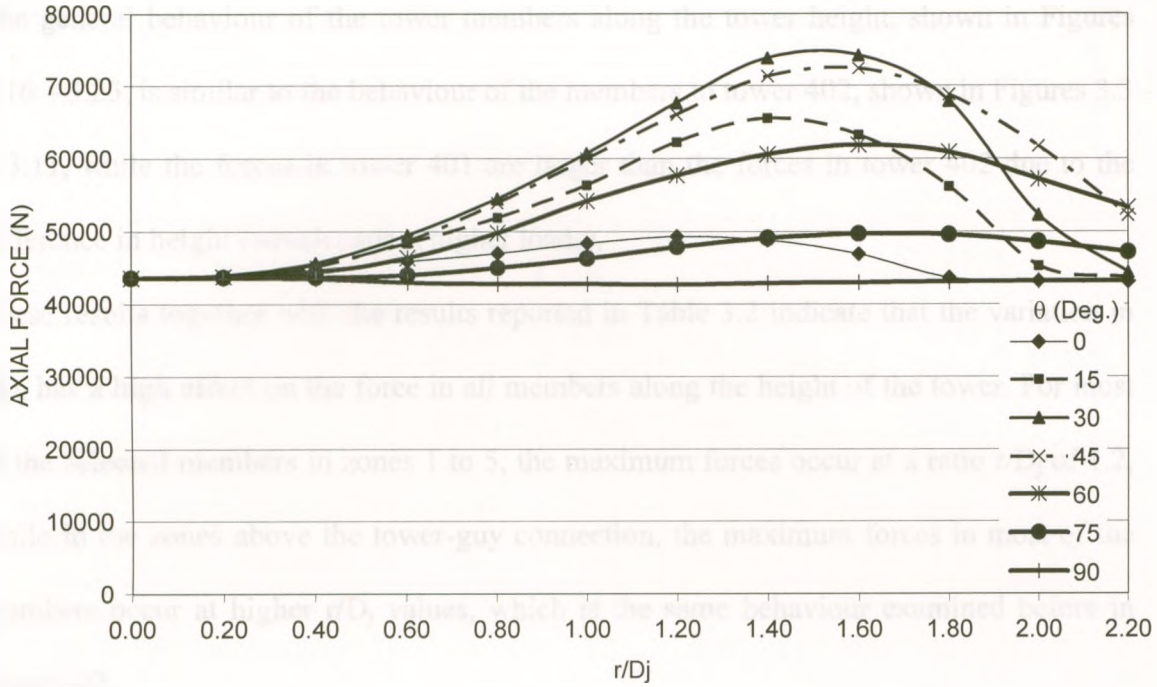

Figure 3.24 Variation of the axial force in the lower chord cross-arm member 616 to changing r/D_j and θ, for D_j = 500 m.

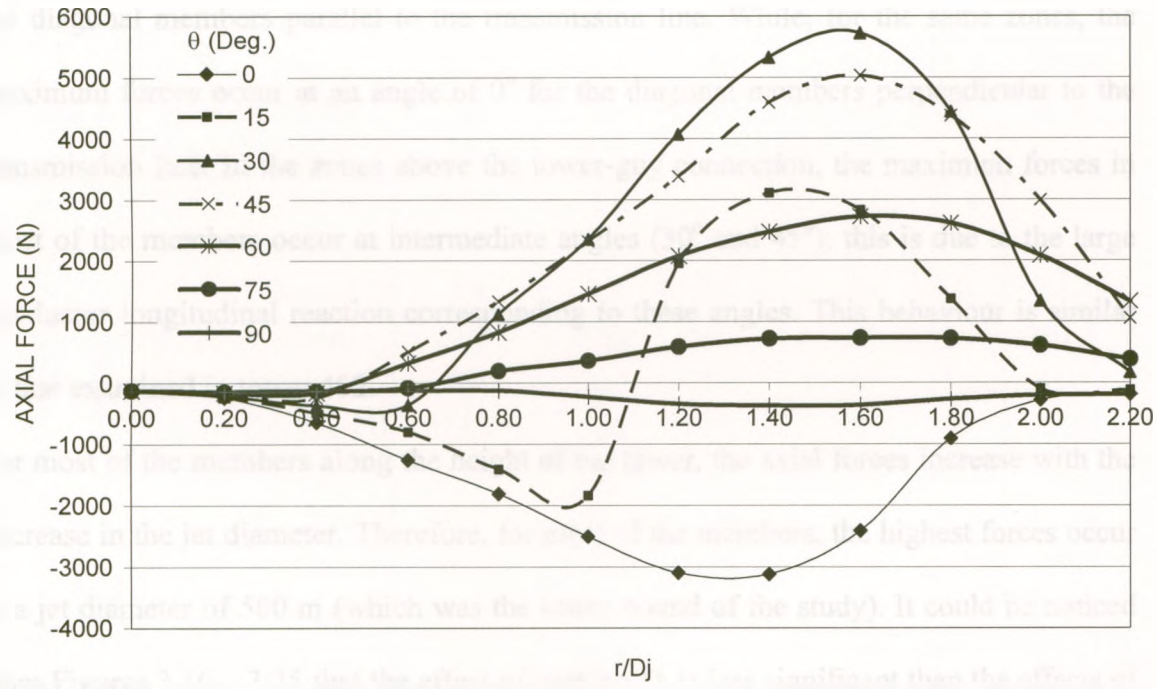

Figure 3.25 Variation of the axial force in chord member 675 to changing r/D_j and θ, for D_j = 500 m.

The general behaviour of the tower members along the tower height, shown in Figures 3.16 – 3.25, is similar to the behaviour of the members in tower 402, shown in Figures 3.3 – 3.11, while the forces in tower 401 are larger than the forces in tower 402 due to the difference in height (which causes higher loads).

These results together with the results reported in Table 3.2 indicate that the variation in r/D_j has a high effect on the force in all members along the height of the tower. For most of the selected members in zones 1 to 5, the maximum forces occur at a ratio r/D_j of 1.2, while in the zones above the tower-guy connection, the maximum forces in most of the members occur at higher r/D_j values, which is the same behaviour examined before in tower 402.

For zones 1 to 5, the maximum forces occur at an angle of 90^o for the chord members and the diagonal members parallel to the transmission line. While, for the same zones, the maximum forces occur at an angle of 0^o for the diagonal members perpendicular to the transmission line. In the zones above the tower-guy connection, the maximum forces in most of the members occur at intermediate angles (30^o and 45^o); this is due to the large conductor longitudinal reaction corresponding to these angles. This behaviour is similar to that examined in tower 402.

For most of the members along the height of the tower, the axial forces increase with the decrease in the jet diameter. Therefore, for most of the members, the highest forces occur at a jet diameter of 500 m (which was the lower bound of the study). It could be noticed from Figures 3.16 – 3.25 that the effect of varying D_j is less significant than the effects of varying r/D_j and θ, which is similar to the behaviour examined before in tower 402. Also, it could be noticed that, with the exception of the uppermost two zones members, the

internal forces resulting from both the ASCE and the downburst analyses have close values.

Table 3.2 Parametric study for the Manitoba Hydro tower type A-401-0

Zone		Member		ASCE	ASCE BWL	Downburst Loading				Capacity (KN)
		No.	Type	Axial Force (KN)	Axial Force (KN)	D_j (m)	r/D_j	θ	Axial Force (KN)	
Zone 1		*F42*	Chord	37.5	11.7	500	1.2	90°	41.6	162.1
		F12	Diagonal I	0.4	0.1	500	1.2	90°	0.5	14.3
		F8	Diagonal II	0.4	2.5	500	1.2	0°	1.5	8.5
Zone 2		*F75*	Chord	29.8	15.2	500	1.2	90°	27.2	178.6
		F118	Diagonal I	4.1	1.1	500	1.2	90°	5.3	15.3
		F91	Diagonal II	1.1	1.2	500	1.4	0°	0.9	11.0
Zone 3		*F330*	Chord	73.7	14.6	500	1.2	90°	76.0	178.6
		F281	Diagonal I	0.3	4.3	500	1.6	30°	1.1	15.3
		F224	Diagonal II	0.4	0.4	500	1.2	0°	1.2	11.0
Zone 4		*F350*	Chord	62.2	37.8	500	1.2	90°	73.0	209.4
		F418	Diagonal I	1.2	4.9	500	1.2	90°	2.0	11.6
		F361	Diagonal II	2.2	2.2	1000	1.2	0°	1.6	21.0
Zone 5		*F372*	Chord	48.2	31.8	500	1.2	90°	54.6	219.5
		F441	Diagonal I	3.0	6.2	500	1.2	90°	3.9	11.9
		F381	Diagonal II	3.4	3.5	500	1.2	0°	3.0	24.0
Zone 6	Tower	*F528*	Chord	9.9	209.0	500	1.6	30°	31.3	301.7
		F538	Diagonal I	0.6	74.3	500	1.6	30°	13.2	45.8
		F532	Diagonal II	13.7	12.6	1000	1.2	0°	8.8	45.8
	Guy C.	*F502*	U. Chord	2.8	227.0	500	1.6	30°	34.2	98.1
		F504	L. Chord	9.7	154.0	500	1.4	30°	29.4	171.9
	Conductor C.	*F581*	U. Chord	45.3	136.0	500	1.6	30°	67.6	65.2
		F616	L. Chord	47.9	166.0	500	1.6	30°	74.3	148.7
Zone 7		*F675*	Chord	3.0	95.5	500	1.6	30°	5.7	52.1
		F699	Diagonal I	0.2	0.3	500	2	45°	0.4	12.0
		F694	Diagonal II	2.7	96.0	500	1.6	30°	6.0	55.3

As shown in Table 3.2, for all of the selected members (with exception of member 581), the capacity of the members is larger than its maximum force. The member 581 (which is an upper chord cross-arm member) has a critical buckling capacity which is lower than the compression force in the member. This is due to the fact that the original design of that member is based on the typical loading (boundary layer uniform wind load, own weight and snow load). This design did not take into account the asymmetric load (which happened at an angle of 30^{o} for downburst loading) causing a high longitudinal reaction. This high longitudinal reaction causes the upper chord cross-arm member to suffer from a compression force that it was not designed to withstand.

3.3.3 THE EFFECT OF TURBULENCE ON THE FORCE IN THE TOWER MEMBERS

3.3.3.1 Turbulence quantification

The Wind Science and Engineering Research Centre at Texas Tech University recorded the gust front from a downdraft on the 4^{th} of June 2002 at the former Reese Air force base, located 20 Km West of Lubbock, Texas, USA. The set of data was fitted by Kim and Hangan (2007), with a set of CFD data corresponding to a downburst with a jet velocity of 29 m/s. Details of these records are provided by Gast (2003) and Orwig and Schroeder (2007).

The same set of data was used by Darwish et al. (2010) to extract the turbulent component. The turbulent component was extracted by subtracting the mean velocity from the full scale velocity reported on site. Further more, Darwish et al. (2010) included this turbulent component in the dynamic analysis of the conductors so as to evaluate the effect of turbulence on the conductor reactions acting at the tower cross-arms. This study

revealed that the response was affected by the background component, while the resonant component was damped out due large aerodynamic damping of the conductors. Hence, Darwish et al. (2010) concluded that the quasi-static analysis was sufficient in assessing the effect of both the mean and turbulent components. It was also concluded that the increase in the reactions due to the background (quasi-static) component of turbulence was 22.5 %. The same method of turbulence extraction used by Darwish et al. (2010) is applied within this chapter. More details of the process of turbulence extraction are provided by Darwish et al. (2010). The extracted turbulent component is added to the mean velocity produced from the scaled CFD data.

3.3.3.2 The sensitivity of the forces in the tower members to turbulence

According to Shehata et al. (2005), the value of the fundamental period of the tower was 0.58 s which is also within the range of the values reported by Amiri (2002) for guyed towers lower than 150 m in height. Darwish et al. (2010) conducted a fast Fourier transformation (FFT) transferring the full scale velocity from the time domain to the frequency domain. It was found that the major portion of the load occurred for a range of frequencies less than 0.05 Hz (corresponding to a range of loading period larger than 20 s). It can be noticed that the range of loading periods is much less than the fundamental period of the tower. Therefore, it is concluded that there is no need to analyze the structure dynamically. Accordingly, the analysis is conducted in a quasi-static manner with and without including the turbulent component as shown in Table 3.1. The axial forces in the members were compared to those resulting from normal wind loading according to the ASCE # 74 (2010) – explained in section 3.3.1 – and the same load in addition to the broken wire load case (BWL) as shown in Table 3.1. The normal wind load, according to ASCE # 74 (2010), exerts a perfectly symmetric load. On the other

hand, the broken wire load involves adding a longitudinal reaction at the cross-arm tips equal to 70 % of the pretension force in the conductor, creating an asymmetric load case which could be used in comparing it to the downburst loading cases at intermediate angles.

It could be noticed that for different members all over the height of the tower, the maximum axial force increases by 15 – 20 % as compared to the forces resulting from analyzing the tower under non-turbulent downbursts. For most of the members in zones 1 – 5, the axial forces due to the normal wind loading are within the same range as the values resulting from the downburst wind loading, with a maximum difference of 8 %. On the other hand, for most of the members in zones 6 and 7, the axial forces due to the normal wind loading are much less than the values resulting from the downburst wind loading. This is caused by the fact that the high forces resulting from the downburst wind loading occur at angles of 30^{o} and 45^{o} for most of the members due to the large longitudinal force from the conductors. However, this longitudinal reaction is less than the concentrated force (70 % of the pretension force) applied in the case of the broken wire load case. This is why the axial forces due to the broken wire load case are higher than the forces resulting from the downburst wind loading for the cross-arm members.

3.3.4 THE EFFECT OF MAGNITUDE OF CONDUCTORS PRETENSIONING

The parametric study done in Section 3.3.1 is repeated while assuming different values for the conductors' pretensioning force. For a fixed value of the conductors' span and weight, the pretensioning force is inversely proportional to the conductors' sag. As such, in this set of analysis, when the pretensioning force is multiplied by a certain factor, the sag is divided by the same factor.

The longitudinal reaction is a result of the second order effect due to the loss of symmetry in loading the conductors (which is apparent most incase of intermediate angles). Figure 3.26 shows the significant effect of the pretension force on the longitudinal reaction, this is due to the major effect of the pretension force on the conductors' stiffness. When the pretension force increases, the stiffness increases, and hence, the longitudinal reaction decreases.

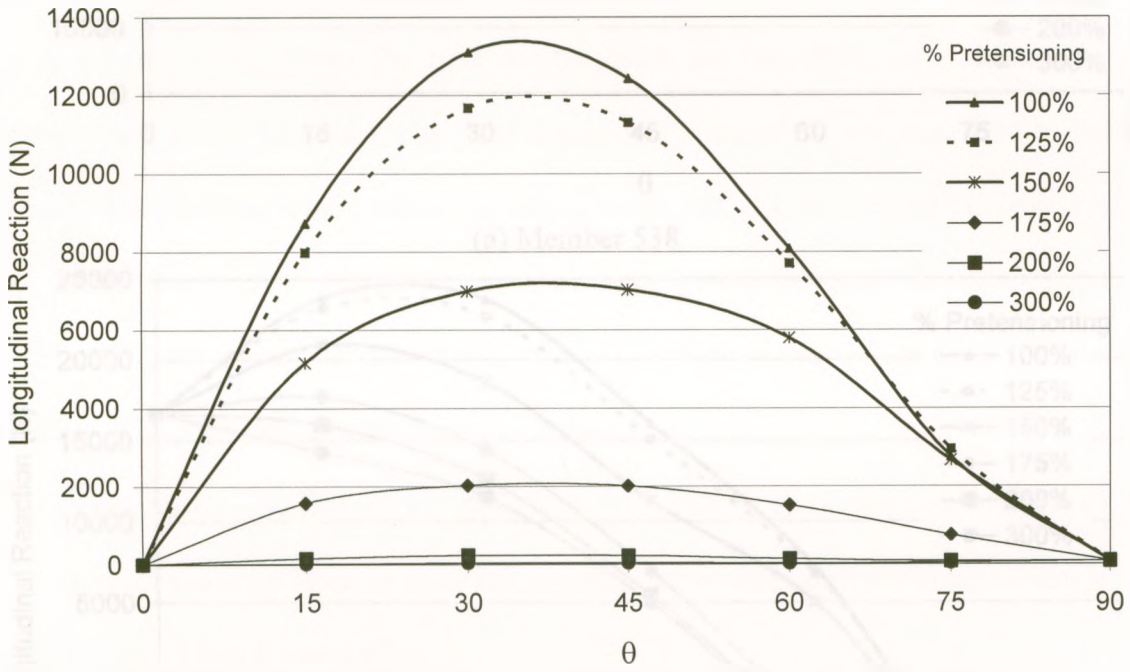

Figure 3.26 Variation of the conductor longitudinal reaction with θ and the pretensioning force, for $r/D_j = 1.6$ and $D_j = 1000$ m.

In Figures 3.26 and 3.27, the highest forces occur when the pretension force is kept to its original value of 82,344 N. While it could be seen that the effect of increasing the pretension force is significant until the pretension force is doubled, increasing this force more than that has a minor effect as very low values for the longitudinal reaction are achieved when the pretension force is doubled.

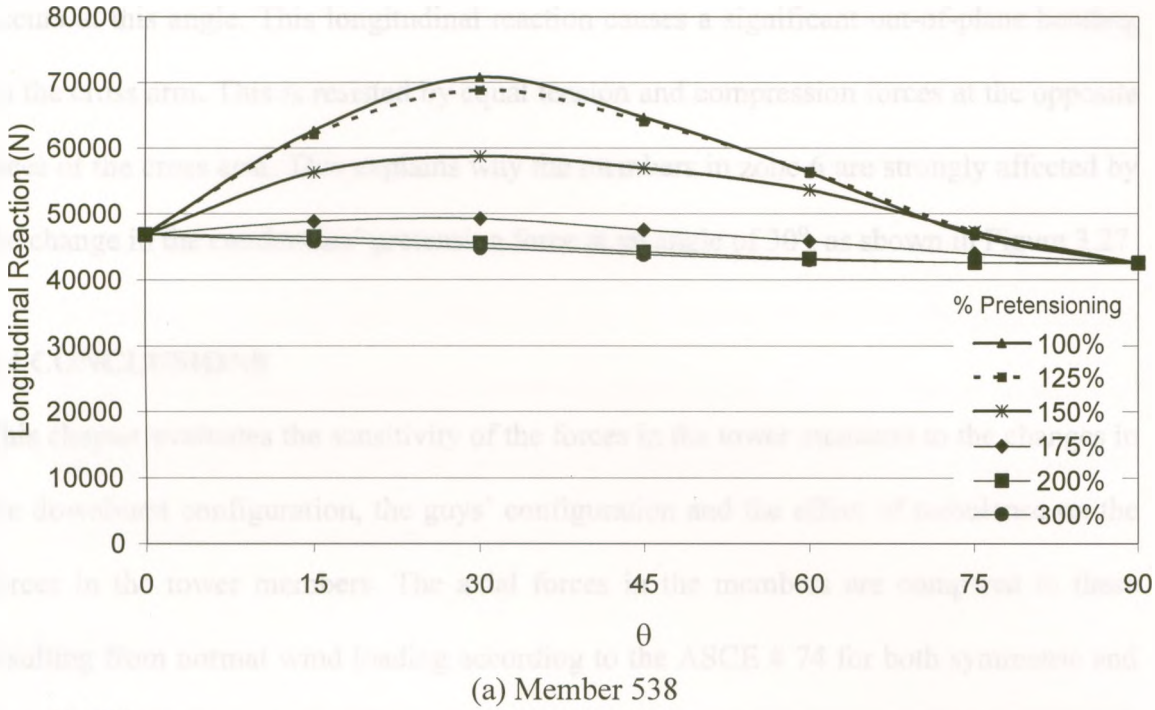

(a) Member 538

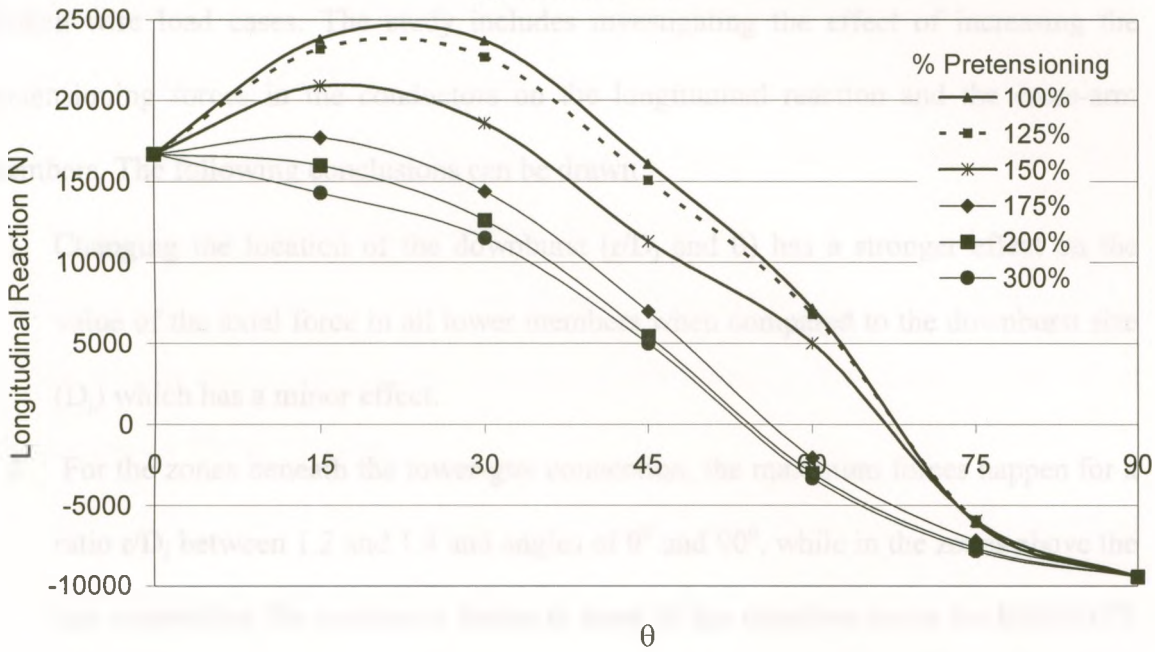

(b) Member 422

Figure 3.27 Variation of the forces in the chord members in Zone 6 with θ and the pretensioning force, for $r/D_j = 1.6$ and $D_j = 1000$ m.

It could be noticed that the effect of changing the pretension force is most prominent at an angle of 30°. It could be also noticed that the maximum value for the longitudinal reaction

occurs at this angle. This longitudinal reaction causes a significant out-of-plane bending on the cross arm. This is resisted by equal tension and compression forces at the opposite faces of the cross arm. This explains why the members in zone 6 are strongly affected by the change in the conductors' pretension force at an angle of 30°, as shown in Figure 3.27

3.4 CONCLUSIONS

This chapter evaluates the sensitivity of the forces in the tower members to the changes in the downburst configuration, the guys' configuration and the effect of turbulence on the forces in the tower members. The axial forces in the members are compared to these resulting from normal wind loading according to the ASCE # 74 for both symmetric and broken wire load cases. The study includes investigating the effect of increasing the pretensioning forces in the conductors on the longitudinal reaction and the cross-arm members. The following conclusions can be drawn:

1. Changing the location of the downburst (r/D_j and θ) has a stronger effect on the value of the axial force in all tower members when compared to the downburst size (D_j) which has a minor effect.
2. For the zones beneath the tower-guy connection, the maximum forces happen for a ratio r/D_j between 1.2 and 1.4 and angles of 0° and 90°, while in the zones above the guy connection the maximum forces in most of the members occur for higher r/D_j values and for angles between 15° and 45° due to the high longitudinal reaction of the conductors corresponding to these angles.
3. The maximum increase in the axial force in the members due to turbulence is 20%.
4. Doubling the pretensioning force in the conductors is sufficient enough to achieve very low values for the longitudinal reaction, hence reducing the forces in the cross-

arm members significantly. However, this would increase threat due to conductor breakage as more potential energy will be dissipated incase of conductor failure

5. The effect of changing the pretensioning force is most prominent at an angle of 30^0 as the maximum value for the longitudinal reaction occurs at this angle.
6. Increasing the height and the changing guy configuration causes negligible changes in the general behaviour of the tower members along the tower height in terms of the sensitivity to changing the downburst configuration, although the values of the forces in the tower members do change.

3.5 REFERENCES

American Society of Civil Engineers (2010). "Guidelines for electrical transmission line structural loading." *ASCE Manuals and Reports on Engineering Practice*, No. 74, N.Y.

Amiri, G. G. (2002). "Downbursts: meteorological features and wind field characteristics." *Computers and Structures*, 80(1), 349-364.

Darwish, M. M., El Damatty, A. A. and Hangan, H.M. (2010) "Dynamic characteristics of transmission line conductors and behaviour under turbulent downburst loading" *Wind and Structures*, 13(4), 327-346.

Davenport, A.G., (1962). "Buffeting of a suspension bridge by storm winds." *Journal of the ASCE Structural Division,* 88(3), 233–264.

Fujita, T. T. (1990). "Downbursts: meteorological features and wind field characteristics." *Journal of Wind Engineering and Industrial Aerodynamics*, 36(1), 75-86.

Gast, K.D., 2003. A comparison of extreme wind events as sampled in the 2002 Thunderstorm Outflow Experiment. Master's Thesis, Texas Tech University, Lubbock.

Gerges, R. R. and El Damatty, A. A. (2002). "Large displacement analysis of curved beams." *Proceeding of CSCE Conference*, Montreal, QC, Canada, ST 100.

Holmes, J.D., H.M. Hangan, J. L. Schroeder, C. L. Letchford, and K. D. Orwig (2008): "A forensic study of the Lubbock-Reese downdraft of 2002" *Wind and Structures, An International Journal*, 11(2), 137-152.

Hangan, H. and Kim, J. (2007). "Numerical simulations of impinging jets with application to downbursts" *Journal of Wind Engineering and Industrial Aerodynamics*, 95(4), 279–298.

Kim, J.D., Hangan, H. and Ho, T.C.E. (2007). "Downburst versus boundary layer induced loads for tall buildings." *Wind and Structures*, 10(5), 481-494.

Koziey, B. and Mirza, F. (1994). "Consistent curved beam element." *Computers and Structures*, 51(6), 643-654.

Loredo-Souza, A. M. and Davenport, A. G. (1998). "The effects of high winds on transmission lines." *Journal of Wind Engineering and Industrial Aerodynamics*, 74-76, 987-994.

Manitoba Hydro Transmission and Civil Design Department (1999), "Bipole 1 & 2 HVDC Transmission Line Wind Storm Failure on September 5, 1996 – Review of Emergency Response, Restoration and Design of These Lines", *Manitoba Hydro*, 98-L1/1-37010-06000, 54.

Mara, T. 2007. The Effects of Multi-Directional Winds on Lattice Sections. MEsc. Thesis, University of Western Ontario, London, Canada.

Mathur, R. K., Shah, A.H., Trainor, P.G.S. and Popplewell, N. (1987). "Dynamics of a Guyed Transmission Tower System." IEEE Transactions on Power Delivery, Vol. PWRD-2, No. 3, pp. 908-916.

Oliveira, M. I., Silva, J.G., Vellasco, P.C. , Andrade, S.A. and Lima, L. R. (2007). "Structural Analysis of Guyed Steel Telecommunication Towers for Radio Antennas." *Journal of the Brazilian Society of Mechanical Science & Engineering*, 29(2), 185-195.

Oakes, D. "Nelson river HVDC transmission line towers." Manitoba Power Conference EHV-DC, Winnipeg, Manitoba, Canada, June 7-10, 1971, 17

Orwig, K.D. and Shcroeder, J.L. (2007). "Near-surface wind characteristics of extreme thunderstorm outflows" *Journal of Wind Engineering and Industrial Aerodynamics*, 95(1), 565-584.

Shehata, A. Y., El Damatty, A. A., and Savory, E. (2005). "Finite element modelling of transmission line under downburst wind loading." *Finite Element in Analysis and Design*, 42(1), 71-89.

Shehata, A.Y. and El Damatty, A.A. (2007). "Behaviour of guyed transmission line structures under downburst wind loading" *Wind and Structures, An International Journal*, 10(3), 249-268

Shehata, A.Y. and El Damatty, A.A. (2008). "Failure analysis of a transmission tower during a microburst" *Wind and Structures, An International Journal*, 11(3), 193-208

Shehata, A. Y., Nassef, A.O. and El Damatty, A. A. (2008). "A coupled finite element-optimization technique to determine critical microburst parameters for transmission towers." *Finite Element in Analysis and Design*, 45(1), 1-12.

Xie, Qiang, Zhang, Yong and Li, Jie (1993). "Investigation on tower collapses of 500 kV Renshang 5237 transmission line caused by downburst 2." *Power System Technology*, 30(10), 59-63.

CHAPTER 4

EQUIVALENT LOADING OF GUYED TRANSMISSION LINE TOWERS TO RESIST DOWNBURSTS

4.1 INTRODUCTION

Electricity is mainly transmitted through conductors, supported by transmission towers. A major cause of power outages is the failure of the towers themselves. Hence, transmission towers are one of the most essential components in the electrical system. These failures have been often attributed to high wind loads in the form of tornadoes and downbursts.

The design codes of transmission towers have typically considered only normal wind loads associated with large-scale synoptic events such as hurricanes and typhoons. Within the last years, high intensity winds (HIW) associated with localized wind events have been subjected to research studies assessing their effects on the transmission line conductors and towers.

There are two main types of electrical transmission towers; self-supported and guyed towers. Self-supported towers carry and transfer loads only through the towers' members. When subjected to lateral loads, the behavior of a self-supported tower is similar to that of a cantilever. On the other hand, guyed towers rely on attached guys, anchored to the ground, to transfer the greater portion of the lateral loads. Guyed towers behave in a similar manner to a simple beam with an overhanging cantilever at the top region above the guys.

A downburst is defined as a strong downdraft that induces an outburst of damaging winds on, or near the ground (Fujita, 1990). The localized nature of the event and the variation of the wind field with time and space are the biggest challenges in performing structural

analysis. Figure 4.1 shows the jet diameter (D_j) and the location of the downburst center relative to the tower (represented by the polar coordinates r and θ). These parameters, together with the jet velocity (V_j), are the downburst characteristics that influence the distribution and magnitudes of the forces acting on the tower and the conductors, as described by Shehata and El Damatty (2007) and Shehata et al. (2008).

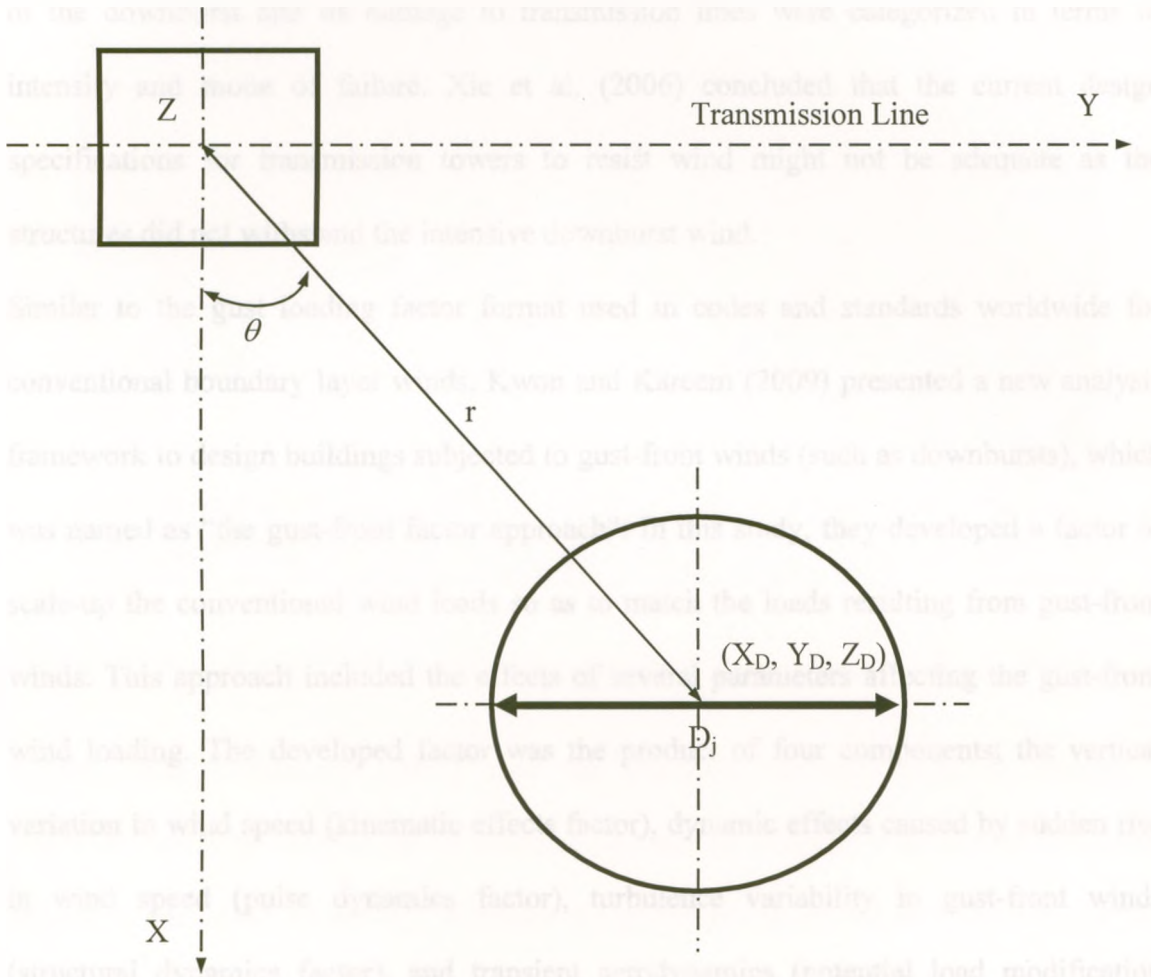

Figure 4.1 Horizontal projection of transmission line and downburst, (Shehata et al., 2005).

Hangan and Kim (2004, 2007) developed and validated a computational fluid dynamic (CFD) model simulating the spatial and time variations of the wind field associated with

downbursts. This fluid dynamic model simulates the large-scale fluctuating mean component of the downburst velocity field.

The results of field investigations of ten downburst-loaded towers that failed at the east of China were presented by Xie et al. (2006). The collapsed towers were classified according to the observed level of collapse severity, where the destruction characteristic of the downburst and its damage to transmission lines were categorized in terms of intensity and mode of failure. Xie et al. (2006) concluded that the current design specifications for transmission towers to resist wind might not be adequate as the structures did not withstand the intensive downburst wind.

Similar to the gust loading factor format used in codes and standards worldwide for conventional boundary layer winds, Kwon and Kareem (2009) presented a new analysis framework to design buildings subjected to gust-front winds (such as downbursts), which was named as "the gust-front factor approach". In this study, they developed a factor to scale-up the conventional wind loads so as to match the loads resulting from gust-front winds. This approach included the effects of several parameters affecting the gust-front wind loading. The developed factor was the product of four components; the vertical variation in wind speed (kinematic effects factor), dynamic effects caused by sudden rise in wind speed (pulse dynamics factor), turbulence variability in gust-front winds (structural dynamics factor), and transient aerodynamics (potential load modification factor).

Shehata et al. (2005) developed a structural analysis numerical model to evaluate the response of transmission lines under downburst loading. This structural analysis model is based on the finite element method. The two-dimensional non-linear curved frame element, shown in Figure 4.2, was used to simulate the conductors and three-dimensional

linear frame elements were used to simulate the tower members. In this model, the CFD data developed by Hangan et al. (2004) was incorporated and scaled-up based on the relative values between the characteristics of a prototype downburst and those used in the CFD model.

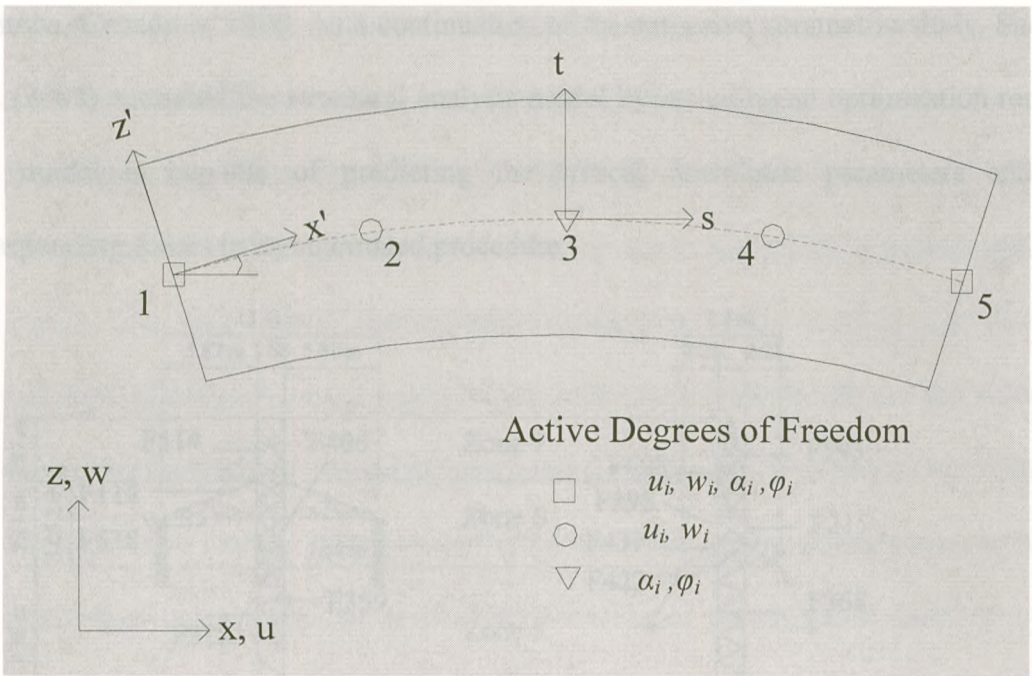

Figure 4.2 Two-dimensional consistent curved frame element (Shehata et al., 2005).

Shehata and El Damatty (2007) used this structural analysis model to conduct a parametric study by varying the jet diameter (D_j) and the location of the downburst center relative to the tower. Figure 4.3 illustrates the guyed transmission tower that was used to perform this parametric study. The analyzed tower was located in Manitoba, Canada, and was one of several towers that collapsed in 1996 during a downburst event. The critical downburst parameters (D_j, r and θ), leading to maximum forces in the tower members, were identified. The study revealed that the critical downburst parameters vary based on the type and location of the members. For example, the chord members of the tower main

body, the diagonal members of the tower main body, and the cross arms members are all found to have different critical downburst parameters. Shehata and El Damatty (2008) extended their numerical scheme by including a failure model for the tower members, which was used to study the progressive collapse of the guyed tower that failed in Manitoba, Canada in 1996. As a continuation of the extensive parametric study, Shehata et al. (2008) extended the structural analysis model by including an optimization routine. This model is capable of predicting the critical downburst parameters and the corresponding forces in an automated procedure.

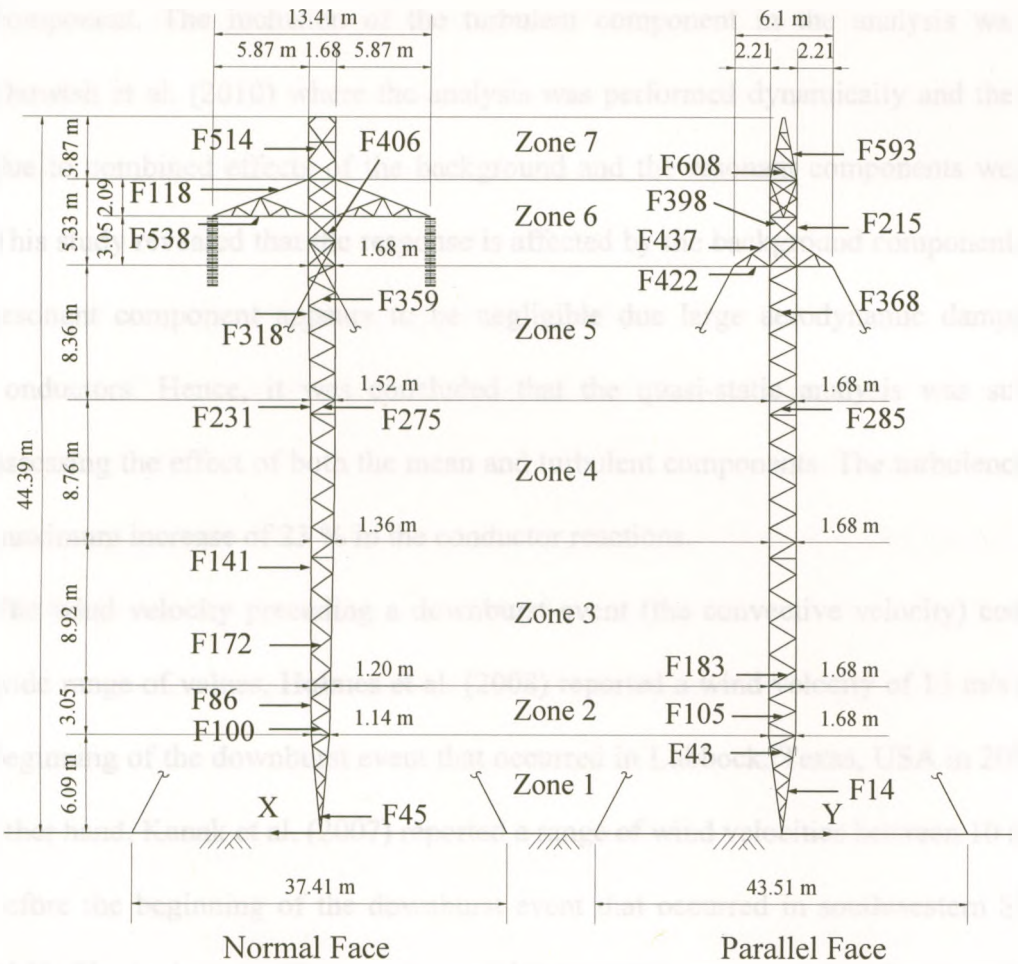

Figure 4.3 Geometry of the modeled lattice transmission tower Type A-402-0 (Shehata et al., 2005).

All of the above studies were conducted quasi-statically using the large-scale fluctuating mean component of the downburst wind field, as predicted numerically by Hangan et al. (2004, 2007). The sufficiency of a quasi-static analysis was justified as the period of the large-scale fluctuating mean component of the downburst load is significantly larger than the fundamental periods of oscillation of both the conductors and the tower. It is expected that the dynamic effect will be of more importance in analyzing the conductors rather than the tower as the conductors have typically larger fundamental periods compared to the tower and, consequently, are closer to the dominant periods of the turbulent component. The inclusion of the turbulent component in the analysis was done by Darwish et al. (2010) where the analysis was performed dynamically and the responses due to combined effects of the background and the resonant components were studied. This study revealed that the response is affected by the background component, while the resonant component appears to be negligible due large aerodynamic damping of the conductors. Hence, it was concluded that the quasi-static analysis was sufficient in assessing the effect of both the mean and turbulent components. The turbulence caused a maximum increase of 23 % in the conductor reactions.

The wind velocity preceding a downburst event (the convective velocity) could have a wide range of values. Holmes et al. (2008) reported a wind velocity of 15 m/s before the beginning of the downburst event that occurred in Lubbock, Texas, USA in 2002. On the other hand, Kanak et al. (2007) reported a range of wind velocities between 10 and 17 m/s before the beginning of the downburst event that occurred in southwestern Slovakia in 2003. The inclusion of the variation of this velocity component with the downburst event was not considered previously when assessing the structural behaviour of transmission lines under downbursts.

The current study focuses on developing equivalent load patterns of downbursts capable of representing the critical design load cases that initiate different modes of failure in guyed transmission towers. Within the first part of the chapter, a parametric study is performed using three different approaches regarding the assumed wind velocity. They involve setting up fixed values for: a) the reference velocity at a height of 10 m, b) reference velocity at the ground wire level, and c) the jet velocity. Hence, a conceptual relation between the reference velocity and the jet velocity is reached.

Following on that, the same parametric study is repeated while adding a spatially uniform convective velocity to the downburst event. Based on the first two parts of this chapter and the results of previous studies performed within this topic, a simple procedure for evaluating equivalent loads associated with three critical downburst configurations for guyed transmission towers is developed. The background and the details of this procedure are provided. Finally a case study is considered in order to validate the proposed procedure. In this case study, tower members internal forces are evaluated using this simplified method and are compared to those resulting from a comprehensive finite element parametric study. It is worth noting that Shehata et al. (2005) reported that the axial (vertical) velocity component of the downburst wind is much smaller than the radial (horizontal) component. Hence, the vertical component of the force is negligible and the current chapter takes only the horizontal component into account.

4.2 DESCRIPTION OF THE MODELED TOWERS

The modeling of the transmission line towers and its guys is done according to the approach developed by Shehata et al. (2005). Two guyed towers transmission line systems, belonging to the company Manitoba Hydro, are used in this study. The first

system is labelled type A-402-0. A sketch of one of the towers belonging to this line is shown in Figure 4.3. The tower is supported using four guys at a height of 38.0 m. Four conductors hang between every two consecutive towers; two from each cross arm side. The conductors are attached to the towers via insulator strings that are allowed to swing in two perpendicular plans. One ground wire is attached between each two consecutive towers at their top edges for lightning protection. The geometric and material properties of the conductors and the ground wires are provided by Shehata et al. (2005). The guys are made of grade 225 galvanized steel wires with 11.68 mm diameters. The insulator strings connecting the conductors to the towers have a length of 4.27 m.

The second transmission line tower is labelled as A-401-0. A sketch of one of the towers belonging to this line is shown in Figure 4.4. It is similar to type A-402-0 towers, with the exception of having a different height and different guy configurations. The tower type A-401-0 is 11 m higher than A-402-0. It has two additional guys located in the vertical plane perpendicular to the transmission line at a height of 19.81 m, while the other four guys are connected to the tower at a height of 45.85 m. The conductors are supported at a height of 48.90 m and the ground wire is supported at the top of the tower at a height of 55.07 m. The span covered by the conductor is 480 m for both towers.

A two-node linear three-dimensional frame element having three translational and three rotational degrees of freedom per node is used to model the tower members and the highly pretensioned guys. Each tower member is modelled using one element, while each guy is discritized into five elements. The system of global axes used in the finite element analysis of the entire transmission line/tower system is shown in Figure 4.1, where the Y-axis coincides with the direction of the transmission line, the Z-axis is the vertical direction, and the X-axis is perpendicular to the transmission line direction. Only one

intermediate tower located at (0, 0, 0), according to the system of the global axes, is considered in the finite element analysis. The stiffness of the adjacent towers is included in the analysis of the conductors and the ground wires as was discussed by Shehata et al. (2005). More details concerning the modeling of the transmission line are provided by Shehata et al. (2005).

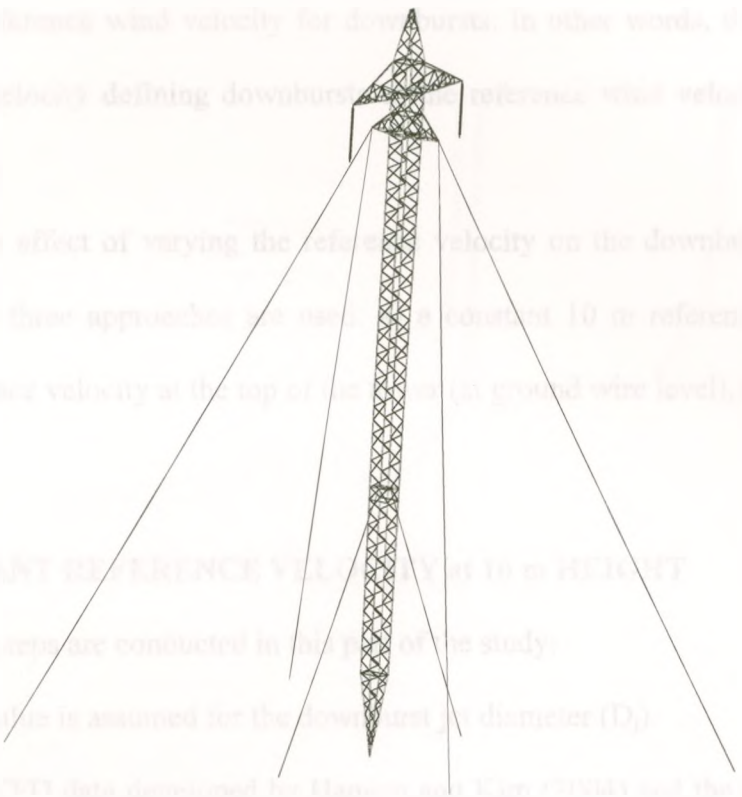

Figure 4.4 Geometry of the modeled lattice transmission tower Type A-401-0

4.3 SELECTION OF THE REFERENCE VELOCITY

In the studies conducted by Shehata et al. (2005), Shehata and El Damatty (2007, 2008) and Shehata et al. (2008), the structural performance of a guyed transmission tower was evaluated while varying the location of the centre of the downburst relative to the centre of the tower. As such, each study involved a large number of quasi-static analyses, each one corresponding to a specific downburst location. In all these analyses, the downburst

jet velocity was assumed to be constant. For a specific site location, the codes of practice and design specify a reference horizontal velocity defined at a certain reference height. In most codes, this reference height is given as 10 m. Meanwhile, the internal design specifications of some utility companies consider the conductor and ground wire levels as the reference heights. The objective of this section is determining a proper method for defining the reference wind velocity for downbursts. In other words, the objective is to relate the jet velocity defining downbursts to the reference wind velocities used in the design practice.

To do that, the effect of varying the reference velocity on the downburst wind field is assessed. Here three approaches are used: a) a constant 10 m reference velocity, b) a constant reference velocity at the top of the tower (at ground wire level), and c) a constant jet velocity.

4.3.1 CONSTANT REFERENCE VELOCITY at 10 m HEIGHT

The following steps are conducted in this part of the study:

1) A certain value is assumed for the downburst jet diameter (D_j).
2) Using the CFD data developed by Hangan and Kim (2004) and the scaling approach proposed by Shehata et al. (2005), the velocity field of this downburst is determined as a function of time and space.
3) The maximum radial velocity at a height of 10 m from the ground is identified within the entire space and time domains.
4) The velocity field is scaled such that this maximum velocity is equal to a certain selected reference velocity. A value of 32.6 m/s is selected as the reference velocity in

this parametric study. This corresponds to the reference wind velocity used in designing the transmission line considered later in this Chapter.

Steps 1 to 4 are repeated for different jet diameters and the maximum profiles of the wind field, corresponding to each diameter, are identified. Figures 4.5a and b show the vertical profile and the longitudinal profile of the maximum radial velocity for different jet diameters, respectively.

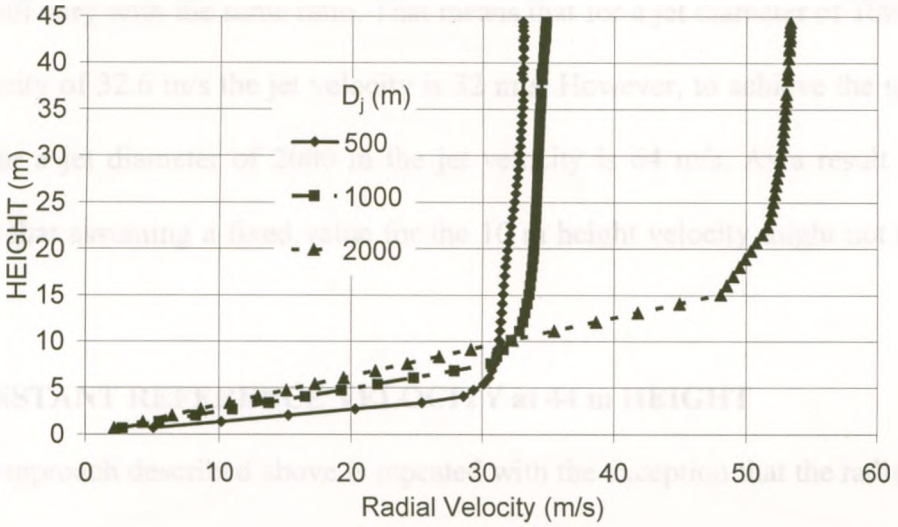

(a) Vertical profile.

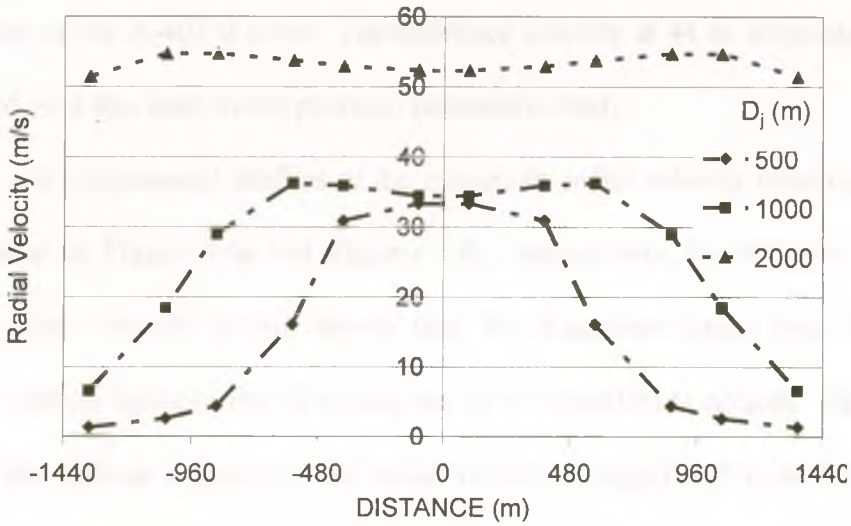

(b) Horizontal profile.

Figure 4.5 Profiles of the radial velocity having a constant 10 m velocity.

The profiles are plotted up to 44 m above the ground, which is the height of the A-402-0 towers. The figure shows that by maintaining a constant velocity at a 10 m height, the velocity increases significantly with the increase in the jet diameter. Beyond a value of 2000 m for the jet diameter, the downburst is enveloping the six spans studied. Hence, very large unrealistic values are obtained at the top level of the tower. This is due to the fact that to match a constant reference velocity while varying the jet diameter the jet velocity will vary with the same ratio. That means that for a jet diameter of 1000 m and a 10 m velocity of 32.6 m/s the jet velocity is 32 m/s. However, to achieve the same 10 m velocity for a jet diameter of 2000 m the jet velocity is 64 m/s. As a result, it can be concluded that assuming a fixed value for the 10 m height velocity might not be a good approach.

4.3.2 CONSTANT REFERENCE VELOCITY at 44 m HEIGHT

The same approach described above is repeated with the exception that the radial velocity is maintained constant at an elevation of 44 m, which represents the level of the ground wire at the top of the A-402-0 tower. The reference velocity at 44 m is maintained at the same value of 32.6 m/s used in the previous parametric study.

The vertical and longitudinal profiles of the maximum radial velocity resulting from this case are plotted in Figure 4.6a and Figures 4.6b, respectively, for different downburst parameters. The vertical profile shows that for diameters larger than 1000 m, a significant variation between the 10 m and the 44 m velocities is noticed. This is due to the fact that the vertical variation of the radial velocity is significant most for the higher jet diameters as the scale of the downburst event is magnified

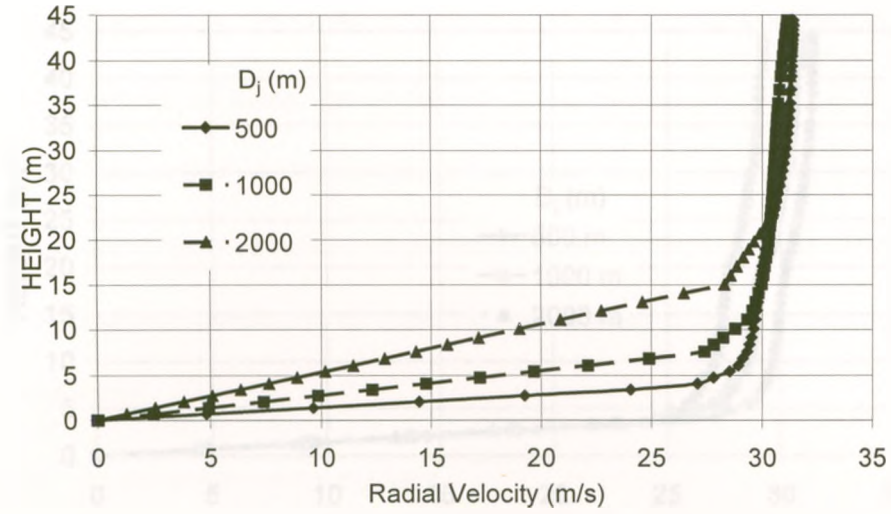

(a) Vertical profile.

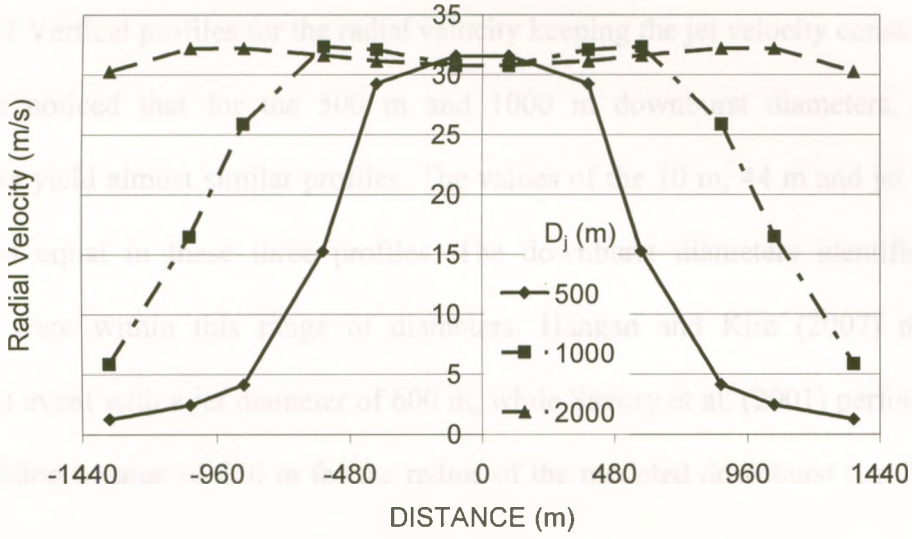

(b) Horizontal profile.

Figure 4.6 Profiles of the radial velocity having a constant 44 m velocity.

4.3.3 CONSTANT JET VELOCITY

The jet velocity is maintained constant at 29 m/s in this parametric study. The vertical profiles for the maximum radial velocities resulting from this case are given in Figure 4.7. It could be noticed that as the jet diameter decreases, the radial velocity increases. It could be also noticed that for the 500 m and 1000 m downburst diameters, the differences in the radial velocities decrease as the height increases such that the difference between the two profiles is very small at a height of 44 m.

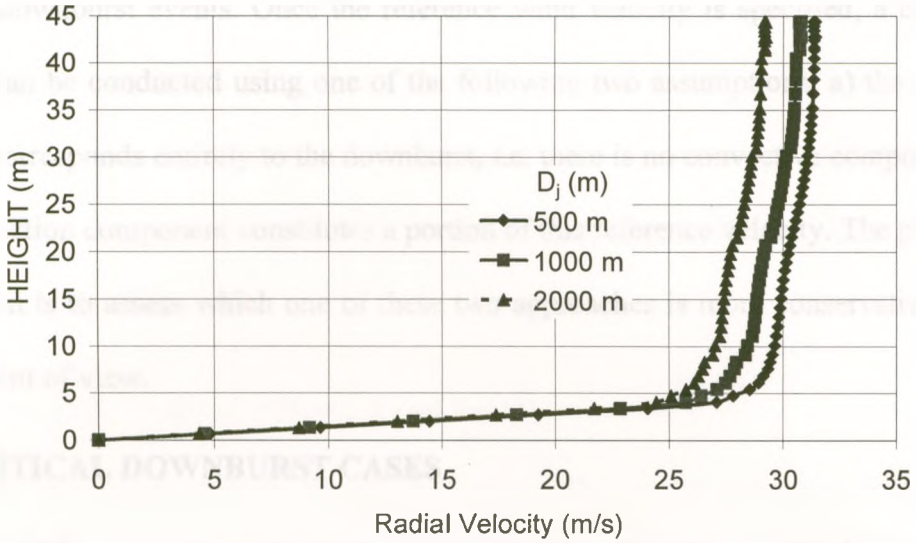

Figure 4.7 Vertical profiles for the radial velocity keeping the jet velocity constant.

It can be noticed that for the 500 m and 1000 m downburst diameters, the three approaches yield almost similar profiles. The values of the 10 m, 44 m and jet velocities are almost equal in these three profiles. The downburst diameters identified in the literature were within this range of diameters. Hangan and Kim (2007) reported a downburst event with a jet diameter of 600 m, while Savory et al. (2001) performed their analysis using a value of 650 m for the radius of the modeled downburst (i.e. D_j = 1300 m).

Based on the above discussion, the following approach is recommended regarding the reference and jet velocities:

1) The downburst parametric study can be conducted by varying the jet diameter.
2) The jet velocity can be assumed to be equal to the 10 m reference velocity.

4.4 CONVECTIVE VELOCITY EFFECT

A downburst event is usually accompanied with a convective velocity wind field. Unlike the downburst wind field, the convective velocity field does not have a significant variation in space. The direction and intensity of this convective velocity will vary for

different downburst events. Once the reference wind velocity is specified, a downburst analysis can be conducted using one of the following two assumptions: a) the reference velocity corresponds entirely to the downburst, i.e. there is no convective component, and b) a convection component constitutes a portion of this reference velocity. The purpose of this section is to assess which one of these two approaches is more conservative from a design point of view.

4.4.1 CRITICAL DOWNBURST CASES

The effect of the convective velocity is expected to depend on the specific downburst load case, which is defined by the location of the downburst relative to the structure. Shehata and El Damatty (2008) have identified three critical load cases that led to three distinct modes of failure for the transmission tower type A-402-0. Figure 4.8 shows the locations of the three critical downburst configurations relative to the targeted tower and the transmission line. Brief descriptions of these configurations and the failure modes are provided below.

4.4.1.1 Case 1 (D_J = 1000 m, r/D_J = 1.6 and $\theta = 30^o$)

This downburst configuration is critical for the conductors cross arms. As shown in Figure 4.8a, the location of the downburst is not symmetric with respect to the tower. As such, the conductors at opposite sides of the towers will be subjected to different loadings. Knowing that the maximum radial velocity occurs for r/D_j ranging between 1.2 and 1.4, it is worth noting that for this case the perpendicular distance from the downburst center to the transmission line is approximately $1.3D_j$. This could explain the large loads on the conductors for this load case. Due to the nonlinear behaviour of the conductors,

this loading will lead to a net force acting on the cross arms along the longitudinal direction of the conductors. As a result, the cross arm will be subjected to an out-of-plan bending effect. As a result, some chord members will be subjected to high compression forces, which they are not probably designed to resist under the load conditions considered in the design.

4.4.1.2 Case 2 (D_J = 500 m, r/D_J = 1.2 and $\theta = 0^o$)

This downburst configuration, shown in Figure 4.8b, can be critical to the members located at the main portion of the tower in the vicinity of the guys. The conductors are subjected to the largest accumulation of transverse forces in this case, which leads to large equivalent bending moment and shear force effects at the guys region.

4.4.1.3 Case 3 (D_j = 500 m, r/D_j = 1.2 and $\theta = 90^o$)

This downburst configuration is shown in Figure 4.8c. Almost no forces act on the conductors under such a configuration. The forces that act on the conductors for the first two cases cause negative moment on the cantilever part of the guyed tower, and consequently, reduce the positive moment developing at the middle potion of the tower. On the other hand, this case, which does not involve conductor forces, leads to maximum straining actions at the middle and bottom portions of the tower.

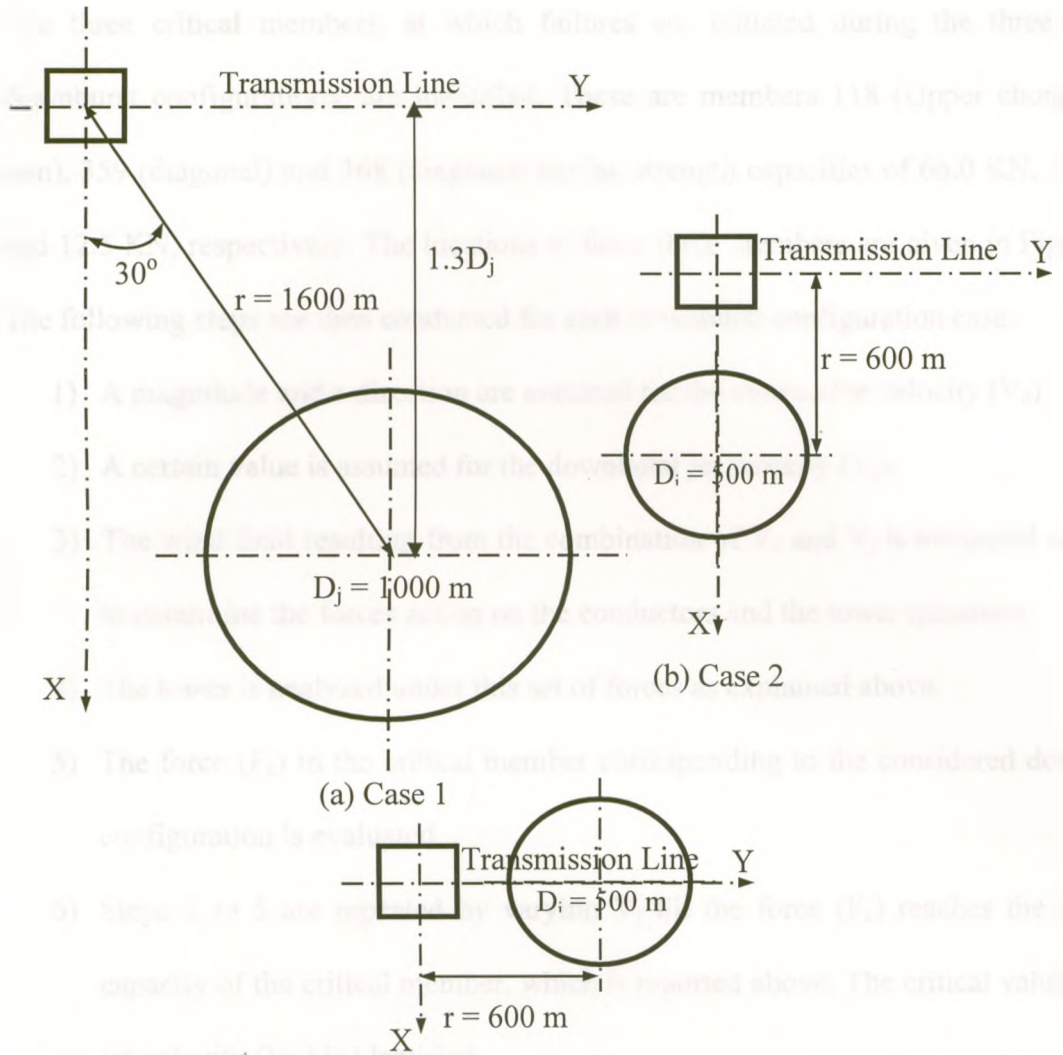

Figure 4.8 The three critical downburst load cases.

4.4.2 EFFECT OF THE CONVECTIVE VELOCITY COMPONENT

A parametric study is conducted in this section to assess the effect of the convective component when conducting downburst analyses. A total reference velocity will be assumed in the design procedure. This velocity can be assumed to be associated entirely with the downburst or can be assumed to contain a convective part. The objective of this part of the study is to check which assumption is more conservative from a design point of view.

The three critical members, at which failures are initiated during the three critical downburst configurations, are identified. These are members 118 (Upper chord cross-arm), 359 (diagonal) and 368 (diagonal) having strength capacities of 66.0 KN, 24.0 KN and 12.5 KN, respectively. The locations of these three members are given in Figure 4.3. The following steps are then conducted for each downburst configuration case:

1) A magnitude and a direction are assumed for the convective velocity (V_c).
2) A certain value is assumed for the downburst jet velocity (V_j).
3) The wind field resulting from the combination of V_c and V_j is evaluated and used to determine the forces acting on the conductors and the tower members.
4) The tower is analyzed under this set of forces as explained above.
5) The force (F_c) in the critical member corresponding to the considered downburst configuration is evaluated.
6) Steps 2 to 5 are repeated by varying V_j till the force (F_c) reaches the strength capacity of the critical member, which is reported above. The critical value for the jet velocity (V_{jc}) is identified.
7) Steps 1 to 6 are repeated while varying the magnitude and direction of the convective velocity (V_c) within a range of 0 and 20 m/s with an increment of 5 m/s.

For the 1st and 2nd cases, the convective velocity is found to have its highest effect when it acts in the direction normal to the transmission line. On the other hand, for the 3rd case, the convective velocity is found to have its highest effect when it is in the direction parallel to the transmission line. The results of this study are provided in Table 4.1. The summations of the convective velocity and the critical jet velocity for each case are evaluated to give the total velocity (V_t). As mentioned earlier, the jet velocity can be

considered to be almost equal to the 10 m reference velocity. As such, the calculated total velocities represent the measured 10 m wind speed at which failures can potentially initiate in the considered tower. The following observations can be drawn from these results:

1) For the asymmetric case (failure mode 1), the minimum value for the total velocity of 40 m/s corresponds to the case of zero convective velocity. As such, for this downburst configuration, it is more conservative to assume that the wind field results totally from the downburst with no convective component.
2) For the other two downburst configurations, regardless of the value of the convective component, the total velocity has always a value of 64 m/s. This means that due to the symmetry of loading within these two cases the effect of the convective component is nearly equal to that of the velocity due to the downburst as the summation of the velocity causing failure is always constant.

Table 4.1 Parametric study measuring the effect of the convective velocity.

V_c (m/s)	Failure mode 1: member 118			Failure mode 2: member 359			Failure mode 3: member 368		
	V_{jc} (m/s)	V_t (m/s)	F_{max} (KN)	V_{jc} (m/s)	V_t (m/s)	F_{max} (KN)	V_{jc} (m/s)	V_t (m/s)	F_{max} (KN)
0	40	40	-66.2	64	64	24.6	64	64	13.0
5	38	43	-68.1	59	64	24.4	59	64	12.9
10	37	47	-69.9	54	64	24.3	54	64	12.8
15	36	51	-70.4	49	64	24.2	49	64	12.7
20	35	55	-69.9	44	64	24.1	44	64	12.6

4.5 EQUIVALENT PATCH LOAD APPROACH

The major objective of this Chapter is to develop approaches for evaluating simple loading that can be used by design engineers to simulate the downburst critical load cases. The numerical model developed by Shehata et al. (2005) is used to establish these

approaches. A description for the philosophy behind each approach is provided in this section.

4.5.1 APPROACH 1: SIMULATING CRITICAL LOAD CASE 1

The philosophy behind this approach is based on the following findings established in previous studies as well as in the current study:

1- Downburst configuration #1, shown in Figure 4.8a, is critical mainly for the conductor cross arms. Hence, it can be used in designing cross arms members.

2- The forces affecting the cross arms result mainly from the longitudinal and transverse components of the reaction forces that develop at the tip of the cross arms as a results of the wind forces acting on the conductors.

3- The typical loading profile along the conductors resulting from this load case is shown in Figure 4.9a. As shown in the figure, this velocity in not symmetric with respect to the middle tower (which is the tower of interest). This asymmetric load can be replaced by the equivalent uniform asymmetric patch load shown in Figure 4.9b. In addition to the transverse force, this profile leads to a longitudinal force acting on the cross arm as a result of the nonlinear behaviour of the conductors. The typical forces transferred from the conductors to the cross-arms due to that load case are shown in Figure 4.10, where the R_{TRANS} and R_{LONG} represent the transverse and the longitudinal reactions of the conductors, respectively. The other forces acting on the cross arm members are quite small compared to R_{TRANS} and R_{LONG} and can be neglected. The springs shown in Figure 4.9a represent the combined stiffness of the insulator and the towers. The procedures for evaluating these properties is provided bye Shehata et al. (2005).

4- In evaluating R_{LONG}, it is conservative to use the configuration shown in Figure 4.9b, in which the loading shown in Figure 4.9a is approximated with a uniform load (W) acting on one side and no loading on the other side of the tower, as shown in Figure 4.9b.

5- The value of the uniform load (W) is related to the velocity (V) as follows:

$$\mathbf{W = 0.5\rho D C_d V^2} \qquad \mathbf{(4.1)}$$

where D is the projected dimension of the conductor perpendicular to the wind flow, ρ is the air density, and C_d is the drag coefficient (equal to 1 for conductors according to ASCE 74 (2010)).

6- In view of the discussion carried out in Section 4.3, V can be considered equal to the 10 m reference velocity (for a jet diameter of 500 m).

7- Once W is evaluated, the longitudinal reaction can be obtained by performing nonlinear structural analysis for the conductor under the load configuration shown in Figure 4.9b.

8- This nonlinear analysis should take into account the effects of sag, pretension force, large deformation and the conductor weight. It is known that the sag (S), the pretension force (T), the span (L) and the conductors' weight (W_c) are related by the following relation:

$$\mathbf{T = W_c L^2/(8S)} \qquad \mathbf{(4.2)}$$

9- It is not conservative to neglect the relatively small transverse load acting on the left side of the tower in Figure 4.9a. The average velocity perpendicular to the conductor is approximately half of the jet velocity. Hence, the distributed wind load on the partially loaded span (L) is approximately one quarter of the

distributed wind load on the fully loaded span (L). Therefore the transverse reaction (shown in Figure 4.10) can be calculated as follows:

$$\mathbf{R_{TRANS} = 0.5WL + 0.5(W/4)L = 0.625WL} \quad \textbf{(4.3)}$$

10- The cross arm members can be designed to resist the internal forces resulting from the forces R_{TRANS} and R_{LONG} acting on the conductors as illustrated in Figure 4.10, taking into consideration that both forces are reversible.

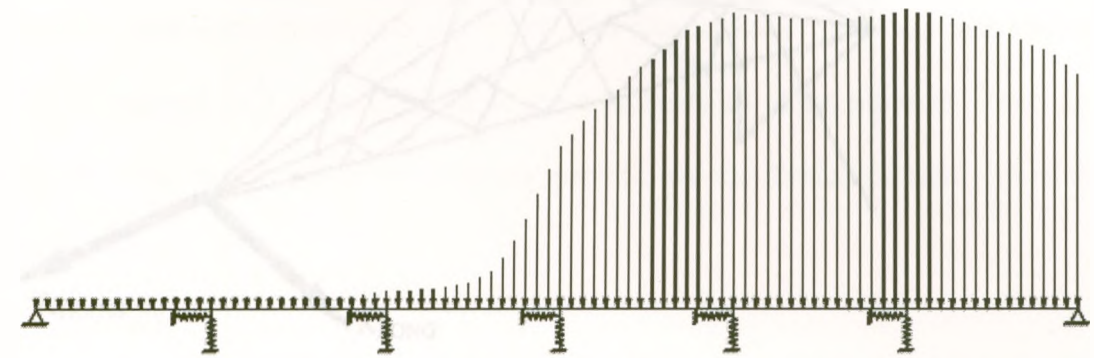

(a) Downburst load.

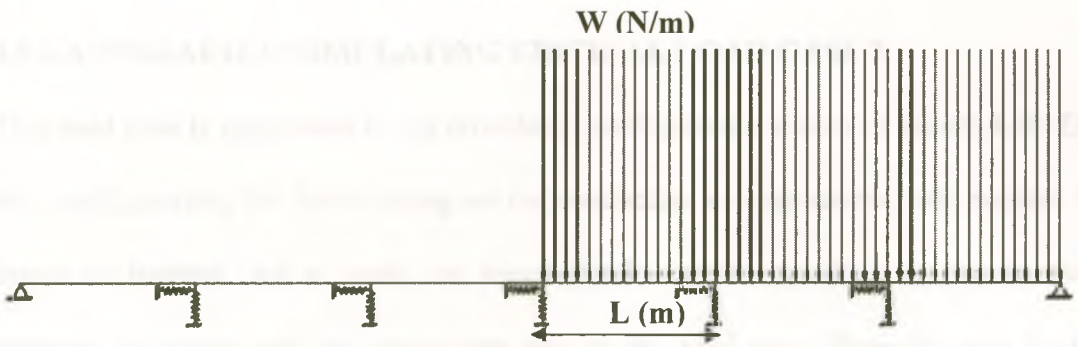

(b) Equivalent load.

Figure 4.9 The load distribution along the conductor for case 1.

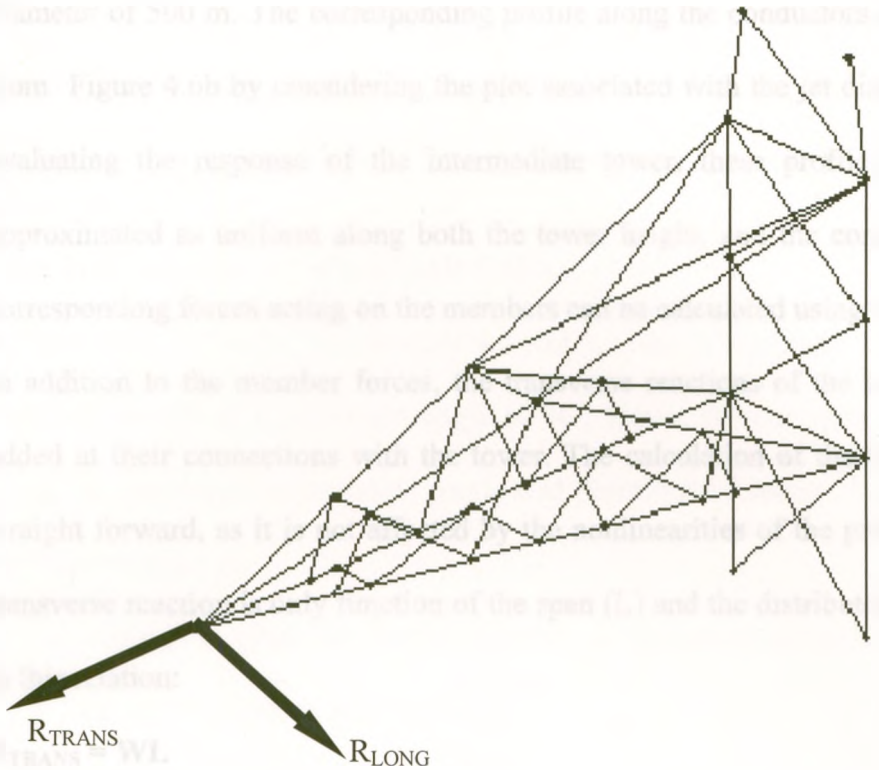

Figure 4.10 Forces transferred from the conductors to the cross-arms due to case 1.

4.5.2 APPROACH 2: SIMULATING CRITICAL LOAD CASE 2

This load case is equivalent to the downburst configuration shown in Figure 4.8b. Due to this configuration, the loads acting on the conductors are symmetric with respect to the tower of interest. As a result, no longitudinal reaction develops at the intersection between the tower and the conductors due to this load case. Basically, this load case should be considered when designing the tower members in the plane perpendicular to the transmission line. It is sufficient to define a velocity profile due to this load case. The associated forces acting on the members and the conductors due to this profile can be then easily determined using available procedures. Based on the studies conducted by Shehata and El Damatty (2007) and Shehata et al. (2008), it is concluded that the critical jet diameter for this load case is 500 m. The vertical profile of the velocity field of this load case can be obtained from Figure 4.7 by considering the plot associated with a jet

diameter of 500 m. The corresponding profile along the conductors can be also obtained from Figure 4.6b by considering the plot associated with the jet diameter of 500 m. For evaluating the response of the intermediate tower, these profiles can be reasonably approximated as uniform along both the tower height, and the conductors lengths. The corresponding forces acting on the members can be calculated using standard procedures. In addition to the member forces, the transverse reactions of the conductors should be added at their connections with the tower. The calculation of the transverse reaction is straight forward, as it is not affected by the nonlinearities of the problem. Basically, the transverse reaction is only function of the span (L) and the distributed load (W) as shown in this relation:

$$R_{TRANS} = WL \qquad (4.4)$$

4.5.3 APPROACH 3: SIMULATING CRITICAL LOAD CASE 3

This load case is equivalent to the downburst configuration shown in Figure 4.8c. Due to this configuration, the load acting on the conductors is negligible. As a result, the longitudinal and transverse reactions at the intersection between the tower and the conductors due to this load case are negligible. This load case should be considered when designing the tower members in the plane parallel to the transmission line. The vertical profile of the velocity field associated with this load case is shown in Figure 4.7 for the jet diameter of 500 m. Similarly, for evaluating the response of the tower, this profile can be reasonably approximated as uniform along the tower height.

4.6 EVALUATION OF LOADS FOR GUYED TRANSMISSION TOWERS

As described previously in Sections 4.3 and 4.4, the critical load cases for the guyed transmission towers are three cases; the asymmetric load case, the symmetric load case at

a projection angle of 0^{o}, and the symmetric load case at a projection angle of 90^{o}. Hence the structure is analyzed based on these three load cases and the members designed for the maximum values of the axial forces resulting from these three cases.

4.6.1 THE ASYMMETRIC LOAD CASE

As previously described in Sections 4.4 and 4.5, the critical load case for the cross-arm members occurs at a projection angle of 30^{o}. Hence these members could be designed using the equivalent asymmetric patch load described in section 4.5.1 through applying the following steps:

1. Assume a value for the jet velocity (a discussion about the selection of V_j is carried out later in Section 4.6.4).
2. Assume a uniform profile for the wind field along both the tower height, and the conductors' lengths with a magnitude equal to the assumed jet velocity.
3. Calculate the distributed load (W) acting on the conductors using Equation 4.1.
4. Determine the span (L), the sag (S) and the conductor self weight (W_c).
5. Acquire the longitudinal reaction acting on the tower through performing a nonlinear analysis.
6. Calculate the transverse reaction using equation 4.3.
7. Apply the loads transferred from the conductors at the tips of the cross-arms.
8. Analyze the tower for the applied loads, taking into account that the loads are reversible.

4.6.2 LOAD CASE 2

As described previously in Sections 4.4 and 4.5, the critical load case for the diagonal members perpendicular to the transmission line occurs at a projection angle of 0^{o}. Hence

these members could be designed using the equivalent symmetric patch load described in Section 4.5.2 through applying the following steps:

1. Assume a value for the jet velocity (a discussion about the selection of V_j is carried out latter in section 4.6.4).
2. Assume a uniform profile for the wind field along both the tower height, and the conductors' lengths with a magnitude equal to the assumed jet velocity.
3. Calculate the distributed load (W) acting on the conductors using Equation 4.1.
4. Calculate the transverse reaction using Equation 4.4.
5. Calculate the corresponding forces acting on the members using standard procedures, e.g ASCE # 74 (2010).
6. Apply the load transferred from the conductors at the tips of the cross-arms.
7. Analyze the tower for the applied loads, taking into account that the loads are reversible.

4.6.3 LOAD CASE 3

As described previously in sections 4.4 and 4.5, the critical load case for the diagonal members parallel to the transmission line and the chord members occurs at a projection angle of 90^{o}. No forces act on the conductors due to this load case. The following steps are applied in this load case:

1. Assume a value for the jet velocity.
2. Assume a uniform profile for the wind field along the tower height with a magnitude equal to the assumed jet velocity.
3. Calculate the corresponding forces acting on the members using standard procedures, e.g ASCE # 74 (2010).

4. Analyze the tower for the applied loads, taking into account that the loads are reversible.

4.6.4 WIND SPEED METEOROLOGICAL DATA

Manitoba Hydro (1999) prepared a report that studied the 1996 failure incident. In this report, it was estimated that gust speeds near the failed towers were in the range of 42 – 50 m/s (150-179 km/hr). This is reasonably consistent with the asymmetric load case discussed in sections 4.3 and 4.4, which shows that the asymmetric downburst, having a jet velocity of 40 m/s, causes the tower cross-arm to fail.

Kanak et al. (2007) reported a downburst event that occurred in southwestern Slovakia in 2003. Within that event, 18 electric transmission line towers were destroyed. Seven of them fell down in a 1.2 km line, where the transmission line was almost perpendicular to the track of the storm. The company responsible for designing the transmission line reported that the structure could withstand a wind speed of 160 Km/hr (44.4 m/s). This suggested that the velocity acting on the transmission line itself was higher than 44.4 m/s. This high velocity causing failure (which could be the maximum velocity within the event) was localized at the location of the failed towers (Kanak et al., 2007).

Dotzek and Friedrich (2009) reported that the peak speeds reached up to 55 m/s during a downburst event that occurred in March, 2001 in the suburbs of Munich, Germany. Within the same study, two other downburst events that occurred within the same region of Munich suburbs in June and July, 2002 were reported. Each one of these events had a peak speed of about 40 m/s.

Unfortunately, the meteorological data are not sufficient to estimate a downburst velocity for various locations. The above studies point out that downburst velocities can reach and

exceed a value of 40 m/s. The wind speeds specified in the building codes are based on database for historical measurements at various locations. It is expected that this database includes some downburst events. As such, with the lack of meteorological data specific for downbursts, it is recommended to use the wind speed values specified in the building codes to estimate the 10 m reference velocity, which as previously mentioned, can be assumed to be equal to the downburst jet velocity.

4.6.5 THE EFFECT OF TURBULENCE

In the ASCE 74 code (2010), the design speed is considered to be a gust velocity. Other design codes are based on a mean velocity. Darwish et al. (2010) used a set of records provided by Gast (2003) and Orwig and Schroeder (2007) to study the effect of downburst turbulence on the conductor reactions. It was concluded that resonant component due to turbulence was damped out due to high aerodynamic damping. It was also concluded that the increase in the reactions due to the background component of turbulence was 22.5 %. Based on the above discussion, the 10 m velocity for the downburst can be assumed to be equal to the reference gust velocity specified in the codes. Alternatively, if the reference velocity represents a mean value, it can be still used in the downburst analysis while magnifying the conductor reactions by a value of 22.5%.

4.7 SOLVED EXAMPLE

An example is considered in this section in order to assess and illustrate the proposed approaches for the evaluation of downburst loads. The transmission tower type A-402 is considered in this example. The loads associated with the three equivalent load cases are evaluated as described in Section 4.6. The tower is analyzed under the three load cases. The forces in the tower members are evaluated, and the maximum force in each member of the tower is determined.

An extensive parametric study is conducted for the same tower by performing a large number of analyses using the time and spatially varying downburst wind field as described by Shehata et al. (2005). This downburst wind field featured a constant jet velocity of 29 m/s. The turbulent component described by Darwish et al. (2010) is added to the downburst field. The absolute maximum forces resulting from this parametric study are determined. Hence, the 10 m reference velocity could be considered approximately equal to the jet velocity – which was 29 m/s. Consequently, the gust design velocity which is used in the equivalent method is approximately 33 m/s.

Comparisons are made between the maximum forces obtained from the extensive parametric study and the envelope of forces obtained from the three simplified load cases. Results of the study are presented in Table 4.2 for specific members of the tower. The locations of these selected members are shown in Figure 4.3. In Table 4.2, the critical downburst configuration for each one of the selected members, resulting from the parametric study, is provided. Also, in the last column of the table the specific simplified load case that leads to a maximum axial force in each member is given. A discussion of the results is provided in Section 4.7.3.

Table 4.2 Results of the analysis of tower 402 under the equivalent loads in comparison to the downburst load.

Zone		Member		Downburst Load				Equivalent load	
		No.	Type	D_j (m)	r/D_j	θ	Axial Force (KN)	Axial Force (KN)	Governing case
1		*14*	Chord	500	1.2	90°	33.2	34.1	Symmetric, 90°
		43	Diagonal I	500	1.4	90°	0.3	0.3	Symmetric, 90°
		45	Diagonal II	500	1.2	0°	2.5	2.6	Symmetric, 0°
2		*86*	Chord	500	1.2	90°	37.6	38.2	Symmetric, 90°
		105	Diagonal I	500	1.2	90°	4.3	4.5	Symmetric, 90°
		100	Diagonal II	500	1.4	0°	1.5	1.7	Symmetric, 0°
3		*141*	Chord	500	1.2	90°	50.7	51.3	Symmetric, 90°
		183	Diagonal I	500	1.2	90°	3.8	4.1	Symmetric, 90°
		172	Diagonal II	500	1.2	0°	0.5	0.6	Symmetric, 0°
4		*231*	Chord	500	1.2	90°	51.4	52.1	Symmetric, 90°
		285	Diagonal I	500	1.2	90°	1.5	1.6	Symmetric, 90°
		275	Diagonal II	500	1.2	0°	5.1	5.2	Symmetric, 0°
5		*318*	Chord	500	1.2	90°	42.7	43.5	Symmetric, 90°
		368	Diagonal I	500	1.2	90°	3.4	3.6	Symmetric, 90°
		359	Diagonal II	500	1.2	0°	6.8	7.0	Symmetric, 0°
6	Tower	*215*	Chord	500	1.6	22.4	22.4	24.9	Asymmetric
		398	Diagonal I	500	1.6	13.5	13.5	15.0	Asymmetric
		406	Diagonal II	500	1.8	12.6	12.6	13.9	Asymmetric
	Guy C.	*437*	U. Chord	500	1.6	35.4	35.4	35.9	Asymmetric
		422	L. Chord	500	1.4	29.5	29.5	30.1	Asymmetric
	Cond. C.	*118*	U. Chord	1000	1.6	55.2	55.2	60.1	Asymmetric
		538	L. Chord	1000	1.6	76.1	76.1	81.0	Asymmetric
7		*593*	Chord	500	1.6	30°	11.0	12.0	Asymmetric
		608	Diagonal I	500	1.2	90°	0.6	0.6	Symmetric, 90°
		514	Diagonal II	500	1.4	30°	4.1	4.7	Asymmetric

4.7.1 THE ASYMMETRIC LOAD CASE

The procedures described in Section 4.6.1 are applied as follows:

1. $V = 33$ m/s
2. $W = 0.5\rho DC_d V^2 = 0.5(1.226)(1)(0.0406)(33)^2 = 26$ N/m
3. $L = 420$ m, $S = 20$ m and $W_c = 58$ N/m
4. The nonlinear analysis leads to $R_{LONG} = 19700$ N

5. $R_{TRANS} = 0.625WL = 0.625(25)(480) = 7800$ N.
6. The tower is analyzed under these loads and the results are presented in Table 4.2.

4.7.2 THE SYMMETRIC LOAD CASES

As described previously in Sections 4.3 and 4.4, the critical load case for the diagonal members perpendicular to the transmission line occurs at a projection angle of 0^o, while the chord members and the diagonal members in the transmission line plane occur at an angle of 90^o. The procedures described in Sections 4.6.2 and 4.6.3 are applied as follows:

1. V = 33 m/s
2. The velocities at the tower joints are considered equal to 33 m/s.
3. For a projection angle of 0^o:
    a. $W = 0.5\rho DC_dV^2 = 0.5(1.226)(1)(0.0406)(29)^2 = 26$ N/m
    b. $R_{TRANS} = WL = (26)(480) = 12480$ N.
    c. The tower loadsat a projection angle of 0^o are calculated according to ASCE 74.
    d. Structural analysis of the loaded tower is performed.
    e. The forces in the diagonal members perpendicular to the transmission line plane are acquired from the analysis of the tower.
4. For a projection angle of 90^o:
    a. The tower loads at a projection angle of 90^o are calculated according to ASCE 74.
    b. Structural analysis of the loaded tower is performed.
    c. The forces in the chord and diagonal members in the transmission line plane are acquired from the analysis of the tower.
5. The results of these analyses are presented in Table 4.2.

4.7.3 COMPARISON OF THE RESULTS

The results shown in Table 4.2 show an agreement – in terms of member axial forces – between the equivalent loading approach and the extensive downburst analysis. The member axial forces produced by the equivalent loading approach are larger than these produced by the extensive downburst analysis. The differences in the member axial forces are minor for almost all members, having a maximum difference of 8 %. This maximum difference occurs in the axial forces in the cross-arm members. As expected, the maximum forces within the cross-arm members occur when the structure is asymmetrically loaded. On the other hand, the maximum forces in the chord members and the diagonal members in the transmission line plane occur when the structure is symmetrically loaded at an angle of 90^{o}, while the maximum forces in the diagonal members perpendicular to the transmission line plane occur when the structure is symmetrically loaded at an angle of 0^{o}.

4.8 CONCLUSIONS

Within this chapter, different options are considered in terms of both the location and the nature, of the design velocity associated to different critical downburst cases. The effect of adding the convective velocity component to the downburst event is studied. The equivalent load corresponding to each of the three critical cases is developed. The following conclusions can be drawn:

1. The analysis of guyed transmission towers under downburst load with a fixed velocity at a height of 44 m provides more realistic results when compared to the results of analysing the same towers under downburst load with a fixed velocity at a height of 10 m.

2. Loading only one side of the transmission line beside the tower under study with a uniform load is effective in calculating the equivalent load representing the load transferred through the conductors within the asymmetric downburst case.

3. In addition to loading the tower body; loading all the spans of the conductor with a uniform load is effective in calculating the equivalent patch load representing the load transferred through the conductors within the second downburst case.

4. Loading only the tower body is effective in calculating the equivalent load representing the third downburst case.

5. The horizontal velocity along the tower height could be considered equal to the 10 m reference velocity.

6. The design velocity should be decided upon through the speed available from sufficient meteorological data acquired from the location of the transmission line to be designed. Thorough statistical analysis is needed so as to determine this design velocity.

7. For the symmetric downburst load cases, the effects of both the convective and jet velocities are significant and the summation of both velocities causing failure is always constant.

8. For the asymmetric downburst load case, the most critical factor is the large longitudinal reaction due to the unbalanced loading caused by the asymmetric downburst load, while the convective velocity has a minor effect when comparing it to the effect of the jet velocity. This case is the most critical for the cross-arm members, as it causes failure at a level of loading earlier than that caused by symmetric load cases.

4.9 REFERENCES

American Society of Civil Engineers (2010). "Guidelines for electrical transmission line structural loading." *ASCE Manuals and Reports on Engineering Practice*, No. 74, N.Y.

Darwish, M. M., El Damatty, A. A. and Hangan, H.M. (2010) "Dynamic characteristics of transmission line conductors and behaviour under turbulent downburst loading" *Wind and Structures*, 13(4), 327-346.

Dotzek, N. and Friedrich, K. (2009) "Downburst-producing thunderstorms in southern Germany: Radar analysis and predictability" *Atmospheric Research*, 93(6), 457-473.

Fujita, T. (1990). "Downbursts: meteorological features and wind field characteristics." *Journal of Wind Engineering and Industrial Aerodynamics*, 36(1), 75-86.

Gast, K.D., 2003. A comparison of extreme wind events as sampled in the 2002 Thunderstorm Outflow Experiment. Master's Thesis, Texas Tech University, Lubbock.

Holmes, J., H.M. Hangan, Schroeder, J., Letchford, L. and Orwig, K. (2008): "A forensic study of the Lubbock-Reese downdraft of 2002" *Wind and Structures*,11, 137-152.

Hangan, H. and Kim, J.D., "Numerical simulation of downbursts", ASCE Structural Congress, Nashville, Te, USA, June, 2004. *(pp.1657-1664)*

Hangan, H. and Kim, J.D. (2007). "Numerical simulations of impinging jets with application to downbursts" *Journal of Wind Engineering and Industrial Aerodynamics*, 95, 279–298.

Kanak, J., Benko, M., Simon, A and Sokol, A. (2007). "Case study of the 9 May 2003 windstorm in south-western Slovakia" *Atmospheric Research*, 83, 162-175.

Kwon, D. and Kareem, A. (2009). "Gust-front factor: New framework for wind load effects on structures." *Journal of Structural Engineering*, 135(6), 717-732.

Manitoba Hydro Transmission and Civil Design Department (1999), "Bipole 1 & 2 HVDC Transmission Line Wind Storm Failure on September 5, 1996 – Review of

Emergency Response, Restoration and Design of These Lines", *Manitoba Hydro*, 98-L1/1-37010-06000, 54.

Orwig, K. and Shcroeder, J. (2007). "Near-surface wind characteristics of extreme thunderstorm outflows" *Journal of Wind Engineering and Industrial Aerodynamics*, 95, 565-584.

Savory, E., Parke, G., Zeinoddini, M., Toy, N., and Disney, P. (2001). "Modelling of tornado and microburst-induced wind loading and failure of a lattice transmission tower." *Engineering Structures*, 23, 365-375.

Shehata, A., El Damatty, A., and Savory, E. (2005). "Finite element modelling of transmission line under downburst wind loading." *Finite Element in Analysis and Design*, 42(1), 71-89.

Shehata, A.Y. and El Damatty, A.A. (2007). "Behaviour of guyed transmission line structures under downburst wind loading" *Wind and Structures*, 10(3), 249-268

Shehata, A.Y. and El Damatty, A.A. (2008). "Failure analysis of a transmission tower during a microburst" *Wind and Structures*, 11(3), 193-208

Shehata, A. Y., Nassef, A.O. and El Damatty, A. A. (2008). "A coupled finite element-optimization technique to determine critical microburst parameters for transmission towers." *Finite Element in Analysis and Design*, 45(1), 1-12.

Xie, Q., Zhang, Y. and Li, J. (2006). "Investigation on tower collapses of 500 kV Renshang 5237 transmission line caused by downburst 2." *Power System Technology*, 30(10), 59-63.

CHAPTER 5

BEHAVIOR OF SELF SUPPORTED TRANSMISSION LINE TOWERS UNDER DOWNBURST LOADING

5.1 INTRODUCTION

Transmission towers are essential components in an electrical system. A major cause of power outages is the failure of the towers during severe natural disasters. These costly failures have been often attributed to high localized wind events, in the form of tornadoes and downbursts (Manitoba Hydro, 1999). Despite these facts, the design codes of transmission towers have typically considered only wind loads associated with large-scale synoptic events, such as hurricanes and typhoons. High intensity winds (HIW), resulting from downbursts, originate from thunderstorms. A downburst was defined by Fujita (1990) as "a strong downdraft that induces an outburst of damaging winds on or near the ground". The boundary layer wind velocity profile of large-scale wind events is typically different from that of a downburst. As such, downbursts can produce different loading and, consequently, different collapse modes, as shown by Kim et al. (2007) for the case of tall buildings.

In general, the structural system of electrical transmission towers can be categorized into two types: (a) self-supporting towers, and (b) guyed towers. Guyed towers rely on attached guys, which are anchored to the ground, to transfer some of the lateral loads imposed on the tower. Under lateral loads, guyed towers behave as simple beams with overhanging cantilevers. The towers are simply supported at their bases, while the guys function as flexible supports. On the other hand, self-supporting towers carry and transfer

loads only through its members. Under lateral loads, a self-supporting tower behaves similar to a cantilever with the tower base fixed to the ground.

Savory et al. (2001) modeled the wind velocity time–histories of transient tornado and microburst events and applied their resulting loads on a lattice self-supported transmission tower. The dynamic analysis performed for the two HIW events predicted a shear failure due to the tornado similar to that observed in the field. However, the microburst did not cause a failure due to its lower intensity (in comparison to the tornado).

Kanak et al. (2007) studied a downburst event that occurred in south-western Slovakia in 2003. At least 18 electric self-supported transmission line towers were destroyed due to that downburst event. Seven of the transmission towers felt down in a 1.2 km line, where the transmission line was almost perpendicular to the track of the storm. The direction of the fallen towers and trees was almost uniform and parallel to the track of the thunderstorm. When observing the towers that failed during the event, it was found that the members in the middle third of the towers' height failed while the uppermost members and lowermost members remained straight. The company responsible for designing the transmission line reported that the structure could withstand a wind speed of 160 Km/hr (44.4 m/s). This suggested that the velocity acting on the transmission line was higher than 44.4 m/s. This high velocity causing failure (which could be the maximum velocity within the event) was appearing to be localized at the location of the failed towers (Kanak et al., 2007).

Hangan and Kim (2007) developed and validated a computational fluid dynamic (CFD) model simulating the spatial and time variations of the fluctuating mean component of the downburst velocity wind field. Shehata et al. (2005) developed a structural analysis

numerical model capable of evaluating the response of transmission lines under the effect of downbursts. In this numerical model, the CFD data developed by Hangan and Kim (2007) was incorporated and scaled-up based on the relative values between the characteristics of a prototype downburst and those used in the CFD model. Shehata et al. (2005) structural analysis model was based on the finite element method, using three-dimensional linear frame elements to simulate the tower members and two-dimensional non-linear curved frame elements to simulate the conductors.

Shehata et al. (2005) reported a value of 0.58 s for the natural period of a 44 m high guyed transmission tower. Based on the fact that the loading period of the mean velocity in a downburst event is greater than 20 s, negating the need to perform a dynamic analysis, Shehata et al. (2005) performed a quasi-static analysis.

Using this structural analysis model, Shehata and El Damatty (2007) conducted a parametric study by varying the jet diameter (D_j) and the location of the downburst center relative to the tower. A guyed transmission tower located in Manitoba, Canada, which collapsed in 1996 due to a downburst event, was used to perform this parametric study. The critical downburst parameters, in terms of the size of the event and its location relative to the tower, leading to maximum forces in the tower members, were identified. The study revealed that the critical downburst parameters vary based on the type and location of the members. Shehata and El Damatty (2008) extended their numerical scheme by including a failure model for the tower members, which was used to study the progressive collapse of the guyed tower that failed in Manitoba, Canada in 1996. An optimization routine was then implemented by Shehata et al. (2008) to predict the critical downburst parameters and the corresponding forces in an automated procedure.

It should be mentioned that the above downburst studies have focused on guyed towers. The current study focuses on the behaviour of self-supported transmission towers under downbursts. The study is conducted numerically using the same model developed by Shehata et al. (2005). A brief description of this numerical model is first introduced. An extensive parametric study is conducted to assess the structural behaviour of a self-supported tower, while varying the downburst parameters, which are defined by the diameter of the downburst jet and the location of the centre of the downburst relative to the centre of the tower. The results of this parametric study are used to assess the variations of the internal forces in various tower's members with the downburst parameters. They are also used to identify the critical downburst configurations that lead to maximum internal forces in various members of the tower. The internal forces associated with the critical downburst configurations are compared to those corresponding to normal wind loads that are typically used in the design. Finally, the structural behaviour of the self-supported tower under such critical downburst configurations is described.

5.2 DESCRIPTION OF NUMERICAL MODEL

As mentioned above, the current study is conducted using the numerical model developed by Shehata et al. (2005). The wind field for downbursts adopted in this model is based on the Computational Fluid Dynamic (CFD) simulation conducted by Hangan and Kim (2004). The variations of the wind field, with time and space, for a small-scale downburst jet having a specific diameter and a certain downward velocity, were determined from this CFD simulation. The downburst velocity field has two components; a radial horizontal component and an axial vertical component. A procedure to scale-up this wind

field and to estimate the wind forces acting on the tower and the conductors due to a full-scale downburst was provided by Shehata et al. (2005). The magnitude and direction of these forces depend on a number of parameters, which are referred to as "the downburst configurations". These parameters are: a) the jet velocity (V_j), b) the jet diameter (D_j), c) the location of the centre of the downburst relative to centre of the tower, which is defined by the polar coordinates r and θ.

Two types of elements are used in Shehata's numerical model. The tower members are modeled using two-nodded linear three-dimensional frame elements having three translational and three rotational degrees of freedom per node. The conductors are modeled using an assembly of two-dimensional nonlinear curved consistent frame elements (Gerges and El Damatty, 2002). This nonlinear model takes into consideration various nonlinear aspects that affect the behaviour of flexible cables, including the effects of sagging, post-tensioning forces, and large deformations. After assuming a specific downburst configuration and evaluating the corresponding downburst forces, the numerical model starts by conducting two independent quasi-static time history analyses for each conductor (one analysis for each velocity component). This set of analyses includes modeling three conductor spans from each side of the tower of interest. It was shown by Shehata et al. (2005) that this number of spans is sufficient to predict the forces transferred from the conductors to the tower. In these analyses, the conductors are supported by nonlinear springs at their connections with the towers. The stiffness of these springs simulates the combined rigidity of the towers and the insulators used to connect the towers cross arms to the conductors. Time history variations for the three components of the reaction force, transferred from the conductors to the tower of interest, were determined from this set of analyses. This is followed by a linear time history quasi-static

analysis for the tower under the combined effects of the downburst wind forces acting on the tower members and the conductors' reaction forces predicted by the first set of analyses. Time history variations for the tower members' internal forces were determined from this set of analysis.

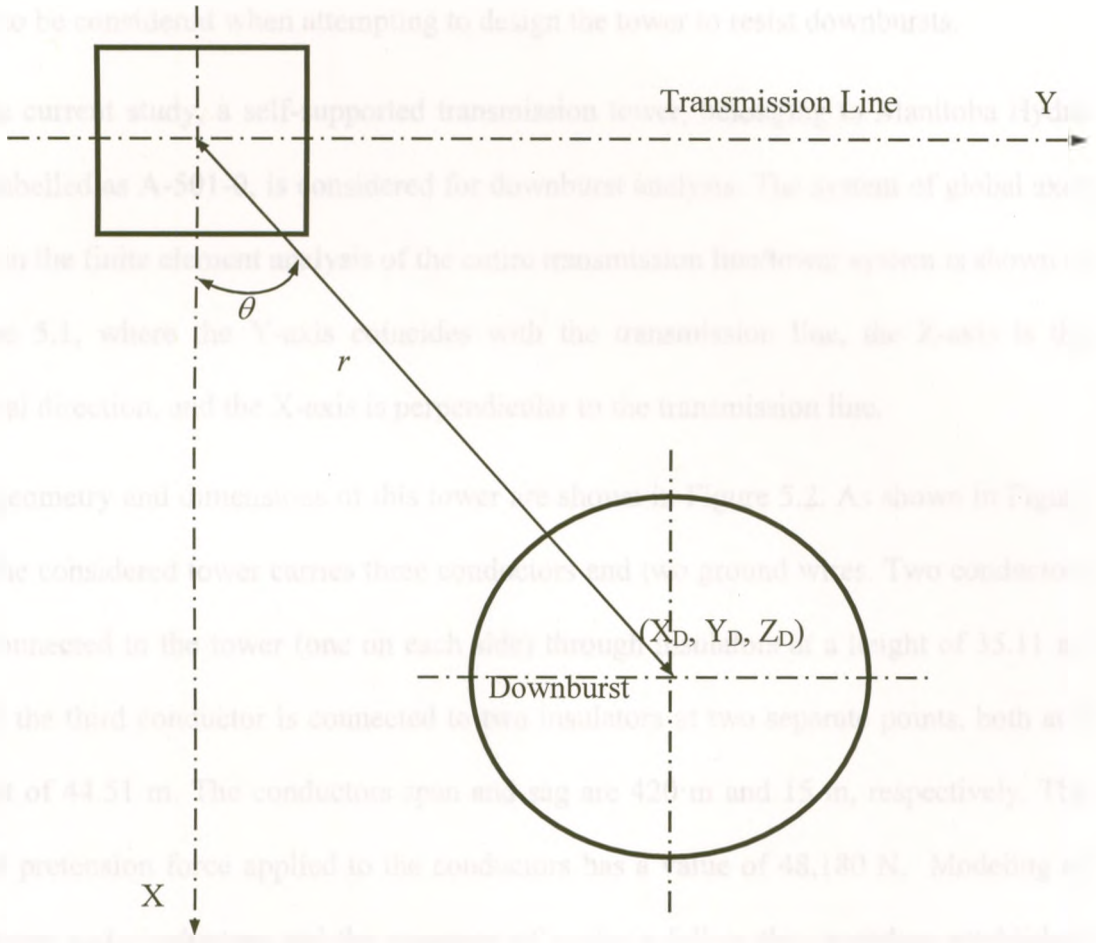

Figure 5.1 Horizontal projection of transmission tower and downburst parameters. (Shehata et al., 2005)

For each member, the absolute maximum internal force determined within the entire time history of the analysis is detected. A parametric study is conducted by repeating the analyses many times through varying the downburst parameters (D_j, r and θ). The jet velocity (V_j) is usually assumed to have a fixed value in this parametric study. The absolute maximum force in each member of the tower obtained from the entire parametric

study can be then determined. The critical downburst configurations (D_j, r and θ) corresponding to this maximum force can be also identified. In general, the tower members can have different critical downburst configurations. Usually, a certain number of critical downburst configurations exist for a tower. These downburst configurations need to be considered when attempting to design the tower to resist downbursts.

In the current study, a self-supported transmission tower, belonging to Manitoba Hydro and labelled as A-501-0, is considered for downburst analysis. The system of global axes used in the finite element analysis of the entire transmission line/tower system is shown in Figure 5.1, where the Y-axis coincides with the transmission line, the Z-axis is the vertical direction, and the X-axis is perpendicular to the transmission line.

The geometry and dimensions of this tower are shown in Figure 5.2. As shown in Figure 5.2, the considered tower carries three conductors and two ground wires. Two conductors are connected to the tower (one on each side) through insulators at a height of 35.11 m, while the third conductor is connected to two insulators at two separate points, both at a height of 44.51 m. The conductors span and sag are 420 m and 15 m, respectively. The initial pretension force applied to the conductors has a value of 48,180 N. Modeling of the tower and conductors and the sequence of analysis follow the procedure established by Shehata et al. (2005).

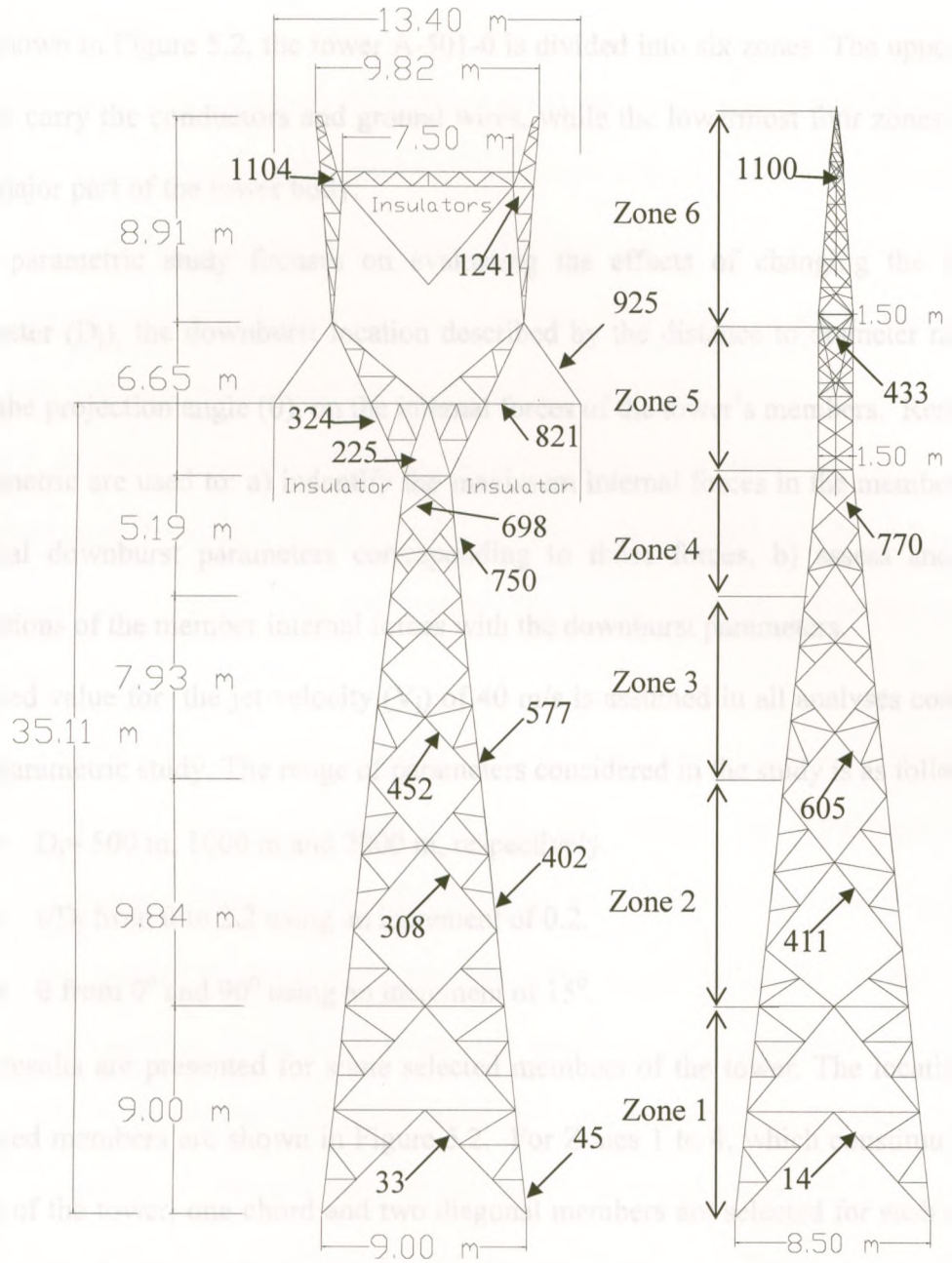

Figure 5.2 Geometry of MH Tower Type A-501

5.3 PARAMETRIC STUDY OF A SELF SUPPORTED TOWER

As shown in Figure 5.2, the tower A-501-0 is divided into six zones. The uppermost two zones carry the conductors and ground wires, while the lowermost four zones constitute the major part of the tower body.

The parametric study focuses on evaluating the effects of changing the downburst diameter (D_j), the downburst location described by the distance to diameter ratio (r/D_j), and the projection angle (θ), on the internal forces of the tower's members. Results of the parametric are used to: a) indentify the maximum internal forces in the members and the critical downburst parameters corresponding to those forces, b) assess and plot the variations of the member internal forces with the downburst parameters.

A fixed value for the jet velocity (V_j) of 40 m/s is assumed in all analyses conducted in this parametric study. The range of parameters considered in the study is as follows:

- D_j= 500 m, 1000 m and 2000 m, respectively.
- r/D_j from 0 to 2.2 using an increment of 0.2.
- θ from 0^o and 90^o using an increment of 15^o.

The results are presented for some selected members of the tower. The locations of the selected members are shown in Figure 5.2. For Zones 1 to 4, which constitute the main body of the tower, one chord and two diagonal members are selected for each zone. The two diagonal members are located in two different planes; parallel and perpendicular to the line direction, and are labelled as diagonal (I) and diagonal (II), respectively. A similar selection is made for zone 6. In addition to the above three types of members, the forces in one upper chord member and one bottom chord member are reported in the conductor cross arm area (zone 5).

5.3.1 MAXIMUM MEMBER FORCES AND CRITICAL DOWNBURST PARAMETERS

The maximum axial forces in the selected members resulting from the parametric study are reported in Table. 5.1. The results are presented with and without the inclusion of the self weight of the structure. The critical downburst configurations corresponding to the maximum forces are reported for each member. In addition, a set of external forces simulating normal wind loads are calculated based on the ASCE 74 (2010) equations using a reference velocity of 40 m/s. The tower is analyzed under this set of forces and the axial loads developing in the selected members are provided in Table 5.1 for purpose of comparison. The following observations can be noticed from the results provided in Table 5.1:

- For the chord members of zones 5 and 6, the maximum forces correspond to D_j = 1000 m, r/D_j = 1.2 and $\theta = 0^o$. At this location, the radial velocity of the downburst becomes perpendicular to the line. This leads to maximum values for the conductor transverse reaction. This is probably the reason that this configuration is the critical one with respect to these members. No unbalanced forces act on the conductors under this configuration and, consequently, no net longitudinal reaction acts on the tower. The r/D_j value of 1.2 leads to the maximum values for the vertical profile of the radial velocities. This explains why this ratio turns out to be critical in this case. The relatively large value for the jet diameter D_j = 1000 m allows a larger length of the conductors to be subjected to large velocity values.

- For chord members of zones 1 to 4, the critical downburst parameters are D_j = 500 m, r/D_j = 1.4 and $\theta = 15^o$. The critical angle is still close to the $\theta = 0^o$ leading to large values for the transverse reactions. In addition, this small offset of the downburst location leads to a longitudinal conductor reaction, which results in a transverse overturning moment resisted by the chord members.
- Most of the diagonal (II) (perpendicular to the line) members have a critical angle $\theta = 0^o$. This downburst location leads to maximum values for the external forces acting in the direction perpendicular to the line.
- For diagonal (I) members, one would expect that that the maximum axial forces occurs at $\theta = 90^o$. This happens for members 14 and 411 located in zones 1 and 2. In other zones, the critical angle varies between 0^o to 60^o. This can be interpreted by the following two reasons: a) since the four legs of the tower are inclined, the plane at which diagonal (I) members exist is not totally parallel to the line. As such, the external forces perpendicular to the line will have a component in this plane, b) the projected area perpendicular to the line is significantly larger than the projected area parallel to the line. This is particularly true at the top portion of the tower, where the critical angles deviate from the 90^o value.
- The upper and lower chord members of zone 5 have intermediate critical angles of $\theta = 30^o$ and 60^o, respectively. This is due to the longitudinal conductor reaction associated with these unbalanced load cases. Large internal forces develop due to the out-of-plane bending resulting from this longitudinal force.

- With the exception of the upper chord of the cross arm, the internal forces resulting from both the ASCE and the downburst analyses have close values. More details about this variation are discussed in Section 5.4.

Table 5.1 Parametric study for the Manitoba Hydro tower type A-501-0

Zone	El.	Type	Downburst Load					ASCE
			Dj (m)	r/Dj	θ	Force including own weight (KN)	Force excluding own weight (KN)	Force (KN)
1	45	Chord	500	1.4	15	329.1	313.2	302.5
	14	Diagonal (I)	500	1.2	90	7.1	7.7	7.1
	33	Diagonal (II)	500	1.2	0	9.9	10.0	12.2
2	402	Chord	500	1.4	15	348.0	334.7	325.8
	411	Diagonal (I)	500	1.2	90	4.7	4.4	4.0
	308	Diagonal (II)	500	1.2	0	14.4	18.8	14.0
3	577	Chord	500	1.4	15	337.6	325.5	319.9
	605	Diagonal (I)	500	1.4	30	6.6	6.2	1.8
	452	Diagonal (II)	500	1.4	15	10.3	4.9	3.9
4	750	Chord	500	1.4	15	314.0	302.8	300.8
	770	Diagonal (I)	1000	1.2	0	-5.5	4.3	4.5
	698	Diagonal (II)	1000	1.2	0	27.8	46.0	50.2
5	324	Chord	1000	1.2	0	86.3	52.3	54.2
	433	Diagonal (I)	500	1.6	30	11.6	9.8	3.0
	225	Diagonal (II)	500	1.4	15	170.2	136.9	139.5
	925	U. Chord	500	1.6	30	46.2	33.4	0.7
	821	L. Chord	500	1.8	60	10.0	2.5	3.3
6	1241	Chord	1000	1.2	0	73.1	72.0	78.7
	1100	Diagonal (I)	500	1.8	60	7.2	1.6	1.6
	1104	Diagonal (II)	1000	1.2	0	21.9	23.4	25.8

5.3.2 SENSITIVITY OF THE TOWER MEMBERS FORCES TO CHANGING THE DOWNBURST CONFIGURATION

The results of the parametric study are used to assess the sensitivity of the tower members internal forces with the three downburst parameters; D_j, r/D_j, and θ. The variations of the axial forces for some selected members, as well as the conductor reactions, with these

parameters are provided in Figures 5.3 to 5.14. The following observations can be detected from these figures:

- The variation in r/D_j has a significant effect on the values of the axial forces for all members of the tower.
- For most of the members, the axial forces increase with the decrease in diameter and the largest forces occur for a jet diameter equal to 500 m (which was the lower bound diameter used in the study).
- For members with a critical jet diameter of 1000 m, the differences between the two curves of 500 m and 1000 m diameters are minute, as shown in Figures 5.3b, 5.5, 5.7, 5.11 and 5.13. It can be concluded from Figures 5.3 to 5.13 that the effect of varying D_j is less significant than the effects of varying r/D_j and θ.
- Figure 5.3a shows that for the chord member located in Zone 1, the difference between the peak values of the two curves representing angles of 15^o and 30^o is approximately 10% with a maximum value occurring at 15^o. The difference between the peaks of the two similar curves decreases in Zone 2 and becomes minor in Zones 3 and 4, as shown in Figures 5.4, 5.6 and 5.8, respectively. Figure 5.10 shows that, for the upper chord cross-arm member located in Zone 5, the difference between the peak values associated with angles of 15^o and 30^o is more than 10% with an absolute maximum value occurring at 30^o. On the other hand for zone 6, the absolute maximum value occurs at an angle of 0^o, as shown in Figure 5.8a.
- As shown in Figure 5.14, a maximum value for the conductor longitudinal reaction of 12,000 N occurs at two values of r/D_j, which are 1.6 and 1.8. They

correspond to two different critical angles of 30° and 45°, respectively. It can be also noticed that the difference between this absolute maximum reaction and the value of 10,500 N, which is the peak reaction for both $\theta = 60^{\circ}$ and 15°, is not very large. Figure 5.14b shows that a maximum value of 26,000 N for the transverse reaction occurs at an r/D_j of 1.2 and an angle of 0°. This is expected as this load case is perfectly symmetric.

- The angle causing the second highest transverse reaction of 24,000 N is 15°. This value is only 8 % lower than the absolute maximum. This explains why the 15° angle causes the maximum axial forces in six of the twenty members presented in Table 5.1. This location of the downburst causes large reactions in both the transverse and the longitudinal directions. The biaxial moment resulting from this case leads to large axial forces in the chord members of zones 1, 2, 3 and 4. This is due to the fact that the chord members of the lower zones are the main mode of transmitting the straining actions resulting from the conductors and the ground wires forces to the ground. This behaviour is different than that of guyed towers, in which the guys transmit these straining actions directly to the ground.

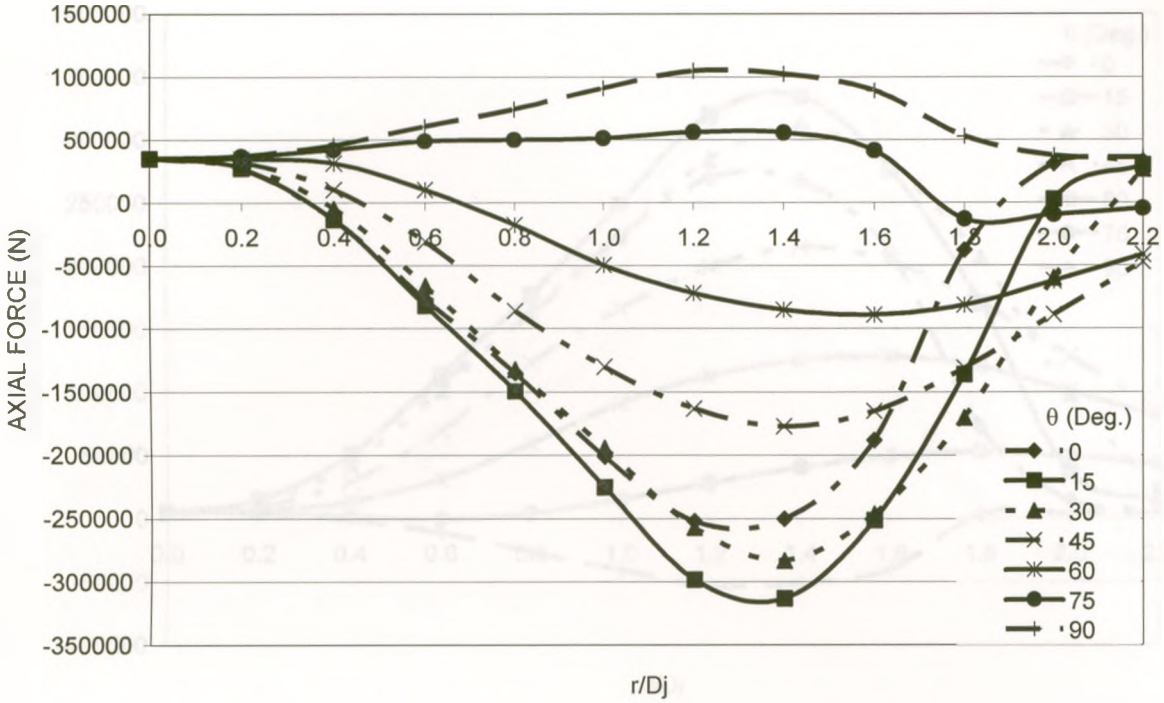

a. Variation of the axial force with r/D_j and θ, for $D_j = 500$ m.

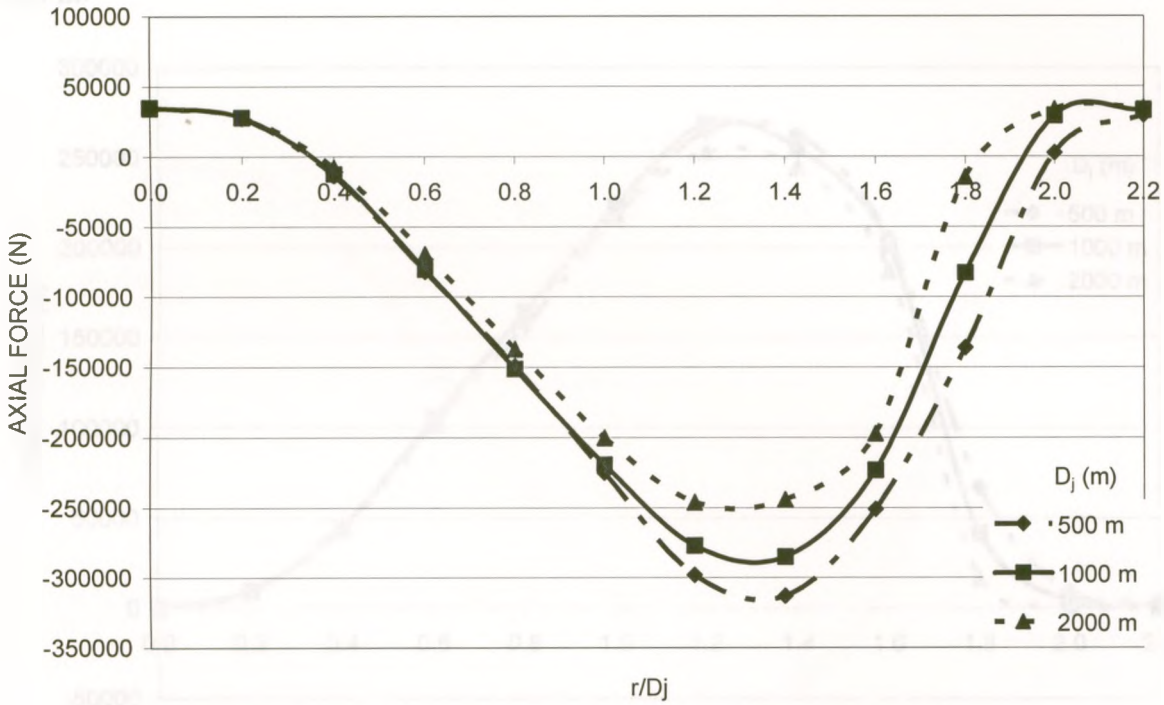

b. Variation of the axial force with r/D_j and D_j, for $\theta = 15^o$.

Figure 5.3 Variation of the axial force in member 45 (Zone 1) with the downburst parameters.

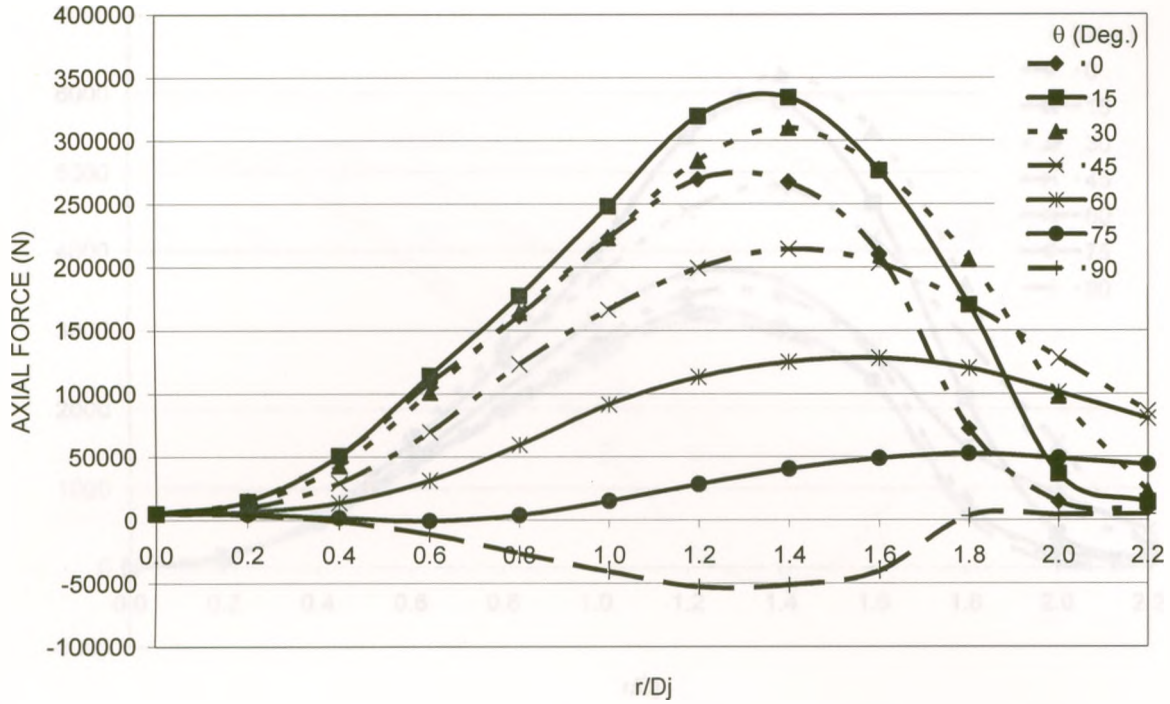

Figure 5.4 Variation of the axial force in member 402 (Zone 2) with r/D_j and θ, for D_j = 500 m.

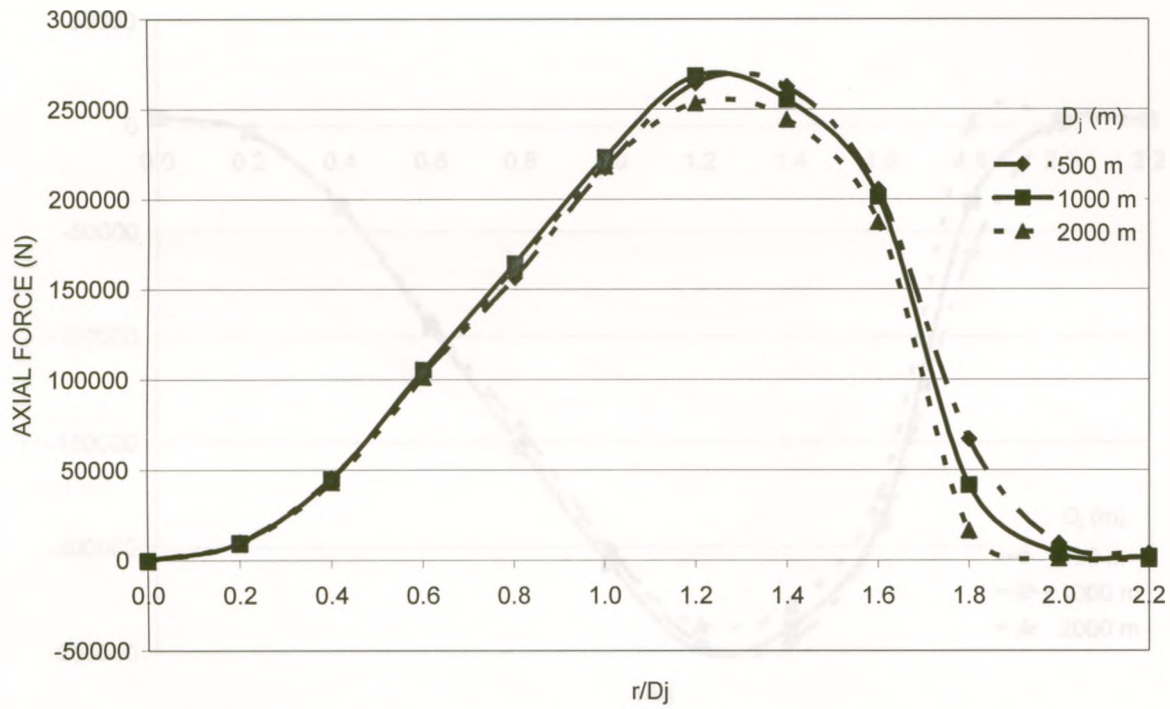

Figure 5.5 Variation of the axial force in member 402 (Zone 2) with r/D_j and D_j, for $\theta = 0^o$.

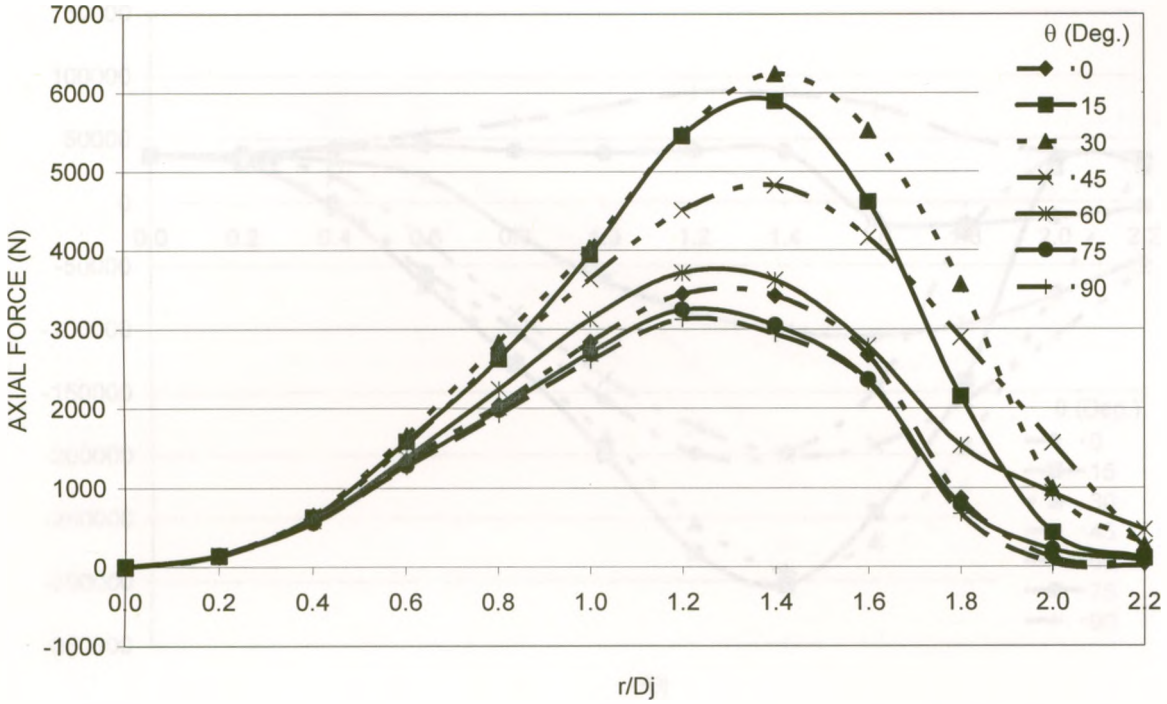

Figure 5.6 Variation of the axial force in member 605 (Zone 3) with r/D_j and θ, for D_j = 500 m.

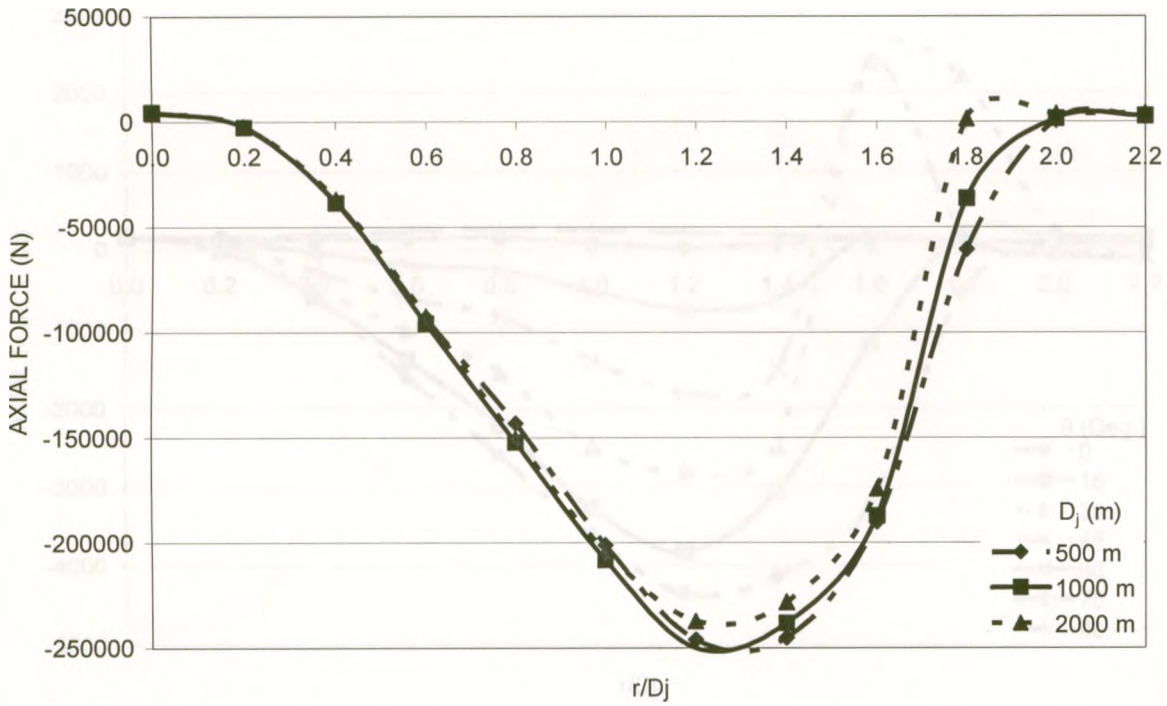

Figure 5.7 Variation of the axial force in member 577 (Zone 3) with r/D_j and D_j, for $\theta = 0^o$.

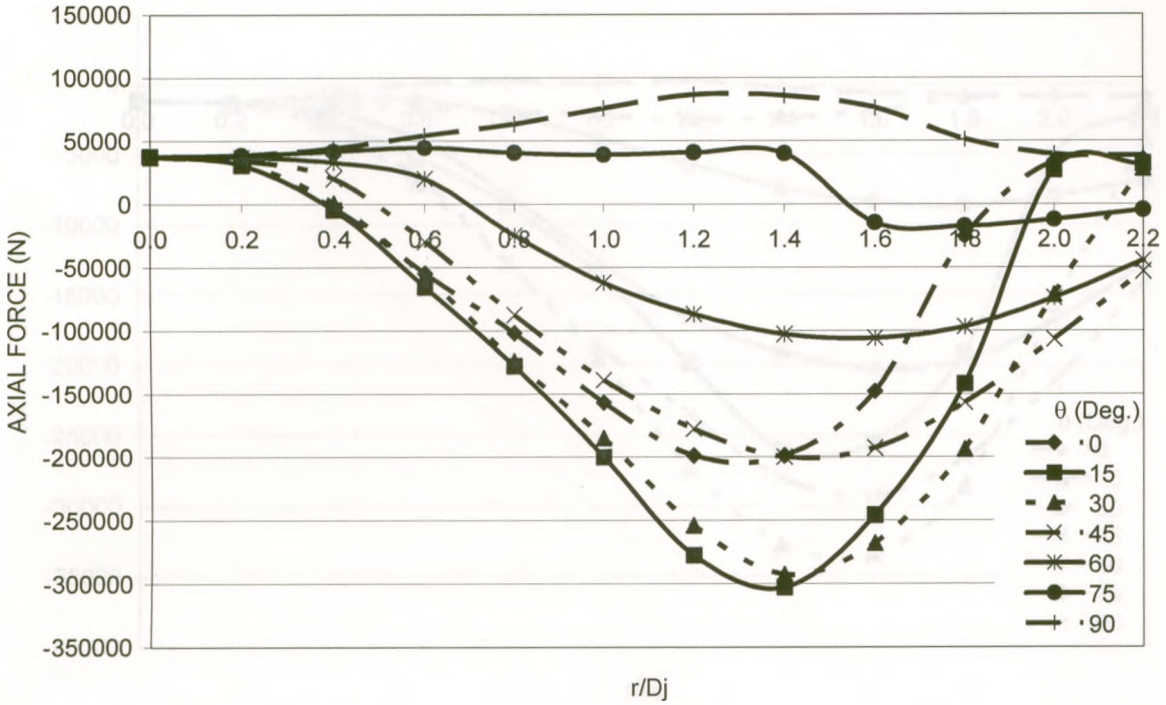

Figure 5.8 Variation of the axial force in member 750 (Zone 4) with r/D_j and θ, for D_j = 500 m.

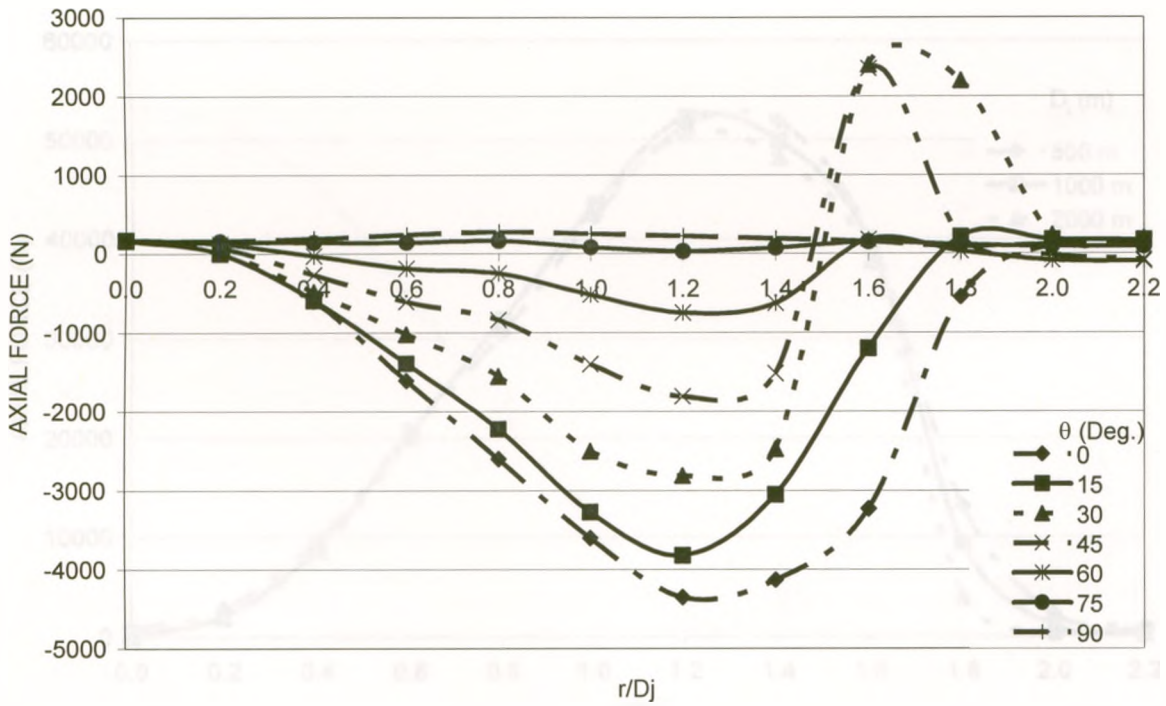

Figure 5.9 Variation of the axial force in member 770 (Zone 4) with r/D_j and θ, for D_j = 1000 m.

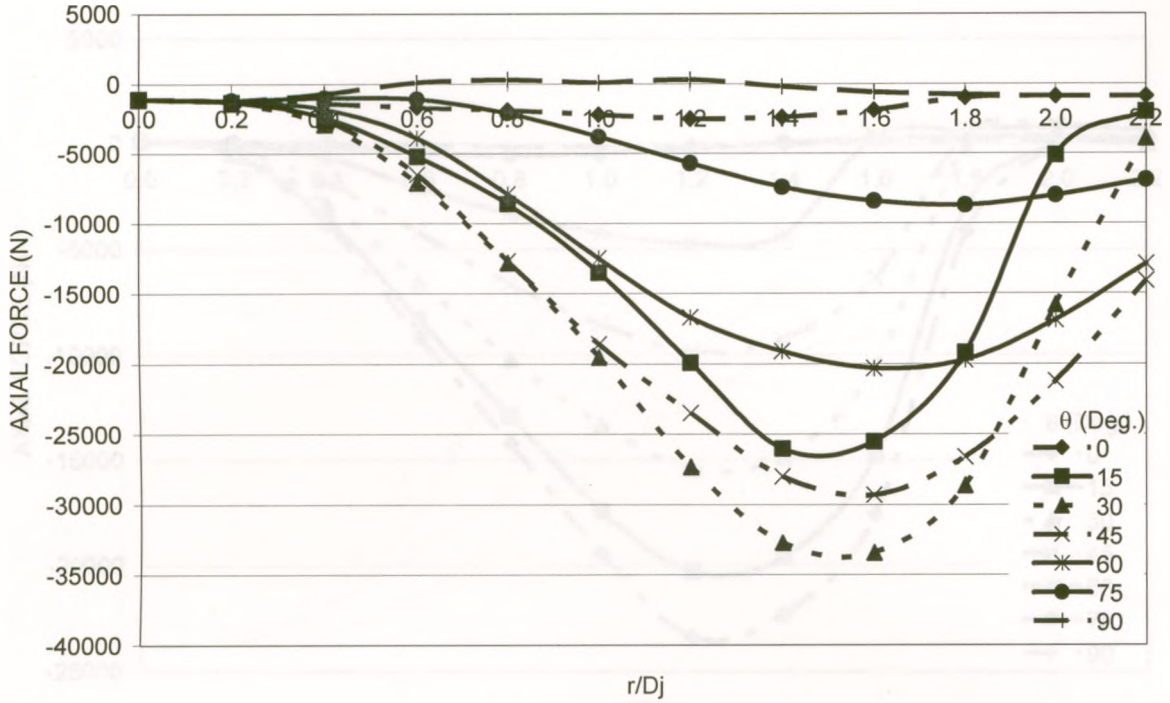

Figure 5.10 Variation of the axial force in member 925 (Zone 5) with r/D_j and θ, for D_j = 500 m.

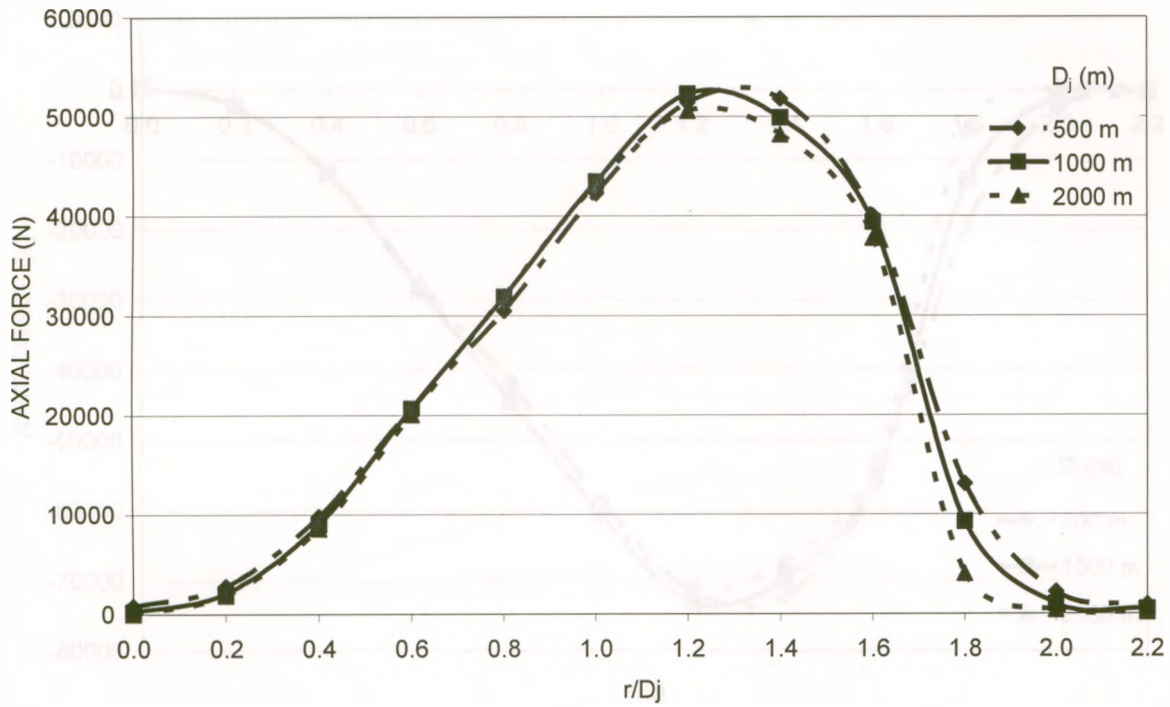

Figure 5.11 Variation of the axial force in member 324 (Zone 5) with r/D_j and D_j, for θ = 0°.

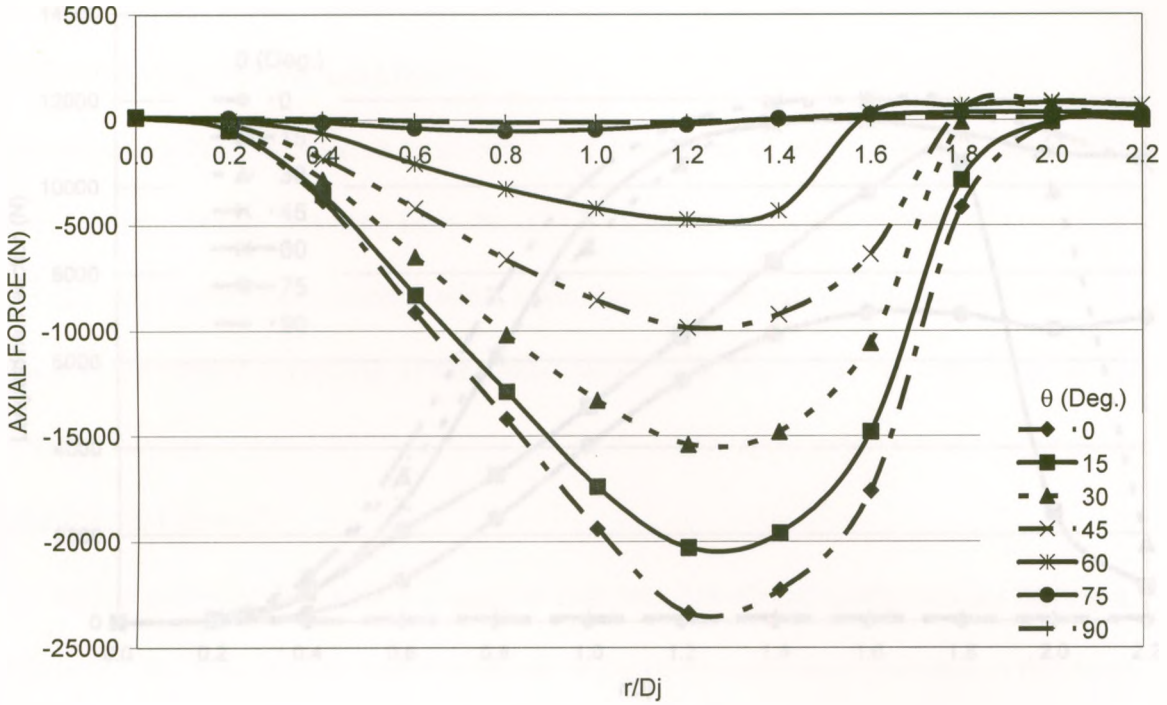

Figure 5.12 Variation of the axial force in member 1104 (Zone 6) with r/D_j and θ, for D_j = 1000 m.

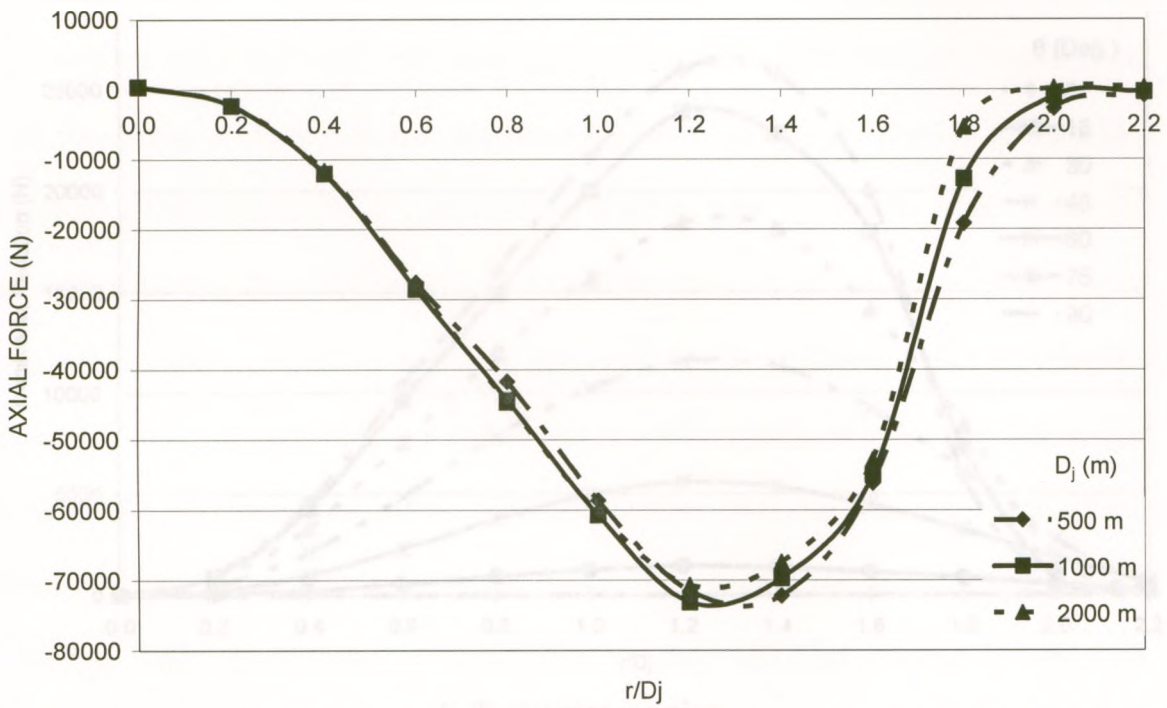

Figure 5.13 Variation of the axial force in member 1241 (Zone 5) with r/D_j and D_j, for θ = 0^o.

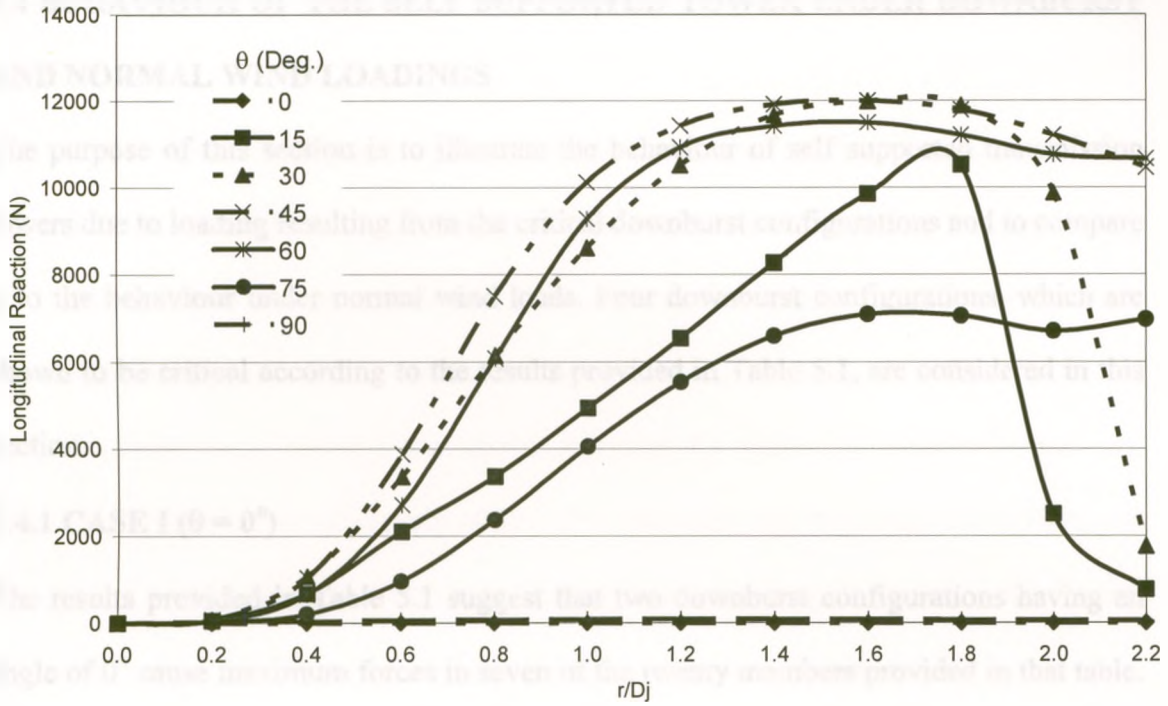

a. Longitudinal reaction.

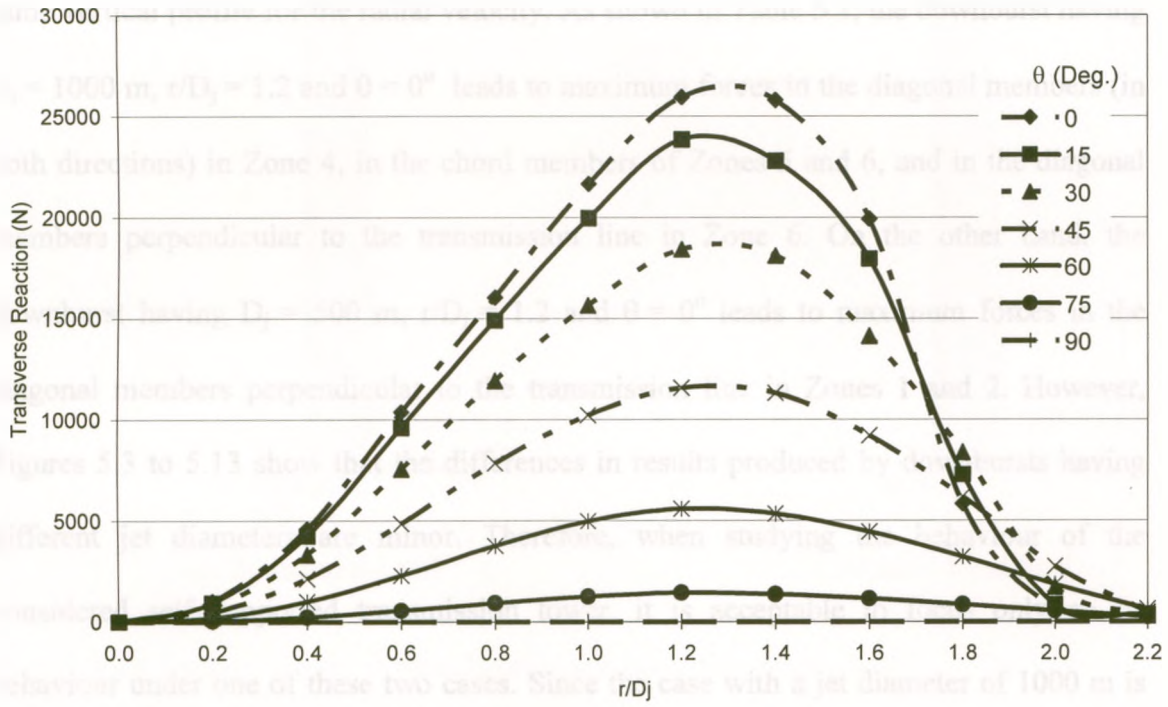

b. Transverse reaction.

Figure 5.14 Variation of the conductor reactions with r/Dj and θ, for D_j = 500 m.

5.4 BEHAVIOUR OF THE SELF SUPPORTED TOWER UNDER DOWNBURST AND NORMAL WIND LOADINGS

The purpose of this section is to illustrate the behaviour of self supported transmission towers due to loading resulting from the critical downburst configurations and to compare it to the behaviour under normal wind loads. Four downburst configurations, which are shown to be critical according to the results provided in Table 5.1, are considered in this section.

5.4.1 CASE I ($\theta = 0^o$)

The results provided in Table 5.1 suggest that two downburst configurations having an angle of 0^o cause maximum forces in seven of the twenty members provided in that table. Both cases have the same of value of 1.2 for the r/D_j ratio and both provide nearly the same vertical profile for the radial velocity. As shown in Table 5.1, the downburst having $D_j = 1000$ m, $r/D_j = 1.2$ and $\theta = 0^o$ leads to maximum forces in the diagonal members (in both directions) in Zone 4, in the chord members of Zones 5 and 6, and in the diagonal members perpendicular to the transmission line in Zone 6. On the other hand, the downburst having $D_j = 500$ m, $r/D_j = 1.2$ and $\theta = 0^o$ leads to maximum forces in the diagonal members perpendicular to the transmission line in Zones 1 and 2. However, Figures 5.3 to 5.13 show that the differences in results produced by downbursts having different jet diameters are minor. Therefore, when studying the behaviour of the considered self supported transmission tower, it is acceptable to focus only on its behaviour under one of these two cases. Since the case with a jet diameter of 1000 m is critical for four of the six members mentioned above, it is chosen to be studied in this

section to represent the behaviour of this tower when it is subjected to a downburst with an angle of 0°.

A simulation for the tower as a vertical column unrestrained along its height and fixed at its base is shown in Figure 5.15. The distributed loads, shown in Figure 5.15a, represent the external forces acting at various locations along the height of the tower due to a downburst having the above mentioned characteristics. In addition to that distributed load, the three concentrated forces shown represent the transverse reactions transferred from the two conductors at a height of 35.11 m; one conductor at a height of 44.51 m, and two ground wires at the top of the tower. Similar forces resulting from normal wind loads, calculated using ASCE No.74 guidelines (2010), are shown in Figure 5.15b.

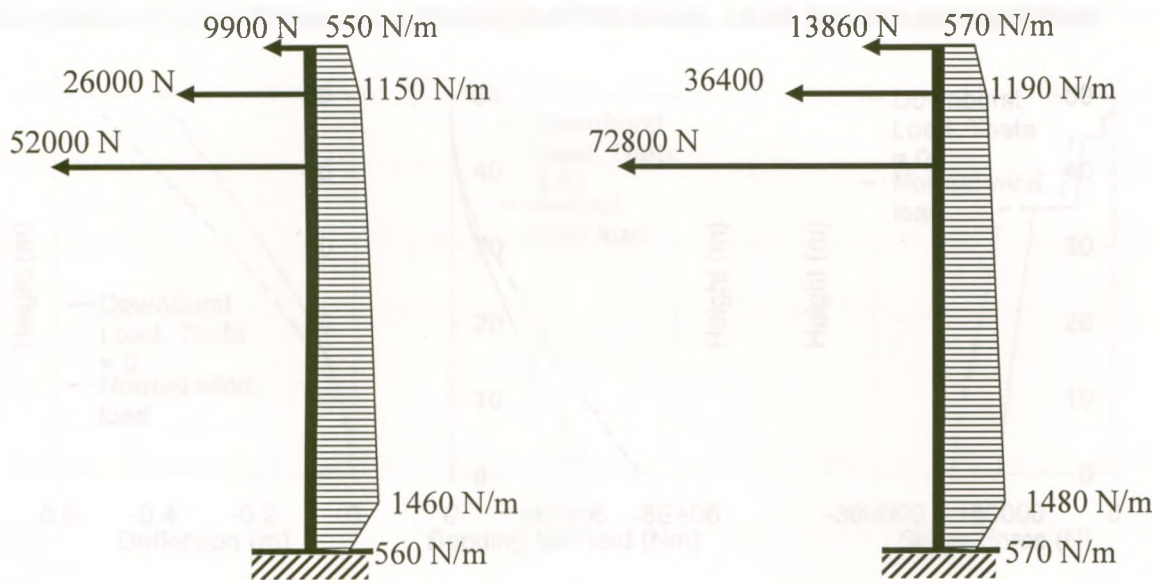

a. Downburst Load

b. Normal wind load

Figure 5.15 Vertical profile of wind loading at a projection angle of 0°.

A comparison between the downburst and the normal wind profiles indicates that the distributed forces acting on the tower are almost equal for both cases. On the other hand,

the forces acting on the conductors due to normal wind loading exceed significantly those due to downburst loading. This could be attributed to the fact that the radial component of the velocity profile decreases when the ratio r/D_j exceeds 1.2. In the considered case, the relative distance r between the centers of the downburst and the tower satisfies a ratio r/D_j of 1.2. However as for the conductors, the effective value of r/D_j at different points will exceed 1.2 and, therefore, smaller forces act at these locations.

Figure 5.16 shows the displacement profile and the variations of the overturning moment and shear force along the height of the equivalent beam due to both the downburst and normal wind loads, respectively. The large conductor forces associated with the normal wind load case lead to larger deflections and larger magnitudes for the overturning moments and shear forces along the height of the tower, which behaves as a cantilever.

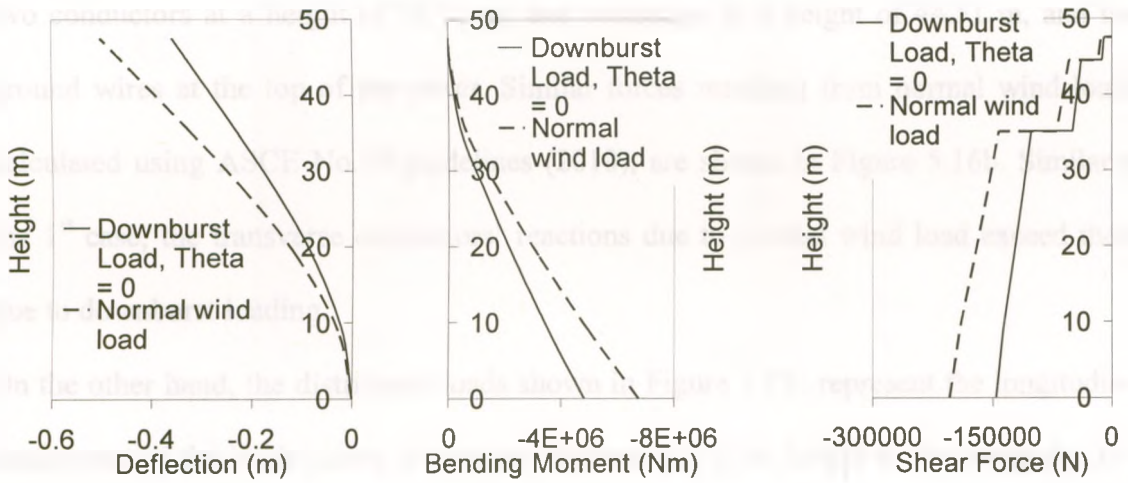

Figure 5.16 Structural behaviour at a projection angle of 0^o.

5.4.2 CASE II ($\theta = 15^o$)

The downburst configuration having D_j= 500 m, r/D_j= 1.4, $\theta = 15^o$ and V_j= 40 m/s is considered in this case. As shown in Table 5.1, this configuration leads to maximum forces in six of the twenty members provided in that table. These members are the chord

members of zones 1, 2, 3 and 4, and the diagonal members perpendicular to the transmission line in zones 3 and 5. The uniqueness of this downburst configuration is that it causes, simultaneously, large longitudinal and transverse reactions in the conductors and ground wires, which are transmitted to the tower. Hence, the behaviour of the tower under this load case is studied twice; once in the transverse plane, and the other in the longitudinal plane.

A simulation similar to that used for the 1st case is shown in Figure 5.17. The distributed loads, shown in Figure 5.17a, represent the transverse component of the loads acting at various locations along the height of the tower due to a downburst having the above mentioned characteristics. In addition to that distributed load, the three concentrated forces shown in the same figure represent the transverse reactions transferred from the two conductors at a height of 35.11 m; one conductor at a height of 44.51 m, and two ground wires at the top of the tower. Similar forces resulting from normal wind loads, calculated using ASCE No.74 guidelines (2010), are shown in Figure 5.16b. Similar to the 1st case, the transverse conductors' reactions due to normal wind load exceed those due to downburst loading.

On the other hand, the distributed loads shown in Figure 5.17c represent the longitudinal component of the loads acting at various locations along the height of the tower due to a downburst having the above mentioned characteristics. In addition to that distributed load, the three concentrated forces shown in the same figure represent the longitudinal reactions transferred from the conductors ground wires to the tower. Similar forces resulting from normal wind loads calculated using ASCE No.74 guidelines (2010) are shown in Figure 5.17d. While no longitudinal reactions are added to the distributed normal wind load as shown in Figure 5.17d, significantly large longitudinal forces are

transferred from the transmission line to the tower in the case of downburst loading shown in Figure 5.17c.

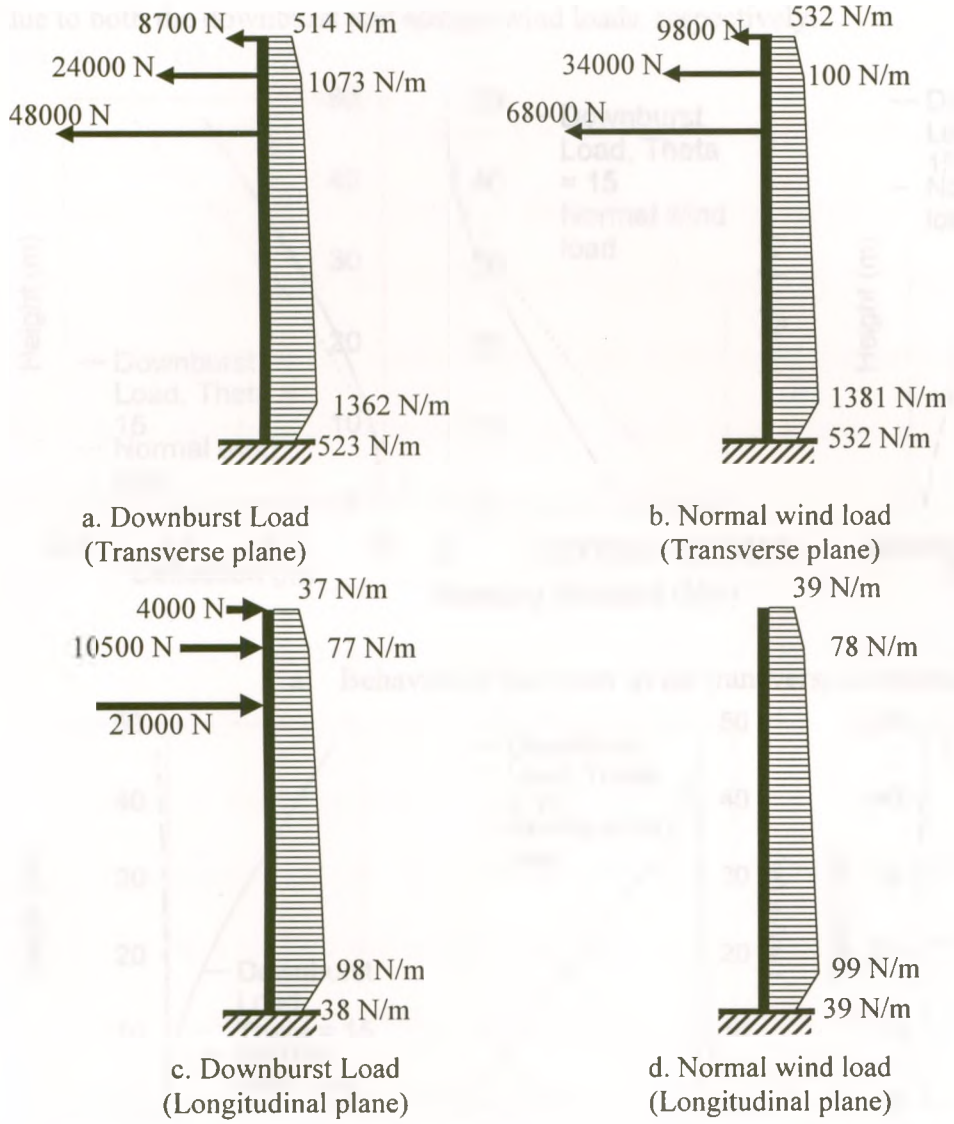

Figure 5.17 Vertical profile of wind loading at a projection angle of 15°.

Figure 5.18a shows the transverse components of the displacement profile and the variations of the overturning moment and shear force in the transverse plane along the height of the equivalent beam due to both the downburst and normal wind loads, respectively. It could be noticed that the straining actions experienced in the transverse plane are very similar to those experienced in the 1st case. Figure 5.18b shows the

transferred from the transmission line to the tower in the case of downburst loading shown in Figure 5.17c.

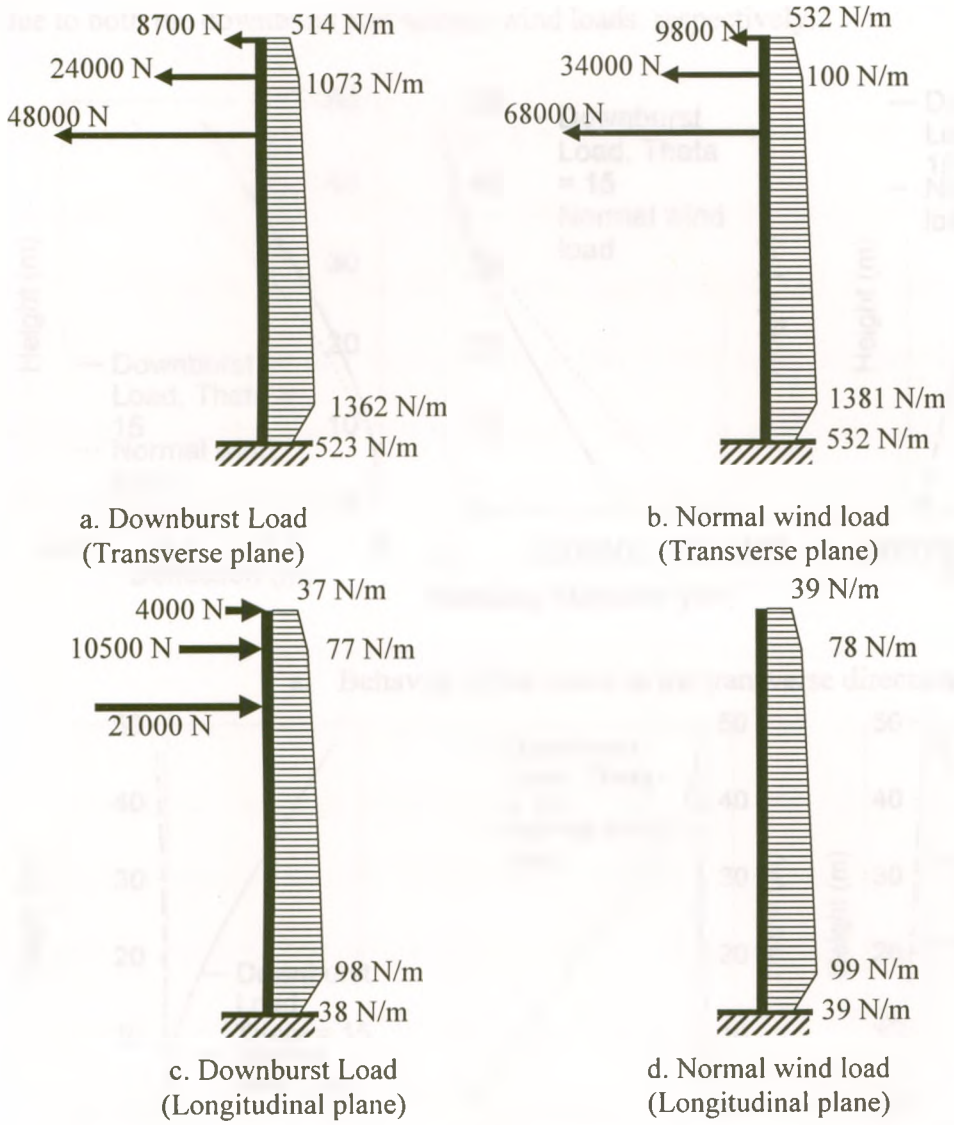

Figure 5.17 Vertical profile of wind loading at a projection angle of 15°.

Figure 5.18a shows the transverse components of the displacement profile and the variations of the overturning moment and shear force in the transverse plane along the height of the equivalent beam due to both the downburst and normal wind loads, respectively. It could be noticed that the straining actions experienced in the transverse plane are very similar to those experienced in the 1st case. Figure 5.18b shows the

longitudinal components of the displacement profile and the variations of the bending moment and shear force in the longitudinal plane along the height of the equivalent beam due to both the downburst and normal wind loads, respectively.

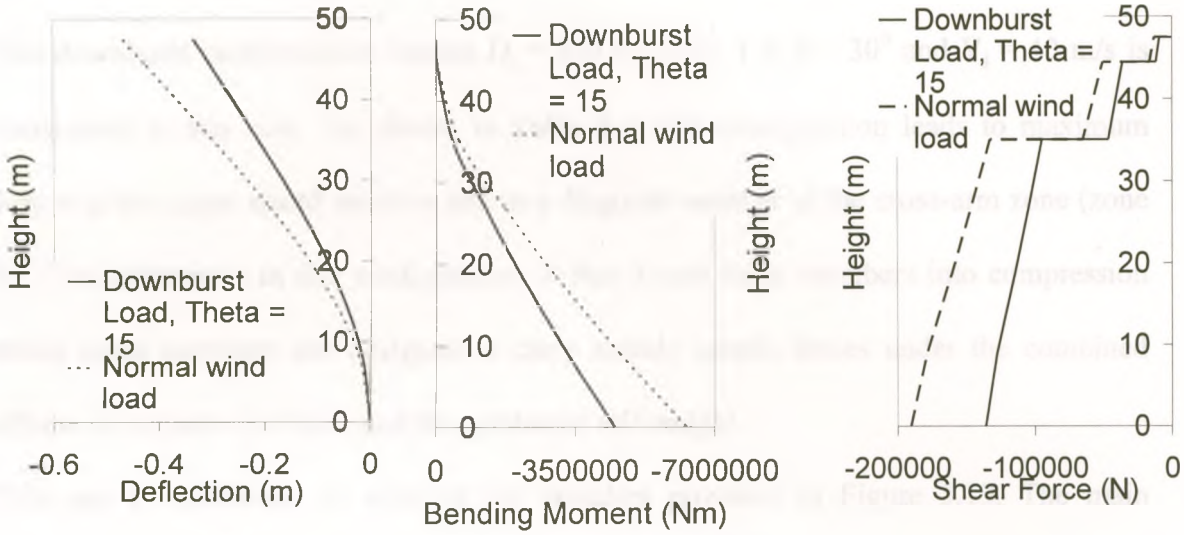

a. Behavior of the tower in the transverse direction.

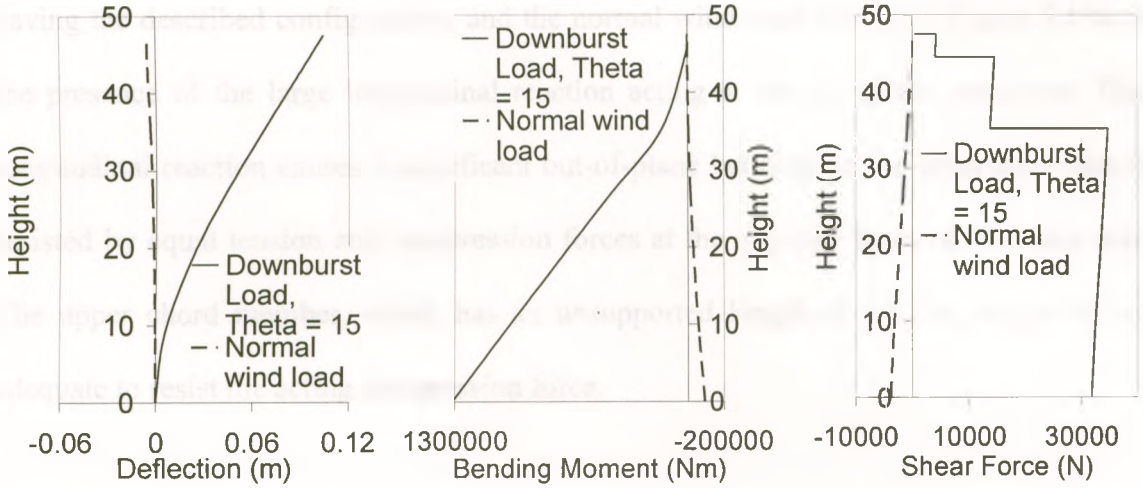

b. Behaviour of the tower in the longitudinal direction.

Figure 5.18 Structural behaviour at a projection angle of 15°.

The large longitudinal forces associated with the downburst load lead to larger deflections and larger magnitudes of the bending moments and shear forces along the height of the tower. This explains why the chord members in Zones 1, 2, 3 and 4 experience high axial

forces under this downburst load case, as these members resist moments resulting from both the longitudinal and transverse reactions.

5.4.3 CASE III ($\theta = 30^o$)

The downburst configuration having D_j = 500 m, r/D_j= 1.6, $\theta = 30^o$ and V_j = 40 m/s is considered in this case. As shown in Table 5.1, this configuration leads to maximum forces in the upper chord member and in a diagonal member of the cross-arm zone (zone 5). The uniqueness in this configuration is that it puts these members into compression while these members are designed to carry mainly tensile forces under the combined effects of normal wind load and the conductor self weight.

This can be explained in view of the sketches provided in Figure 5.19. The main difference between the forces shown in Figure 5.19a for the case of downburst loading, having the described configuration, and the normal wind load, shown in Figure 5.19a, is the presence of the large longitudinal reaction acting at the tip of the cross-arm. This longitudinal reaction causes a significant out-of-plane bending on the cross arm. This is resisted by equal tension and compression forces at the opposite faces of the cross arm. The upper chord member, which has an unsupported length of 4.37 m, might not be adequate to resist the acting compression force.

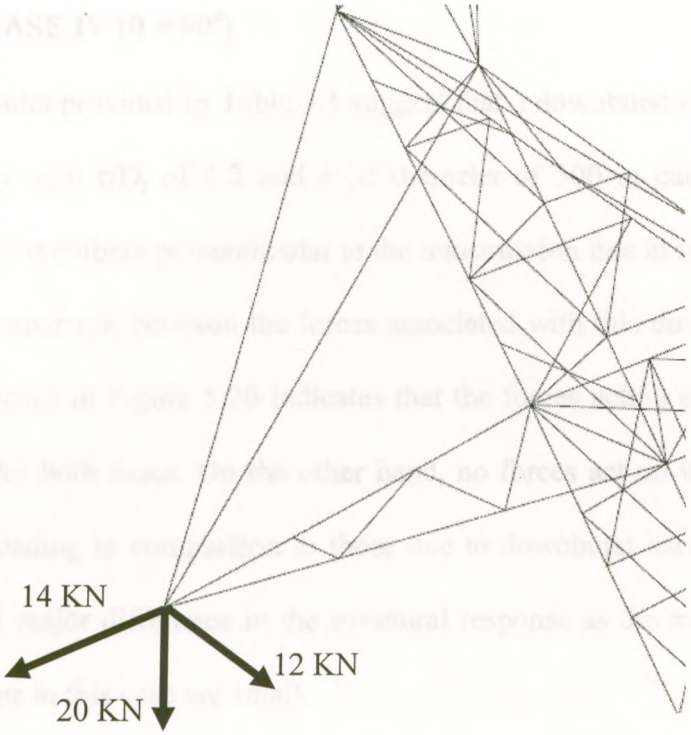

a. Downburst load in addition to the conductor self weight.

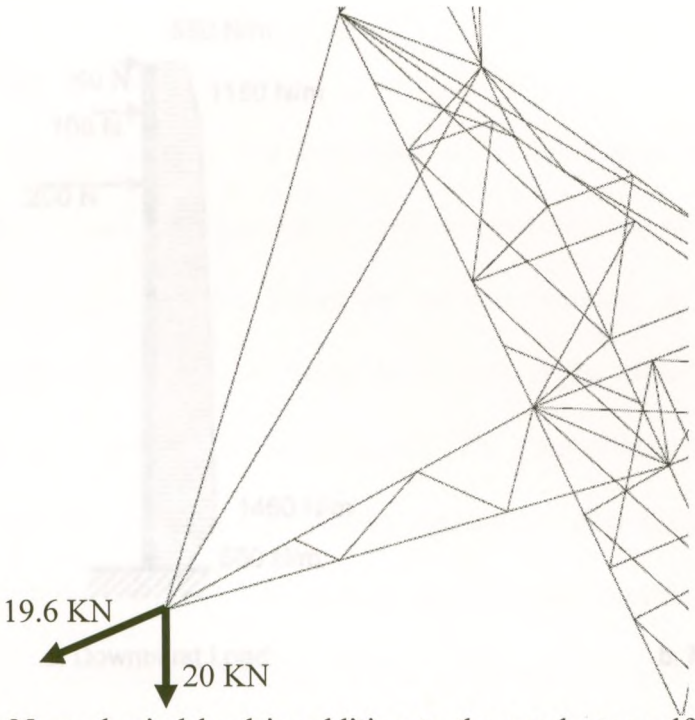

b. Normal wind load in addition to the conductor self weight.

Figure 5.19 Forces transferred from conductors under different wind loads at a projection angle of 30°.

5.4.4 CASE IV ($\theta = 90^{o}$)

The results provided in Table 5.1 suggest that a downburst configuration having an angle of 0^{o}, a ratio r/D_j of 1.2 and a jet diameter of 500 m causes maximum forces in the diagonal members perpendicular to the transmission line in the lowermost two zones.

The comparison between the forces associated with this downburst and the normal wind case shown in Figure 5.20 indicates that the forces acting on the tower body are almost equal for both cases. On the other hand, no forces act on the conductors due to normal wind loading in comparison to those due to downburst loading. However, this does not cause a major difference in the structural response as the magnitudes of the longitudinal reactions in this case are small.

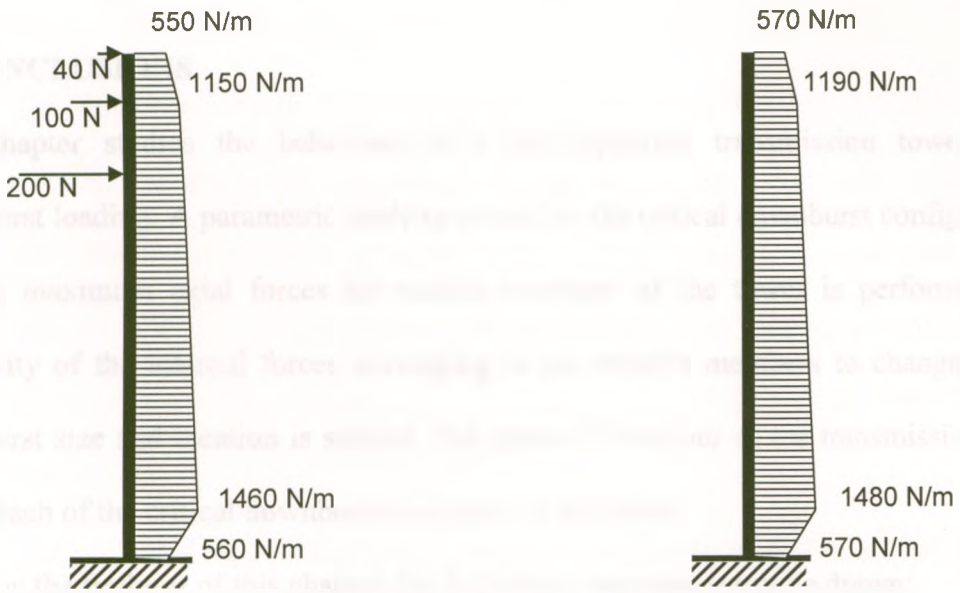

Figure 5.20 Vertical profile of wind loading at a projection angle of 90^{o}.

Figure 5.21 shows the displacement profile and the variations of the bending moment and shear force along the height of the equivalent beam due to both the downburst and normal

wind loads, respectively. The absence of conductor forces in the case of normal wind load leads to slightly smaller deflections (4 % difference), and slightly smaller magnitudes (4 % difference) of the bending moments and shear forces along the height of the tower.

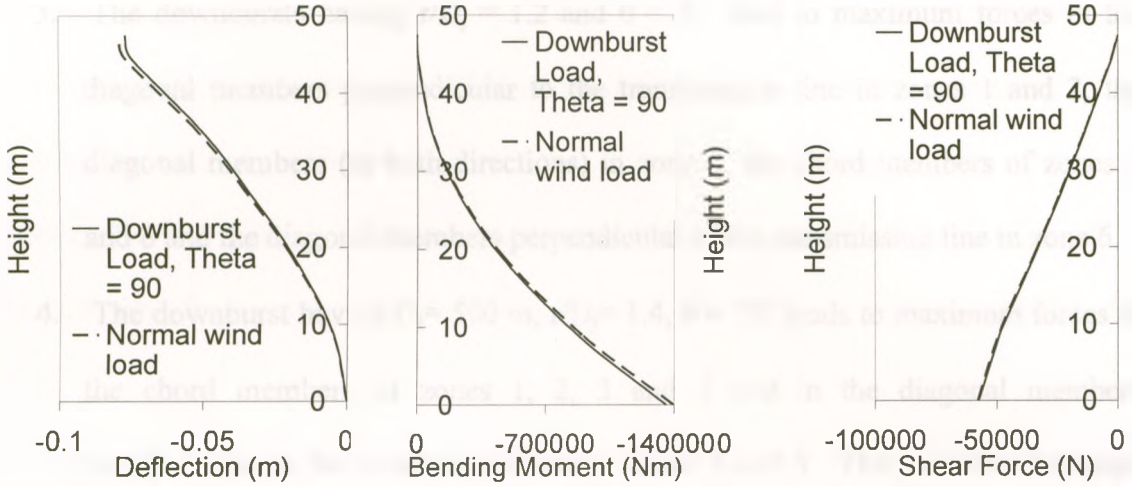

Figure 5.21 Structural behavior at a projection angle of 90°.

5.5 CONCLUSIONS

This chapter studies the behaviour of a self-supported transmission tower under downburst loading. A parametric study to determine the critical downburst configurations causing maximum axial forces for various members of the tower is performed. The sensitivity of the internal forces developing in the tower's members to changes in the downburst size and location is studied. The general behaviour of the transmission tower due to each of the critical downburst load cases is described.

Based on the findings of this chapter, the following conclusions can be drawn:

1. Changing the location of the downburst (r/D_j and θ) has a stronger effect on the value of the axial force in all tower members when compared to the downburst size (D_j) which has a minor effect.

2. Due to the higher radial velocities for r/D_j of 1.2 and 1.4, the downbursts locations corresponding to these ratios cause critical load cases for the first four zones. Larger critical ratios occur for some members in the uppermost two zones.
3. The downbursts having $r/D_j = 1.2$ and $\theta = 0^o$ lead to maximum forces in the diagonal members perpendicular to the transmission line in zones 1 and 2, the diagonal members (in both directions) in zone 4, the chord members of zones 5 and 6 and the diagonal members perpendicular to the transmission line in zone 6.
4. The downburst having $D_j = 500$ m, $r/D_j = 1.4$, $\theta = 15^o$ leads to maximum forces in the chord members of zones 1, 2, 3 and 4 and in the diagonal members perpendicular to the transmission line in zones 3 and 5. This is due to the large forces transferred simultaneously from the conductors and ground wires in both the longitudinal and transverse directions.
5. The downburst configuration having $D_j = 500$ m, $r/D_j = 1.6$, $\theta = 30^o$ leads to maximum forces in the upper chord member and a diagonal member in the cross-arm zone (zone 5). The members are subjected to compression axial forces under this configuration. These members have relatively large unsupported length and might not have been designed to resist compression under normal wind loads and own weight.
6. The typical design of the transmission line according to ASCE no. 74 could be considered sufficient to resist downburst winds at angles of 0^o and 90^o while for moderate angles (e.g. 15^o and 30^o) these design procedures are insufficient due to the large longitudinal reactions occurring in these cases.

5.6 REFERENCES

American Society of Civil Engineers (2010). "Guidelines for electrical transmission line structural loading." *ASCE Manuals and Reports on Engineering Practice*, No. 74, N.Y.

Darwish, M. M., El Damatty, A. A. and Hangan, H.M. (2010) "Dynamic characteristics of transmission line conductors and behaviour under turbulent downburst loading" *Wind and Structures*, 13(4), 327-346.

Fujita, T. T. (1990). "Downbursts: meteorological features and wind field characteristics." *Journal of Wind Engineering and Industrial Aerodynamics*, 36(1), 75-86.

Gerges, R. R. and El Damatty, A. A. (2002). "Large displacement analysis of curved beams." *Proceeding of CSCE Conference*, Montreal, QC, Canada, ST 100.

Hangan, H. and Kim, J. (2007). "Numerical simulations of impinging jets with application to downbursts" *Journal of Wind Engineering and Industrial Aerodynamics*, 95(4), 279–298.

Kim, J.D., Hangan, H. and Ho, T.C.E. (2007). "Downburst versus boundary layer induced loads for tall buildings." *Wind and Structures*, 10(5), 481-494.

Koziey, B. and Mirza, F. (1994). "Consistent curved beam element." *Computers and Structures*, 51(6), 643-654.

Manitoba Hydro Transmission and Civil Design Department (1999), "Bipole 1 & 2 HVDC transmission line wind storm failure on September 5, 1996 – review of emergency response, restoration and design of these lines", *Manitoba Hydro*, 98-L1/1-37010-06000, 54.

Mathur, R. K., Shah, A.H., Trainor, P.G.S. and Popplewell, N. (1987). "Dynamics of a guyed transmission tower system." IEEE Transactions on Power Delivery, Vol. PWRD-2, No. 3, pp. 908-916.

Shehata, A. Y., El Damatty, A. A., and Savory, E. (2005). "Finite element modelling of transmission line under downburst wind loading." *Finite Element in Analysis and Design*, 42(1), 71-89.

Shehata, A.Y. and El Damatty, A.A. (2007). "Behaviour of guyed transmission line structures under downburst wind loading" *Wind and Structures, An International Journal*, 10(3), 249-268

Shehata, A.Y. and El Damatty, A.A. (2008). "Failure analysis of a transmission tower during a microburst" *Wind and Structures, An International Journal*, 11(3), 193-208

Shehata, A. Y., Nassef, A.O. and El Damatty, A. A. (2008). "A coupled finite element-optimization technique to determine critical microburst parameters for transmission towers." *Finite Element in Analysis and Design*, 45(1), 1-12.

Wang, X., Lou, W., Li, H. and Chen, Y (2009). "Wind-induced dynamic response of high-rise transmission tower under downburst wind load" *Journal of Zhejiang University*, 43(8), 1520-1525.

Xie, Qiang, Zhang, Yong and Li, Jie (1993). "Investigation on tower collapses of 500 kV Renshang 5237 transmission line caused by downburst 2." *Power System Technology*, 30(10), 59-63.

CHAPTER 6

CONCLUSIONS

6.1 SUMMARY AND CONCLUSIONS

The current thesis investigates the structural characteristics, sensitivity and the structural design of transmission line structures under downburst wind loading. The study is motivated by the scarcity of special structural design code provisions for transmission line structures under such localized high intensity wind events. The study is conducted numerically and considers several types of the Manitoba Hydro transmission lines of which 19 towers failed during a downburst event in 1996. The research conducted in this thesis involves the following phases:

1) Assess the dynamic behaviour of the transmission line conductors under downburst loading. A turbulence signal is extracted from a set of full-scale data and then added to the mean component of the downburst wind field previously evaluated from a CFD analysis. Dynamic analysis is performed using various downburst configurations to estimate the effect of turbulence.
2) Evaluate the sensitivity of the forces in the guyed tower members to changing the downburst configurations, the tower height, guys configuration, turbulence, and change in the level of pretensioning in the conductors.
3) Study different options in terms of the location and nature of the design velocity associated to different modes of failure of guyed transmission towers. Develop an equivalent load corresponding to each of the three modes of failure.

4) Extend the numerical model to study the behaviour of self supported transmission line towers under downburst loading. Study, the sensitivity of the tower members to changes in the downburst size and location.

The general conclusions pertaining to each of the four research phases are presented below.

6.1.1 DYNAMIC CHARACTERISTICS OF TRANSMISSION LINE CONDUCTORS AND THEIR BEHAVIOUR UNDER TURBULENT DOWNBURST LOADING

This chapter assesses the dynamic behaviour of the line conductors under downburst loading. A non-linear numerical model is developed and used to predict the natural frequencies and mode shapes of conductors at various loading stages. A turbulence signal is extracted from a set of full-scale data. It is added to the mean component of the downburst wind field previously evaluated numerically. Dynamic analysis is performed using various downburst configurations. The following conclusions can be drawn from this chapter:

1. The magnitude of the pretension force has a major effect on the natural frequencies, reactions and mode shapes of the conductor. As the pretension force increases, the natural periods of the structure decreases, and the deflection at the connection between the towers and the cables increases, causing the structure to behave more as a cable than a beam.
2. The inclusion of the flexibility of the towers and insulators at the towers/conductor connections, rather than assuming fully hinged boundary conditions, has a significant effect on the natural frequencies and mode shapes.

3. Neither the level of loading nor the downburst load configuration has any significant effect on the natural periods and the mode shapes of the conductor.
4. The response due to turbulence increases significantly with the increase in the filtering periods, until a filtering period of 40 s. Beyond this value, the response remains almost unchanged. This suggests that 40 s is a suitable averaging period, agreeing with the findings of Holmes et al. (2008).
5. Due to the large aerodynamic damping, the resonant component of the turbulence is damped out when the damping is included in the analysis, leaving the background component to play the major role in the quantification of the effect of turbulence. Hence, the quasi-static analysis is sufficient enough in assessing the effect of turbulence.
6. Considering the 40 s averaging period, the inclusion of turbulence increases the deflection and the internal forces by about 20 % for the considered downburst intensity.

6.1.2 CHARACTERISTICS OF TRANSMISSION LINE GUYED TOWERS AND ITS BEHAVIOUR UNDER DOWNBURST LOADING

This chapter evaluates the sensitivity of the forces in the tower members to the changes in the downburst configuration, the guys' configuration and the effect of turbulence on the forces in the tower members. The axial forces in the members are compared to these resulting from normal wind loading according to the ASCE # 74 for both symmetric and broken wire load cases. The study includes investigating the effect of increasing the pretensioning forces in the conductors on the longitudinal reaction and the cross-arm members. The following conclusions can be drawn:

1. Changing the location of the downburst (r/D_j and θ) has a stronger effect on the value of the axial force in all tower members when compared to the downburst size (D_j) which has a minor effect.
2. For the zones beneath the tower-guy connection, the maximum forces happen for a ratio r/D_j between 1.2 and 1.4 and angles of 0^o and 90^o, while in the zones above the guy connection the maximum forces in most of the members occur for higher r/D_j values for angles between 15^o and 45^o due to the high longitudinal reaction of the conductors corresponding to these angles.
3. The maximum increase in the axial force in the members due to turbulence is 20%.
4. Doubling the pretensioning force in the conductors is sufficient enough to achieve very low values for the longitudinal reaction, hence reducing the forces in the cross-arm members significantly.
5. The effect of changing the pretensioning force is sounding most at an angle of 30^0 as the maximum value for the longitudinal reaction occurs at this angle.
6. Increasing the height and changing guy configuration cause negligible changes in the general behavior of the tower members along the tower height in terms of the sensitivity to changing the downburst configuration although the values of the forces in the tower members have changed.

6.1.3 EQUIVALENT LOADING OF GUYED TRANSMISSION LINE TOWERS TO RESIST DOWNBURSTS

Within this chapter, different options are considered in terms of both, the location and the nature, of the design velocity associated to different critical downburst cases. The effect

of adding the convective velocity component to the downburst event is studied. The equivalent load corresponding to each of the three critical cases is developed. The following conclusions can be drawn:

1. The analysis of guyed transmission towers under downburst load with a fixed 44 m velocity provides more realistic results when compared to the results of analysing the same towers under downburst load with a fixed 10 m velocity.

2. Loading only one side of the transmission line beside the tower understudy with a uniform load is effective in calculating the equivalent load representing the load transferred through the conductors within the asymmetric downburst case.

3. In addition to loading the tower body; loading all the spans of the conductor with a uniform load is effective in calculating the equivalent patch load representing the load transferred through the conductors within the second downburst case.

4. Loading only the tower body is effective in calculating the equivalent load representing the third downburst case.

5. The horizontal velocity along the tower height could be considered equal to the 10 m reference velocity.

6. The design velocity should exceed the speed available from sufficient meteorological data acquired from the location of the transmission line to be designed.

7. For the symmetric downburst load cases, the effects of both the convective and jet velocities are significant and the summation of both velocities causing failure is always constant.

8. For the asymmetric downburst load case, the major source of criticality is the large longitudinal reaction due to the unbalanced loading caused by the asymmetric downburst load, while the convective velocity has a minor effect when comparing it to the effect of

the jet velocity. This case is the most critical, as it causes failure at a level of loading earlier than that caused by symmetric load cases.

6.1.4 BEHAVIOR OF SELF SUPPORTED TRANSMISSION LINE TOWERS UNDER DOWNBURST LOADING

This chapter studies the behaviour of a self-supported transmission tower under downburst loading. A parametric study to determine the critical downburst configurations causing maximum axial forces for various members of the tower is performed. The sensitivity of the internal forces developing in the tower's members to changes in the downburst size and location is studied. The general behaviour of the transmission tower due to each of the critical downburst load cases is described.

Based on the findings of this chapter, the following conclusions can be drawn:

1. Changing the location of the downburst (r/D_j and θ) has a stronger effect on the value of the axial force in all tower members when compared to the downburst size (D_j) which has a minor effect.
2. Due to the higher radial velocities for r/D_j of 1.2 and 1.4, the downbursts locations corresponding to these ratios cause critical load cases for the first four zones. Larger critical ratios occur for some members in the uppermost two zones.
3. The downbursts having $r/D_j = 1.2$ and $\theta = 0^o$ lead to maximum forces in the diagonal members perpendicular to the transmission line in zones 1 and 2, the diagonal members (in both directions) in zone 4, the chord members of zones 5 and 6 and the diagonal members perpendicular to the transmission line in zone 6.
4. The downburst having $D_j = 500$ m, $r/D_j = 1.4$, $\theta = 15^o$ leads to maximum forces in the chord members of zones 1, 2, 3 and 4 and in the diagonal members perpendicular to

the transmission line in zones 3 and 5. This is due to the large forces transferred simultaneously from the conductors and ground wires in both the longitudinal and transverse directions.

5. The downburst configuration having D_j = 500 m, r/D_j= 1.6, $\theta = 30^o$ leads to maximum forces in the upper chord member and a diagonal member in the cross-arm zone (zone 5). The members are subjected to compression axial forces under this configuration. These members have relatively large unsupported length and might not have been designed to resist compression under normal wind loads and own weight.
6. The typical design of the transmission line according to ASCE no. 74 could be considered sufficient to resist downburst winds at angles of 0^o and 90^o while for moderate angles (e.g. 15^o and 30^o) these design procedures are insufficient due to the large longitudinal reactions occurring in these cases.

6.2 RECOMMENDATIONS FOR FUTURE RESEARCH

The thesis investigates numerically the structural behaviour and the structural design of several structural configurations of transmission line structures located in an open country terrain exposure and subjected to downburst wind loading. For future research, the following investigations are suggested:

- Conduct similar studies by considering different configurations of transmission lines.
- Conduct similar studies by considering transmission lines with larger spans and higher heights.
- Consider the effect of different terrain exposures, such as urban and suburban areas and unobstructed coastal areas, as well as the topology of the ground.
- Study different retrofitting techniques for transmission line structures.